Mathematical Model for IL-6-Mediated Tumor Growth, and Targeted Treatment

by

Fereshteh Nazari

A Dissertation Presented in Partial Fulfillment
of the Requirements for the Degree
Doctor of Philosophy

Approved July 2017 by the
Graduate Supervisory Committee:

Trachette L. Jackson, Co-Chair
Carlos Castillo-Chavez, Co-Chair
Sherry Towers
Yun Kang

ARIZONA STATE UNIVERSITY

August 2017

ABSTRACT

Head and neck squamous cell carcinoma (HNSCC), the sixth most common cancer type worldwide, accounts for more than 630,000 new cases and 350,000 deaths annually. Drug-resistance and tumor recurrence are the most challenging problems in head and neck cancer treatment. It is hypothesized that a very small fraction of stem-like cells within HNSCC tumor, called cancer stem cells (CSCs), is responsible for tumor initiation, progression, resistance and recurrence. It has also been shown that IL-6 secreted by head and neck tumor-associated endothelial cells (ECs) enhances the survival, self-renewal and tumorigenic potential of head and neck CSCs. In this study we will use a mathematical multi-scale model which operates at the intracellular, molecular, and tissue level to investigate the impacts of EC-secreted IL-6 signaling on the crosstalk between tumor cells and ECs during tumor growth. This model will be calibrated by using the experimental in vivo data.

Eventually the model will be modified to explore the responses of head and neck cancer cells to combination therapy involving Tocilizumab (an anti-IL-6R antibody) and Cisplatin (the most frequently used chemotherapy for head and neck cancer). The model will be able to predict the final proportion of CSCs in response to endothelial cell-secreted IL-6 and drug therapies. The model will be validated by directly comparing the experimental treatment data and the model predictions. This could potentially provide a condition under which we could control enlargement of the head and neck CSC pool and tumor recurrence. It may also suggest the best bounds for Cisplatin and/or Tocilizumab dose and frequency to be tested in the clinical trial.

ACKNOWLEDGMENTS

This work bears the marks of so many teachers and mentors who have shaped my intellectual journey. I am deeply grateful to my advisors, Dr. Trachette L. Jackson and Dr. Carlos Castillo-Chavez for their stalwart commitment through this process and for showing me that the joy of research comes in the balance of structure and creativity. I am also grateful to my committee member and Dr. Sherry Towers. Their invaluable insight, inspiration, and encouragement have been instrumental in my development as a researcher.

I am grateful for the friendships I made here at ASU, especially at the Simon A. Levin Modeling Sciences Center. Special thanks goes to Arlene Evangelista, Michael lin, Kamaldeen Okuneye, Oyita Udiani, Derdei Bichara, Juan Renova, Baltazar Espinosa, Victor Moreno, Komi Messan, Daniel Burkow, Miles Manning, Dustin Padilla, Jordan Bates and many others with whom I share amazing memories from these past 3 years. I am truly indebted to my friends Monireh Malekirad, Saba Rajabi, Tahoora Nazer, Mahshid Zandi and Sheida Badvipour for their loving generosity, and to Sherry Woodley, Dawn Bies and Margaret Murphy-Tillis who tirelessly went to bat for me. Finally, I give my most profound gratitude to my family– my parents Jalil and Sorayya; and Sahel, Nassim, Farzaneh, Orsa, Nima, Kiyan and Melody – for believing in me. I love you all.

TABLE OF CONTENTS

CHAPTER Page

CHAPTER Page

LIST OF TABLES

Table Page

LIST OF FIGURES

Figure Page

Figure Page

Figure Page

Figure Page

Figure Page

Chapter 1

INTRODUCTION

Cancer is one of the major public health challenges globally, and is the second leading cause of death in the United States Siegel *et al.* (2017). The American Cancer Society recently estimated that approximately 1,700,000 new cancer cases are expected to be diagnosed in 2017, which is equivalent to more than 4,600 new cases each day Siegel *et al.* (2017). Figure 1.1 shows the average annual incidence rate of all cancer types combined for the years 2009 to 2013 per 100,000 individuals in the US population by state. Despite all the treatment improvements and medical advances, cancer-related death rates are still extremely high. More than half a million Americans die from cancer each year. It is estimated that cancer will cause 600,920 deaths in the US in 2017, corresponding to about 1,650 deaths per day Siegel *et al.* (2017). Collectively, the cancer incidence and mortality rates make it a deadly disease that affects the vast majority of the population globally, and not just in the US. Therefore, it is crucially important that more research is aimed at investigating the causes of cancer and developing new therapeutic treatment strategies.

Cancer can be defined as a genetic disease caused by the accumulation of mutations in somatic cells Altrock *et al.* (2015). During the multiple steps of evolution from normal to cancerous, altered somatic cells acquire the capabilities of sustaining proliferative signaling, evading growth suppressors, resisting cell apoptosis, enabling replicative immortality, inducing angiogenesis, and activating invasion and metastasis Altrock *et al.* (2015); Hanahan and Weinberg (2011b). In particular, these mutated cells do not obey the highly regulated processes of normal

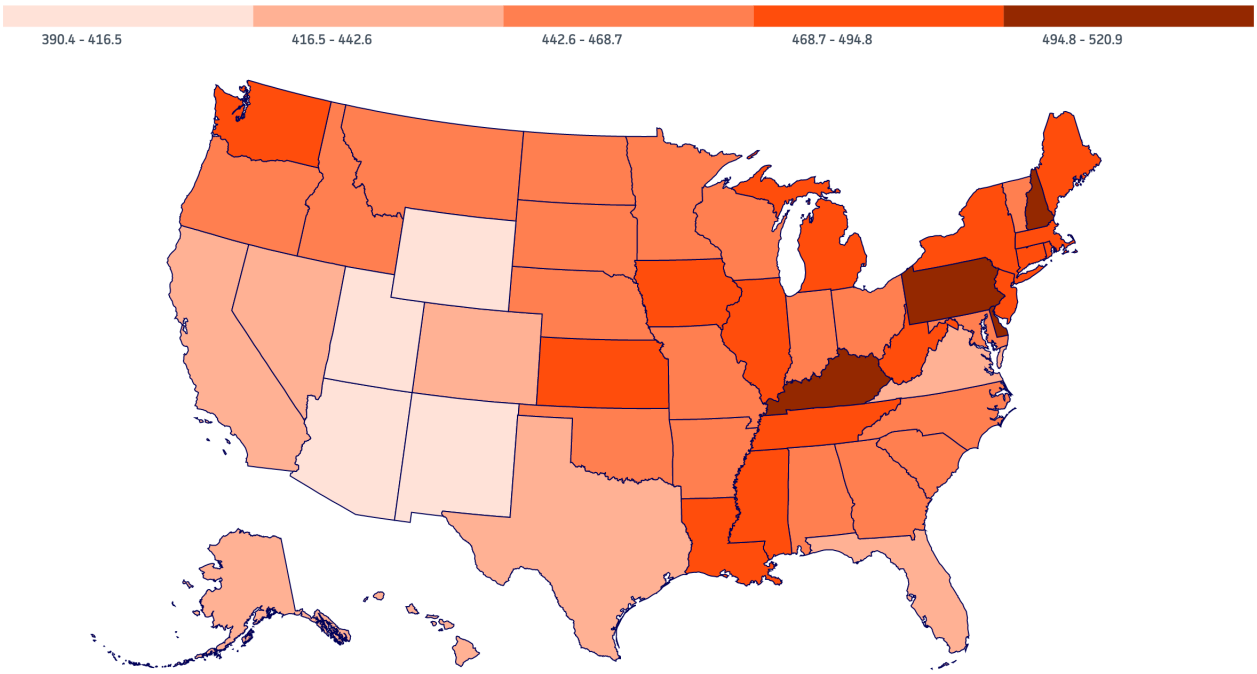

Figure 1.1: Incidence Rates of all Cancer Types Combined for the Years 2009-2013. Average annual rate per 100,000, age adjusted to the 2000 US standard population. *Data sources: North American Association of Central Cancer Registries (NAACCR), 2016*

cell division and death, which can result in tumor initiation Jackson *et al.* (2014). Fortunately, not all the tumors can survive the early stages of tumor growth. To progress towards malignancy and further invasion, tumor cells rely on interactions with stromal cells for a continuous supply of nutrients. There are also multiple additional factors that aid the persistence of newly formed tumors within a tissue. Namely, stochastic DNA replication errors in cells, crosstalk between tumor cells and the tissue microenvironment, radiation exposures and diet are some of the factors contributing to carcinogenesis of tumors.

There are two well-known theories explaining the malignancy potential of mutated tumor cells. According to the *stochastic hypothesis*, tumor cells display ho-

mogeneity in sense that each cell has an equal potential to initiate and propagate tumors, as well as metastasize. Therefore, this implies that there is no selectivity between the cancer cells in a tissue Dick (2009). The stochastic model explains heterogeneity in tumors by spontaneous shifts in cell phenotypes Albers *et al.* (2012). However, there is an abundance of emerging evidence that supports an alternative hypothesis that tumors are initiated and maintained by a population of tumor cells that have many of the biological characteristics of normal adult stem cells. This model, the *cancer stem cell (CSC) hypothesis*, is based on the notion that tumors, like those found in adult tissues, arise from multipotent cells that exhibit the ability to self-renew and give rise to differentiated tissue cells Krishnamurthy *et al.* (2014); Nör *et al.* (2014); Zhu *et al.* (2014). Additionally, it states that the bulk of the tumor tissue is composed of rapidly proliferating cells called transit-amplifying cells and post-mitotic differentiated cells. These cells do not contribute to tumor initiation. They are derived from the cancer stem cells by differentiation, but are not capable of tumor initiation by themselves Prince and Ailles (2008); Reya *et al.* (2001).

An extensive number of studies have utilized these two theories to describe tumor initiation, its heterogeneous structure, and tumor progression in different types of cancer Albers *et al.* (2012); Civenni *et al.* (2011); Girouard and Murphy (2011); Gupta *et al.* (2011); Quintana *et al.* (2008); Taghizadeh *et al.* (2010). For instance, one study demonstrated that in melanomas about 25% of unsorted cells were able to initiate tumors in immunocompromised mice, supporting the stochastic model Quintana *et al.* (2008). In other recent works, evidence contrary to the stochastic model has been presented. For instance, cells with high levels of $CD44^{HIGH}$ $ALDH^{HIGH}$ expression (cancer stem cells) taken from a primary human head and neck tumor were able to create tumors in mice much more often than cells with

low expression of these markers, which supports the cancer stem cell hypothesis Krishnamurthy *et al.* (2014). Furthermore, it was shown that $CD44^{HIGH}ALDH^{HIGH}$ cells were more tumorigenic and created more aggressive tumors than their counterparts with low levels of CD44 and ALDH, providing more evidence in favor of the cancer stem cell (CSC) hypothesis. It is hypothesized that CSCs are responsible for tumor initiation, progression resistance and recurrence Hermann *et al.* (2010); Krishnamurthy *et al.* (2014); Prince *et al.* (2007). Markers for cancer stem cells have now been identified in a variety of malignancies, including tumors of the blood, breast, colon, brain, and head and neck Krishnamurthy *et al.* (2014).

Head and Neck Squamous Cell Carcinomas

Head and neck squamous cell carcinoma (HNSCC) is the sixth most common cancer in the world, diagnosed in approximately 400,000-600,000 people globally each year Neiva *et al.* (2009); Parfenov *et al.* (2014); Pearson *et al.* (2016). High risk strains of human papilloma virus (HPV), alcohol consumption and tobacco use are the most common risk factors for HNSCC Pearson *et al.* (2016). Survival rates in patients with head and neck cancer are poor and have not improved during the last three decades, despite extensive basic and clinical research Neiva *et al.* (2009); Pulte and Brenner (2010).

Conventional treatment for head and neck cancer has consisted of surgery and radiation combined with and/or followed by chemotherapy. Cisplatin is the most common chemotherapeutic agent prescribed for the treatment of HNSCC Nör *et al.* (2014). Although Cisplatin is able to help to raise the quality of life of patients with HNSCC, it does not considerably improve the 5-year survival rete due to drug-

resistance and metastasis.

Attempts to understand the mechanisms behind the tumorigenic process and drug-resistance of tumors led to the discovery of HNSCC cancer stem cells Krishnamurthy *et al.* (2014). HNSCC cancer stem cells are a small population of HNSCC tumors which are uniquely tumorigenic, multipotent cancer cells endowed with the ability to self-renew Krishnamurthy *et al.* (2014); Pearson *et al.* (2016). Furthermore, it was shown that HNSCC tumor cells have a heterogeneous hierarchical structure and are capable of distant metastasis. All together, these facts support the idea of cancer stem cell hypothesis for HNSCC tumors. Unlike most cells within a tumor, cancer stem cells (CSC) are often resistant to conventional chemo- and/or radiation therapy, making it necessary to design new therapeutic approaches that target these cancer stem cells Finkel *et al.* (2016). However, direct targeting and ablation of CSCs might cause toxicities related to the unintended elimination of normal stem cells Krishnamurthy *et al.* (2014). It has also been demonstrated that growth and survival of CSCs are highly influenced by tumor micro-environmental factors and molecular signaling, including cytokines like interleukin-6 (IL-6) Krishnamurthy *et al.* (2014). IL-6 is a protein (signaling molecule) secreted by T-cells, macrophages and osteoblasts, and which acts as both a pro-inflammatory cytokine and an anti-inflammatory myokine. More interestingly, it has been revealed that HNSCC CSCs reside in perivascular niches and that IL-6 secreted by endothelial cells (ECs) in the tumor niche enhances the survival, self-renewal and tumor initiation potentials of CSCs in primary head and neck tumor Krishnamurthy *et al.* (2014). In fact, IL-6 phosphorylates Signaling Transducer and Activator of Transcription 3 (STAT3) via binding to its natural receptor, IL-6R, and the transmembrane cytokine receptor, gp130 (and signaling through the Janus kinases). Phos-

phorylation of STAT3 is an indicative of stemness Krishnamurthy *et al.* (2014). Therefore, targeting the IL-6-induced signaling pathways may inhibit the survival and self-renewal potential of CSCs. Thus, drugs that block the cross-talk between endothelial cells and CSCs within the perivascular niche may inhibit and/or control tumor growth. This is a potential alternative treatment that could be used in combination with conventional therapies.

One of the main challenges in studying CSCs and developing anti-IL-6 therapies has been development of efficient in vitro and/or in vivo methods to understand the impacts of CSCs on the pathobiology of HNSCC. One of the reasons for this is the need to perform most studies with primary HNSCC specimens, which are difficult to obtain. In addition, in vivo experimentation is expensive and time consuming, and in vitro methods have limited capacity for expansion of head and neck cancer stem cells. Along with experimental methods, mathematical and computational modeling approaches provide a useful framework to study cancer progression since they can integrate biological parameters and make predictions across different time and/or spatial scales. Moreover, mathematical models provide a powerful tool to facilitate drug development and pre-clinical evaluation of efficacy, which cannot be easily understood by using conventional wet-lab experiments alone Olsen and Siegelmann (2013); Tang *et al.* (2014); Wang *et al.* (2015). Among the recent mathematical techniques commonly used today, multiscale models have been widely applied to model tumor growth, tumor-induced angiogenesis and treatment Altrock *et al.* (2015); Deisboeck *et al.* (2011); Jackson *et al.* (2014); Jain *et al.* (2008); Olsen and Siegelmann (2013); Perfahl *et al.* (2011); Plank *et al.* (2004); Sanga *et al.* (2006); Shirinifard *et al.* (2009); Tang *et al.* (2014); Tee and Distefano Iii (2004); Wang *et al.* (2013). Most existing models, however, suf-

fer from the lack of (1) sufficient resolution to evaluate drug effects at the cellular level; (2) validation of the model predictions using the actual experimental data; and (3) inclusion of tumor cell heterogeneity and tumor cell plasticity.

Statement of Purpose

The fact that HNSCC CSCs form only a small portion of the total tumor burden, but may play a disproportionately important role in determining tumor growth and treatment outcomes shapes the goals of this study. The overarching objective is to develop a predictive computational framework that will: (1) advance our current understanding of the differential impact of IL-6 on CSC self-renewal and HNSCC growth; and (2) optimize the clinical use of combination therapy involving targeted treatment with Tocilizumab (an anti-IL-6R antibody) and Cisplatin.

This project has two main parts. Part I is to build and calibrate an integrated cellular and molecular model for the IL-6 dependent growth HNSCC tumors from a small population of cancer stem-like cells and use it, and its extensions, to: (1) derive functional relationships among self-renewal and cell death and IL-6 concentration, 2) predict the response of HNSCC to Tocilizumab, an anti-IL6 antibody and 3) incorporate the mechanism of action of Cisplatin and quantify its influence on the tumor growth and stem cell proportion post-treatment.

Part II is to extend this model to a fully multi-scale framework designed to investigate the role of IL-6 and CSCs in the bidirectional communication (i.e. crosstalk) between endothelial cells and tumor cells that contributes to and enhances key aspects of tumorigenesis and can lead to evasive therapeutic resistance.

In Chapter 1, we build and analyze a preliminary mathematical model for the growth of tumors from a small population of cancer stem-like cells and use it to predict tumor growth dynamics and cellular composition. In chapter 2, we extend the model introduced in Chapter 1 to include the molecular level details of tumor cell-secreted IL-6 signaling and its impacts on tumor growth and CSC self-renewal. We also run preliminary simulations of the response of cancer cells to Tocilizumab. Finally, in Chapter 3, we expend the model introduced in Chapter 2 to describe endothelial cell-tumor cell crosstalk. The model in Chapter 3 includes tumor angiogenesis, vascular tumor growth, and response to treatment. This model operates at three levels: (1) intracellular, (2) cellular and (3) tissue levels are integrated to describe IL-6 signaling and silencing, cancer stem cell driven tumor growth, and combination therapy with Tocilizumab and Cisplatin.

Chapter 2

DEVELOPMENT AND ANALYSIS OF A MATHEMATICAL MODEL BASED ON THE CANCER STEM CELL HYPOTHESIS

The main goal of this chapter is to build and analyze a preliminary mathematical model for the growth of tumors from a small population of cancer stem-like cells and use it to predict tumor growth dynamics and cellular composition. According to the CSC hypothesis, tumors have a hierarchical structure and originate from a small number of tumor initiating cells. These cancer stem cells (CSCs) are capable of both self-renewal and differentiation, thereby producing all the distinct cell types found within a tumor and contributing to heterogeneity Michor (2008). During the process of CSC differentiation, one of the two daughter cells retains it's "stemness", whereas the other differentiates into other cell types with little or no ability to self-renewal Al-Hajj *et al.* (2003); Cabrera *et al.* (2015); Michor (2008); Zhu *et al.* (2014). Therefore, following the CSC hypothesis, we develop a mathematical model that assumes CSCs initiate and sustain tumor growth and that the bulk of the tumor tissue is derived through the differentiation of CSCs. We perform a rigorous mathematical analysis of the system of equations and use the model to predict the asymptotic behavior of CSCs at equilibrium and over the tumor's exponential growth phase. We also carry out a local sensitivity analysis in oder to suggest the most influential parameters on the final percentage of the CSCs at different stages of tumor growth. Eventually, this model will be extended in order to study the impact of tumor microenvironmental factors and molecular signaling on

the tumor growth dynamics as well as tumor response to combination therapy.

2.1 Modeling Cancer Stem Cell Driven Tumor Growth

In this section we develop a mathematical model for cancer stem cell-driven tumor growth in order to investigate the dynamics of cancer initiation and progression, as well as to determine the ultimate proportion of CSCs within a growing tumor. Since tumors that arise from CSCs include both tumorigenic and non-tumorigenic cells Michor (2008), our model tracks the temporal evolution of cancer stem cells and non-CSCs, including both progenitor and terminally differentiated cells (Figure 3.1).

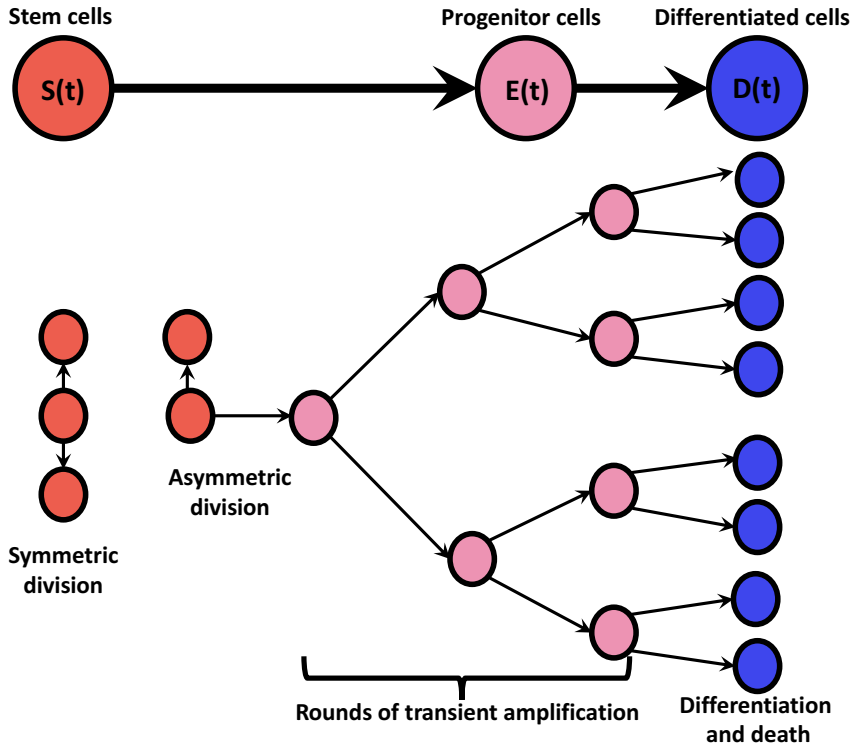

Figure 2.1: Schematic Diagram of the Stem Cell Division Processes Considered in the Amplifying Factor Mathematical Model

Table 3.1 tabulates each model variable along with the units.

Table 2.1: List of Model Variables

Variable	Description	Units
S	HNSCC stem cells	# of cells
E	HNSCC progenitor tumor cells	# of cells
D	HNSCC differentiated tumor cells	# of cells

Cancer cell equations

The total cellular composition of a tumor at time t is divided into cancer stem cells $S(t)$, transient amplifying/progenitor tumor cells $E(t)$ and terminally differentiated tumor cells $D(t)$. Equation (2.1.1), below, describes temporal changes in the cancer stem cell (S) population:

$$\underbrace{\frac{dS}{dt}}_{\text{Stem cell}} = \underbrace{\alpha_S P_S(S)\, S}_{\text{Stem cell self-renewal}} - \underbrace{\delta_S\, S}_{\text{Stem cell death}} \tag{2.1.1}$$

CSCs divide at rate, $_S$. The first term in (2.1.1) assumes that stem cells can either symmetrically renew with the probability of $P_S(S)$, creating two identical daughter cells that retain "stemness", or, with the probability of $(1 - P_S(S))$, they can asymmetrically differentiate into one stem and one progenitor cell. It is assumed that the self-renewal probability, $P_S(S)$, varies depending on the total cancer stem cell population size. The second term of (2.1.1) assumes that CSCs die at a death rate, δ_S.

Equations (2.1.2) and (2.1.3) describe temporal changes in the progenitor and terminally differentiated cell populations.

$$\frac{dE}{dt} = \underbrace{A_{in}\,\alpha_S(1-P_S(S)S}_{\substack{\text{Amplified}\\ \text{stem cell differentiation}}} - \underbrace{\alpha_E\,E}_{\substack{\text{Progenitor cell}\\ \text{differentiation}}} - \underbrace{\delta_E\,E}_{\text{progenitor cell death}} \tag{2.1.2}$$

$$\frac{dD}{dt} = \underbrace{A_{out}\,\alpha_E E}_{\substack{\text{progenitor ce ll}\\ \text{differentiation}}} - \underbrace{\delta_D\,D}_{\text{differentiated cell death}} \tag{2.1.3}$$

As depicted Figure 3.1, progenitor cells (2.1.2) undergo a limited number (w) of mitotic cycles, so called transit-amplifying (TA) cell divisions, before entering a post-mitotic terminally differentiated state Al-Hajj and Clarke (2004); Clarke and Fuller (2006). In this model, instead of adding w sub-compartments of progenitor cells, it is assumed that each differentiated stem cell is amplified on upon entry into the progenitor. This is a simplified version of the model developed in Ganguly and Puri (2006) and this approach has also been used in Gentry and Jackson (2013). The assumptions about amplification imply that the efflux from the stem compartment is augmented by a factor A_{in} as soon as the cells enter the progenitor pool as shown in the first term in (2.1.2).

The second term in (2.1.2) assumes that progenitor cells transition to fully differentiated cells via TA cell division at rate α_E. Finally, the second term in (2.1.2) assumes that progenitor cells die at rate δ_E.

Immediately before leaving the progenitor compartment, cells are further amplified by a factor $A_{out} = 2$ because the transition from progenitor to terminally differentiated cells results in the loss of one progenitor cell and the gain of two

terminally differentially cells as shown in the first term in (2.1.3). These two amplification factors are selected such that $A_{in} \times A_{out} = 2^w$, where $w =$ the number of successive stages of TA cell divisions before transforming into mature cell Ganguly and Puri (2006). Terminally differentiated cells live for a specified amount of time and then die at rate δ_D.

The probability of cancer stem cell self-renewal

The probability of CSC self-renewal, P_S, can be regulated by extrinsic and intrinsic chemical signaling as well as environmental (niche) constraints. Certain environmental cues can promote self-renewal, while others promote differentiation. Similarly, proteins produced by stem cells themselves can affect self-renewal in an autocrine manner. Many published mathematical models use a Hill function Anderson and Mackey (2001); Bernard *et al.* (2003); Gentry and Jackson (2013); Wang *et al.* (2010), which can be derived from receptor-ligand binding kinetics, to describe the effect of chemical signals on the probability of symmetric self-renewal. For these reasons, our model assumes the following functional form for the probability of stem cell-self renewal:

$$P_S(S) = \frac{(P_{S_{max}} - P_{S_{min}})P_{N_s}^n}{P_{N_s}^n + S^n} + P_{S_{min}}. \tag{2.1.4}$$

As the number of cancer stem cells approaches zero, the probability of symmetric self-renewal approaches the maximum value, $P_{S_{max}}$. Conversely, as the number of CSCs approaches infinity, the probability of symmetric self-renewal approaches a minimum value, $P_{S_{min}}$. The parameter P_{N_s} may be interpreted as the number of stem cells for which the probability of symmetric self-renewal is halfway between the maximum and minimum values. Higher values of the exponent $n > 1$ increase

the sensitivity of stem cells to signals that promote symmetric self-renewal. Figure 2.2 plots the probability of CSC self-renewal as a function of cell number for the baseline parameters of the model and for two different choices of the parameter P_{N_s}.

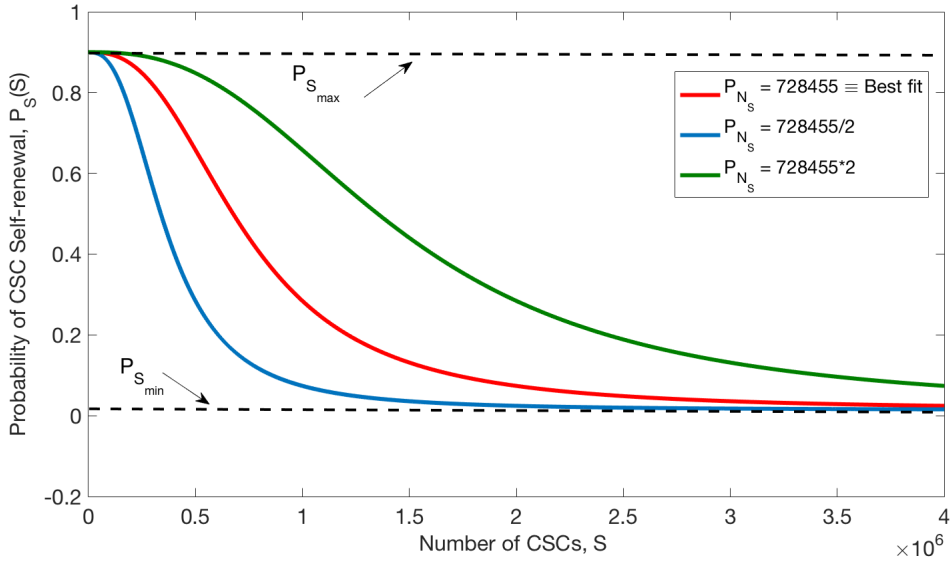

Figure 2.2: The Probability of Stem Cell Self-renewal, P_S, as a Function of Stem Cell Number.

Thus, the model system that we study, referred to as the Amplification Factor Model hereafter, is given by:

Amplification Factor Model

$$\begin{aligned} \frac{dS}{dt} &= \alpha_S P_S(S) S - \delta_S S \\ \frac{dE}{dt} &= A_{in}\, \alpha_S (1 - P_S(S)) S - \alpha_E E - \delta_E E \end{aligned} \tag{2.1.5}$$

$$\frac{dD}{dt} = 2\,\alpha_E E - \delta_D D$$

2.2 Basic Mathematical Analysis of the Amplification Factor Model

In the subsections below, we present some of the general results of our basic mathematical analysis of model 2.1.5. This type of analysis allows us to better understand the dynamic behavior that this model can exhibit.

2.2.1 Positiveness of the solutions

Proposition 2.2.1 *Let the initial condition for model 2.1.5 be $S(0) > 0$ and $E(0) > 0$ and $D(0) > 0$. Then, the solutions $(S(t), E(t), D(t))$ of model 2.1.5, with positive initial data, will remain positive for all time $t > 0$.*

Let assume that $S(0) > 0$, $E(0) > 0$, $D(0) > 0$ and t_1 is the smallest upper bound of all times that one of the three solutions, $S(t)$, $E(t)$ and $D(t)$ becomes zero. That is,

$$t_1 = Sup\,\{t > 0 : S(t) > 0,\ C(t) > 0,\ D(t) > 0\} > 0$$

Now, by contradiction, assume the case that $S(t_1) = 0$. Then, from the first equation in model 2.1.5 for all $t \in [0, t_1]$ we have:

$$\begin{aligned}\frac{dS}{dt} &= \alpha_S P_S(S) S - \delta_S S \\ &= \left\{ \alpha_S \left[\frac{(P_{S_{max}} - P_{S_{min}}) P_{N_s}^n}{P_{N_s}^n + S^n} + P_{S_{min}} \right] - \delta_S \right\} S.\end{aligned}$$

Now, let

$$L = Min\left\{\alpha_S\left[\frac{(P_{S_{max}} - P_{S_{min}})P_{N_s}^n}{P_{N_s}^n + S^n} + P_{S_{min}}\right] - \delta_S \ : \ t \in [0, t_1]\right\}.$$

Then,

$$\frac{dS(t)}{dt} \geq LS(t),$$

which implies that

$$\frac{\frac{dS}{dt}}{S} = \frac{\frac{dS}{S}}{dt} = \frac{d(ln(S)}{dt} \geq L, \quad \text{for } \ t \in [0, t_1].$$

That is,

$$ln(S(t_1)) - ln(S(0)) \geq Lt_1.$$

Thus,

$$S(t_1) \geq S(0)e^{Lt_1} > 0, \quad \text{for } \ t \in [0, t_1].$$

This a contradiction to the assumption that $S(t_1) = 0$. Thus, $S(t) > 0$ for all positive times whenever $S(0) > 0$. Similarly, it can be shown that $C(t)$ and $D(t)$ are positive for all time $t > 0$ if the initial values $C(0) > 0$ and $D(t) > 0$.

2.2.2 Boundedness of solutions

Proposition 2.2.2 *Solutions of model 2.1.5 are bounded provided $\alpha_S < \delta_S$.*

Assume that $\alpha_S < \delta_S$. Then we show that $S(t)$ is bounded under the given condition. Since by definition $P_S(S)$ is less than or equal to one, from the first equation in model 2.1.5 we have:

$$\frac{dS}{dt} = \alpha_S P_S(S)S - \delta_S S$$

$$\leq \alpha_S S - \delta_S S$$
$$= (\alpha_S - \delta_S) S.$$

Therefore,

$$S(t) \leq C_1 e^{(\alpha_S - \delta_S)t},$$

where, C_1 is an arbitrary constant. Hence, $S(t)$ is bounded whenever $\alpha_S < \delta_S$. Similarly, for the second equation in model 2.1.5, we have:

$$\begin{aligned}\frac{dE}{dt} &= A_{in}\, \alpha_S (1 - P_S(S)) S - \alpha_E E - \delta_E E \\ &\leq A_{in}\, \alpha_S S - \alpha_E E - \delta_E E \\ &= A_{in} \alpha_S S - (\alpha_E + \delta_E) E\end{aligned}$$

We showed that $S(t)$ is bounded whenever $\alpha_S < \delta_S$, which means that under the given assumption, there exists an upper-bound, U_S, for $S(t)$ for all time t such that

$$S(t) \leq U_S, \quad \text{for all } \ t > 0,$$

which implies that

$$\begin{aligned}E(t) &\leq e^{-(\alpha_E + \delta_E)t} \left(A_{in} \alpha_S U_S \int e^{(\alpha_E + \delta_E)t} dt + C_2 \right) \\ &= \frac{A_{in} \alpha_S U_S}{(\alpha_E + \delta_E)} + C_2 e^{-(\alpha_E + \delta_E)t}\end{aligned}$$

Hence, $E(t)$ is bounded whenever $S(t)$ is bounded. That is, $E(t)$ is bounded whenever $\alpha_S < \delta_S$. Similarly, it can be easily shown that $D(t)$ is bounded whenever $E(t)$ is bounded. Thus, $D(t)$ is bounded whenever $\alpha_S < \delta_S$. This completes the proof of

the proposition.

2.2.3 Existence of non-negative equilibria

In this section, the possible equilibrium point(s) of model 2.1.5 will be explored. Setting the right hand side of model 2.1.5 equal to zero and solving for S, E and D, we will obtain $\mathcal{E}_0 = (0, 0, 0)$ as a trivial equilibrium of model 2.1.5. Before finding the non-trivial equilibrium of model 2.1.5, we assess the condition under which $\mathcal{E}_0$ becomes unstable, thereby removing the possibility of eliminating the tumor. To study the local stability of $\mathcal{E}_0 = (0, 0, 0)$, we just need to look at the signs of all the eigenvalues of the Jacobian of the system evaluated at $(0, 0, 0)$ given by:

$$J_{(0,0,0)} = \begin{bmatrix} \alpha_S P_{S_{max}} - \delta_S & 0 & 0 \\ A_{in}\alpha_S(1 - P_{S_{max}}) & -(\alpha_E + \delta_E) & 0 \\ 0 & 2\alpha_E & -\delta_D \end{bmatrix}.$$

The eigenvalues of matrix $J_{(0,0,0)}$ are given by:

$$\begin{aligned} \lambda_1 &= \alpha_S P_{S_{max}} - \delta_S, \\ \lambda_2 &= -(\alpha_E + \delta_E) < 0, \\ \lambda_3 &= -\delta_D < 0. \end{aligned}$$

This implies that model 2.1.5 has a trivial equilibrium $\mathcal{E}_0 = (0, 0, 0)$ that is unstable if $\alpha_S P_{S_{max}} - \delta_S > 0$ and is stable if $\alpha_S P_{S_{max}} - \delta_S < 0$.

Now, assume

$$\text{Condition}(i): \quad \alpha_S P_{S_{min}} < \delta_S < \alpha_S P_{S_{max}}$$

then the zero equilibrium $\mathcal{E}_0$ becomes unstable and a new equilibrium point "may" emerge.

Continuing to assume that condition (i) satisfied, now let

$$\mathcal{E}_1 = (S^*, E^*, D^*), \tag{2.2.1}$$

be an arbitrary equilibrium of model 2.1.5, where S^*, E^* and D^* are obtained from setting the right-hand-sides of the equations in model 2.1.5 to zero. The nontrivial steady states are given by:

$$S^* = P_{N_s}\left(\frac{\alpha_S P_{S_{max}} - \delta_S}{\delta_S - \alpha_S P_{S_{min}}}\right)^{1/n} \tag{2.2.2}$$

$$E^* = \frac{(\alpha_S - \delta_S)A_{in}}{(\alpha_E + \delta_E)}\, S^* \tag{2.2.3}$$

$$D^* = \frac{2\alpha_E}{\delta_D}\, E^*. \tag{2.2.4}$$

Condition (i) guarantees positiveness of S^*. Therefore, S^* and consequently E^* and D^* exist and are positive whenever condition (i) holds and:

$$\text{Condition } (ii): \quad \alpha_S > \delta_S$$

To find a relation between the existence of the trivial and non-trivial equilibria let us first define the ***effective reproduction rate*** ($\mathcal{R}_e$) as the ratio of the "effective stem cell self-renewal" ($\alpha_S P_{S_{max}} - \alpha_S P_{S_{min}}$) over the "effective stem cell death" (i.e., $\delta_S - P_{S_{min}}\alpha_S$).

$$\mathcal{R}_e = \frac{\text{effective stem cell self-renewal}}{\text{effective stem cell death}} = \frac{\alpha_S P_{S_{max}} - \alpha_S P_{S_{min}}}{\delta_S - P_{S_{min}}\alpha_S} = \frac{\alpha_S(P_{S_{max}} - P_{S_{min}})}{\delta_S - P_{S_{min}}\alpha_S}$$

Remark 1: According to Condition (i), $\mathcal{R}_e > 0$.

Remark 2: It is assumed that the effective stem cell death happens whenever $P_S(S) = P_{S_{min}}$.

Now, expanding and simplifying factors in the equation of $\mathcal{R}_e$, we obtain:

$$\mathcal{R}_e = \frac{\alpha_S P_{S_{max}} - \delta_S}{\delta_S - \alpha_S P_{S_{min}}} + 1$$

Thus, equilibrium point $\mathcal{E}_1 = (S^*, E^*, D^*)$ given by Eqns. (2.2.2), (2.2.3) and (2.2.4) can be re-written as

$$S^* = P_{N_s}(\mathcal{R}_e - 1)^{1/n} \tag{2.2.5}$$

$$E^* = \frac{(\alpha_S - \delta_S)A_{in}}{(\alpha_E + \delta_E)}\, S^* \tag{2.2.6}$$

$$D^* = \frac{2\alpha_E}{\delta_D}\, E^* \tag{2.2.7}$$

It is worth mentioning that second inequality in Condition (i) results in $\delta_S < \alpha_S$ since $P_{S_{max}} \leq 1$. Furthermore, Condition (i) is equivalent to $\mathcal{R}_e > 1$. Thus, Condition (i) along with the definitions of S^*, E^*, D^* and $\mathcal{R}_e$ lead us to the following proposition.

Proposition 2.2.3 *Model 2.1.5 has a non-negative non-trivial equilibrium whenever condition (i) holds. In other words, model 2.1.5 has a non-trivial equilibrium whenever $\mathcal{R}_e$ exceeds unity, $\mathcal{R}_e > 1$.*

From the biological point of view, Proposition 2.2.3 says that the model 2.1.5 has a non-negative equilibrium point exists whenever the "effective self-renewal rate of stem cells" is greater than "effective death rate of stem cells" and this is just as would be expected.

2.2.4 Local stability of equilibria

Proposition 2.2.4 *The trivial equilibrium point $\mathcal{E}_0 = (0, 0, 0)$ is stable whenever $\alpha_S P_{S_{max}} < \delta_S$. Otherwise, it is unstable.*

Remark: Instability condition of $\mathcal{E}_0 = (0, 0, 0)$ is in agreement with the necessary condition for existence of non-zero equilibrium of model 2.1.5.

At the trivial equilibrium point $(0, 0, 0)$, substituting $S = 0$ into the definition of $P_S(S)$ gives $P_S(0) = P_{S_{max}}$. As a result $\alpha_S P_{S_{max}}$ is the maximum rate of stem cell self-renewal. Thus, Proposition 2.2.4 says that once the maximum rate of CSC self-renewal becomes greater than their death rate, then the trivial equilibrium point $(0, 0, 0)$ loses stability and completely eradicating the tumor is no longer possible. Therefore, when $(0, 0, 0)$ is unstable, small perturbations in the reproduction or death rates can lead to the persistence of a tumor. This result is biologically reasonable since as the reproduction rate is greater than the death rate, the tumor tends to grow rather than die out.

Now assume that conditions (i) and (ii) are satisfied, which makes $(0, 0, 0)$ unstable and (as we showed above) a new equilibrium, $\mathcal{E}_1$, emerges. To study the stability of this nontrivial equilibrium, we will look at the eigenvalues of the

Jacobian of model 2.1.5 evaluated at $\mathcal{E}_1$, which is given by:

$$J_{\mathcal{E}_1}(S^*, E^*, D^*) = \begin{bmatrix} B_1 & 0 & 0 \\ B_2 & -(\alpha_E + \delta_E) & 0 \\ 0 & 2\alpha_E & -\delta_D \end{bmatrix}.$$

$$\begin{aligned} B_1 &= \frac{\alpha_S(P_{S_{max}} - P_{S_{min}})P_{N_s}^n}{P_{N_s}^n + (S^*)^n}\left(1 - \frac{n(S^*)^n}{P_{N_s}^n + (S^*)^n}\right) + \alpha_S P_{S_{min}} - \delta_S \\ B_2 &= \frac{A_{in}\,\alpha_S(P_{S_{max}} - P_{S_{min}})P_{N_s}^n}{P_{N_s}^n + (S^*)^n}\left(\frac{n(S^*)^n}{P_{N_s}^n + (S^*)^n} - 1\right) + A_{in}\alpha_S(1 - P_{S_{min}}) \end{aligned}$$

Using the fact that at non-trivial equilibrium $P_S(S^*) = \frac{\delta_S}{\alpha_S}$, B_1 can be reduced such that:

$$J_{\mathcal{E}_1}(S^*, E^*, D^*) = \begin{bmatrix} \frac{\alpha_S(P_{S_{max}} - P_{S_{min}})P_{N_s}^n}{P_{N_s}^n + (S^*)^n}\left[-\frac{n(S^*)^n}{P_{N_s}^n + (S^*)^n}\right] & 0 & 0 \\ B_2 & -(\alpha_E + \delta_E) & 0 \\ 0 & 2\alpha_E & -\delta_D \end{bmatrix},$$

with the following eigenvalues:

$$\begin{aligned} \gamma_1 &= \frac{\alpha_S \overbrace{(P_{S_{max}} - P_{S_{min}})}^{positive} P_{N_s}^n}{P_{N_s}^n + (S^*)^n}\overbrace{\left(-\frac{n(S^*)^n}{P_{N_s}^n + (S^*)^n}\right)}^{negative} + \overbrace{\alpha_S P_{S_{min}} - \delta_S}^{negative\ by\ Condition(i)} \\ \gamma_2 &= -(\alpha_E + \delta_E) < 0 \\ \gamma_3 &= -\delta_D < 0 \end{aligned}$$

Therefore, since all the eigenvalues are negative, we can conclude that the positive non-trivial equilibrium, $\mathcal{E}_1$ is always locally stable which leads to the following

proposition.

Proposition 2.2.5 *The positive non-trivial equilibrium of model 2.1.5 is always locally asymptotically stable.*

From the biological point of view, Proposition 2.2.5 suggests that as long as the death rate of CSCs is bounded by Condition (i) ($\alpha_S P_{S_{min}} < \delta_S < \alpha_S P_{S_{max}}$), the tumor persists to grow and reaches to an equilibrium level, $\mathcal{E}_1$. Interestingly, violating Condition (i) leads to exponential growth of tumor. Assume that

$$\delta_S < \alpha_S P_{S_{min}} \tag{2.2.8}$$

then we have

$$\frac{dS}{dt} = \alpha_S \frac{(P_{S_{max}} - P_{S_{min}}) P_{N_S}^n}{P_{N_S}^n + S^n}\, S + \overbrace{(\alpha_S P_{S_{min}} - \delta_S)}^{\text{Positive}} S > 0.$$

Therefore, S grows exponentially whenever $\delta_S < \alpha_S P_{S_{min}}$. Furthermore, for a chosen set of parameter values (explained in Section 2.4), Figure 2.3 numerically illustrates that various death rates of CSCs can results in different tumor growth dynamics. The blue line shows the tumor volume over days when Condition (i) satisfies. We keep all the parameter values fixed except δ_S. Decreasing δ_S to a value less than $\alpha_S P_{S_{min}}$ leads to an unbounded (exponential) growth of tumor (orange line).

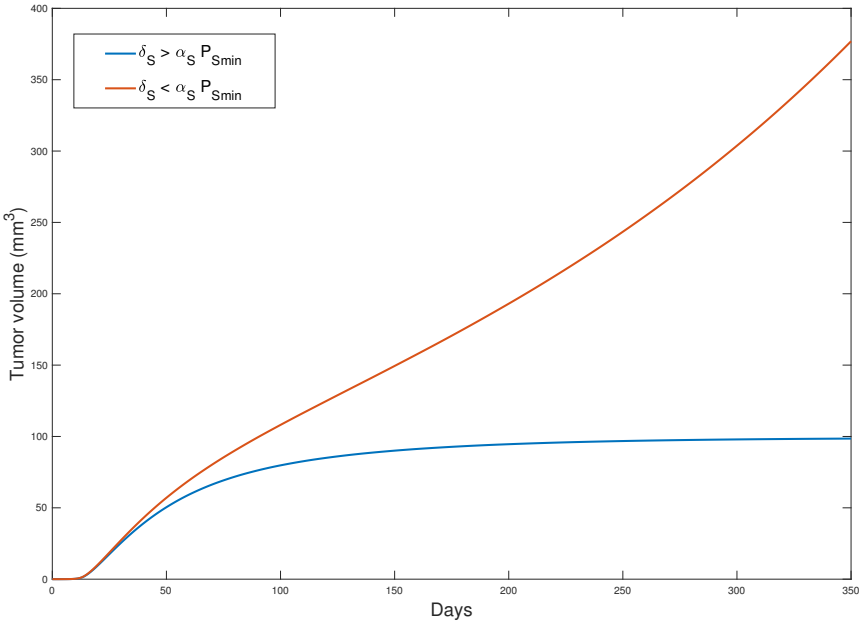

Figure 2.3: Bounded vs Exponential Growth of Tumor Volume. The blue line numerically illustrates the bounded growth of tumor volume when $\delta_S < \alpha_S P_{S_{min}}$. The orange line numerically shows that when $\delta_S > \alpha_S P_{S_{min}}$, the tumor volume growth exponentially.

2.3 Characterizing Tumor Composition

Most tumors are a heterogenous mixture of cells with some degree of differentiation. One of the conjectures of the cancer stem cell hypothesis is that a small population of CSC gives rise to the bulk of the tumor cells with more differentiated phenotypes. However is not at completely clear that CSCs are necessarily a small minority within a tumor Johnston *et al.* (2010). In fact, recent studies have raised the possibility that various types of tumors may contain widely different proportions of CSCs Johnston *et al.* (2010). In this section we explore tumor composition, in terms of CSC proportion, at steady state and during the tumor's exponential growth phase. We further provide an explanation for the variation in the observed CSC percentage.

2.3.1 Cancer stem cell fraction at the steady state

In order to find the proportion of cancer stem cells at the steady state, we use Eqns. 2.2.5-2.2.7 and define:

$$T = \frac{S^*}{S^* + E^* + D^*} = \frac{1}{1 + \frac{(\alpha_S - \delta_S)A_{in}}{\alpha_E + \delta_E} + \frac{2\alpha_E(\alpha_S - \delta_S)A_{in}}{\delta_D(\alpha_E + \delta_E)}}. \tag{2.3.1}$$

Recall that at steady state, according to Condition (ii), $\alpha_S > \delta_S$. That is, T is always a positive value. Now let

$$M = \frac{(\alpha_S - \delta_S)A_{in}}{\alpha_E + \delta_E} + \frac{2\alpha_E(\alpha_S - \delta_S)A_{in}}{\delta_D(\alpha_E + \delta_E)},$$

then T can be re-written as:

$$T = \frac{1}{1 + M}.$$

Depending on the parameter values, T, the fraction of CSCs at the steady state, can be either very small and close to zero or this fraction could also be close to one. For example, the values of α_S being nearly the same as δ_S (but larger) leads to high CSC fraction, while large values of Ain or small values of δ_D leads to low CSC fraction. That is, when the CSC division rate is very close to the CSC death rate, then there is a high probability that tumor dies out because PCs do not have a chance to populate (Eq. 2.2.3). Furthermore, high values of A_{in} implies that each progenitor or transient amplifying cell undergoes a large number of rounds of amplification before differentiating into a terminally differentiated cell which results in a fast (slow) growth rate of PCs (CSCs).

Partial derivatives of M with respect to the parameters $(\alpha_S - \delta_S)$ and A_{in} reveal that any increase in α_S and A_{in} decreases the fraction of CSCs at steady state:

$$\begin{aligned} \frac{\partial M}{\partial(\alpha_S - \delta_S)} &= A_{in}\left[\frac{\delta_D + 2\alpha_E}{\delta_D(\alpha_E + \delta_E)}\right] \\ \frac{\partial M}{\partial A_{in}} &= (\alpha_S - \delta_S)\left[\frac{\delta_D + 2\alpha_E}{\delta_D(\alpha_E + \delta_E)}\right] \end{aligned}$$

Moreover, partial derivatives of M with respect to α_E (not shown) shows that depending on the value of $\Delta = \delta_D - 2\alpha_E$, T can be either negatively or positively correlated to α_E. That is, the balance between the number of TA cell divisions and the rate of division of CSCs influences the percentage of CSCs at the steady state. Moreover, the balance between the rate of differentiation of progenitor cells and the death rate of differentiated cells not only can impact the proportion of progenitor cells but also can influence the proportion of CSCs at the steady state. In the next section we will numerically illustrate the correlation between CSCs proportion and the aforementioned parameter values.

2.3.2 Asymptotic behavior of CSCs

As discussed earlier, moving from bounded to exponential growth requires increases in the division rate of CSCs, α_S, and/or decreases in the death rate of CSCs, δ_S, such that:

$$\delta_S < \alpha_S P_{S_{min}}. \tag{2.3.2}$$

Note that the inequality (2.3.2) contradicts Condition (i) and consequently there is no longer a steady state and solutions of model 2.1.5 will grow exponentially.
Exploring the long-term asymptotic behavior of components of model 2.1.5 en-

ables us to obtain an estimate of the proportion of the cancer stem cells in the tumor as time approaches infinity. In this case, we have:

$$\lim_{t\to\infty} P_S(S(t)) \approx P_{S_{min}}.$$

Thus for long times, the model 2.1.5 can be approximated by following system of linear ordinary differential equations:

$$\begin{aligned}
\frac{dS}{dt} &\approx (\alpha_S P_{S_{min}} - \delta_S)S \\
\frac{dE}{dt} &\approx A_{in}\ \alpha_S(1 - P_{S_{min}})S - \alpha_E E - \delta_E E \\
\frac{dD}{dt} &\approx 2\ \alpha_E E - \delta_D D
\end{aligned}$$

These equations can be explicitly solved and the solutions are given by:

$$\begin{aligned}
S_a(t) &= C_0\ e^{\beta t} \\
E_a(t) &= \frac{A_{in}\alpha_S(1 - P_{S_{min}})}{\beta + \alpha_E + \delta_E} C_0\ e^{\beta t} + C_1\ e^{-(\alpha_E + \delta_E)t} \\
D_a(t) &= \frac{2\ \alpha_E A_{in}\ \alpha_S(1 - P_{S_{min}})}{(\beta + \delta_D)(\beta + \alpha_E + \delta_E)} C_0\ e^{\beta t} + \frac{2\alpha_E}{\delta_D - (\alpha_E + \delta_E)} C_1 e^{-(\alpha_E + \delta_E)t} + C_2\ e^{-\delta_D t}
\end{aligned}$$

where, $\beta = \alpha_S P_{S_{min}} - \delta_S$ is the net growth rate of cancer stem cells and C_0, C_1 and C_2 are arbitrary constants which satisfy in the initial condition of the system. However, since we assumed that $t \to \infty$, the above solutions can be reduced to:

$$S_a(t) = C_0\ e^{\beta t}$$

$$E_a(t) = \frac{A_{in}\alpha_S(1 - P_{S_{min}})}{\beta + \alpha_E + \delta_E} C_0\, e^{\beta t}$$

$$D_a(t) = \frac{2\,\alpha_E A_{in}\,\alpha_S(1 - P_{S_{min}})}{(\beta + \delta_D)(\beta + \alpha_E + \delta_E)} C_0\, e^{\beta t}$$

Now we can use the approximations above to estimate the proportion of cancer stem cells in the tumor during the long-term, exponential growth phase.

$$\begin{aligned} T_\infty &= \lim_{t\to\infty} \frac{S(t)}{S(t) + E(t) + D(t)} \\ &\approx \frac{S_a(t)}{S_a(t) + E_a(t) + D_a(t)} \\ &= \frac{C_0\, e^{\beta t}}{C_0\, e^{\beta t} + \frac{A_{in}\alpha_S(1-P_{S_{min}})}{\beta+\alpha_E+\delta_E} C_0\, e^{\beta t} + \frac{2\,\alpha_E A_{in}\,\alpha_S(1-P_{S_{min}})}{(\beta+\delta_D)(\beta+\alpha_E+\delta_E)} C_0\, e^{\beta t}} \\ &= \frac{1}{1 + \frac{A_{in}\alpha_S(1-P_{S_{min}})}{\beta+\alpha_E+\delta_E} + \frac{2\,\alpha_E A_{in}\,\alpha_S(1-P_{S_{min}})}{(\beta+\delta_D)(\beta+\alpha_E+\delta_E)}} \end{aligned}$$

Now, let

$$F = \frac{A_{in}\alpha_S(1 - P_{S_{min}})}{\beta + \alpha_E + \delta_E} + \frac{2\,\alpha_E A_{in}\,\alpha_S(1 - P_{S_{min}})}{(\beta + \delta_D)(\beta + \alpha_E + \delta_E)}. \tag{2.3.3}$$

Then, T_∞ can be rewritten as

$$\frac{S_a(t)}{S_a(t) + E_a(t) + D_a(t)} = \frac{1}{1+F}. \tag{2.3.4}$$

Partial derivatives of F suggest that, the proportion of CSCs during the exponential growth phase, T_∞, is highly correlated to the values of α_S and A_{in}. This result suggests that decreasing the proliferation rate of CSCs and/or reducing the number of TA divisions for progenitor cells can effectively decrease the final proportion of the CSCs within a tumor.

2.4 Numerical Simulations

In this section, we first introduce a representative set of parameter values and numerically simulate tumor growth over time for various growth scenarios. In addition, we illustrate how the proposed parameters relationships derived in Section 2.3 influence the proportion of the CSCs in the tumor.

2.4.1 Parameter values

Input parameters necessary to characterize the dynamics of the CSC, progenitor and differentiated cell pools include the cell division and death rates as well as the probability of stem and progenitor cell self-renewal. The proportion of cancer stem cells (CSCs) within a tumor varies widely among cancer types and cell lines Liu *et al.* (2013). CSCs make up only a fraction of 1% of the proliferating cells in the bone marrow and approximately $1-10\%$ of the proliferating cells in epithelial cancers. Parameter values for cancer stem cells (including symmetric/asymmetric division rates) also vary widely across tumor types. In Gao *et al.* (2013) the cell-cycle length is approximated around $T_c = 25$ hours which is in agreement with

the result given in Driessens *et al.* (2012) in which T_c is estimated to be varying between one and two days. Therefore, for our numerical simulations we use $\alpha_E = ln2/1.04$ and $\alpha_S \in [ln2/1.04/2\ ,\ ln2/1.04]$. The death rate of differentiated cancer cells, δ_D, has varied widely in a window between 0.01 per day to 15-18 per week in previous studies Gentry and Jackson (2013); Molina-Peña and Álvarez (2012); Rodriguez-Brenes *et al.* (2015); Weekes *et al.* (2014). Finally, under this assumed hierarchical structure, CSCs live longer than both progenitor and differentiated caner cells Clarke and Fuller (2006), so the maximum death rate of progenitor and differentiated cells (δ_E, δ_D) is chosen to be larger than the death rate of CSCs, δ_S. A representative set of baseline parameter values is provided in Table 2.2.

Table 2.2: Baseline Parameter Values For the Amplification Model

Parameters	**Baseline Values**	**Units**	**Reference**
A_{out}	2	dimensionless	Ganguly and Puri (2006)
α_S	0.6	$\frac{1}{day}$	Driessens *et al.* (2012)
			Gao *et al.* (2013)
α_E	$\frac{log(2)}{1.04}$	$\frac{1}{day}$	Driessens *et al.* (2012)
			Gao *et al.* (2013)
$P^*_{S_{min}}$	0.014	dimensionless	Weekes *et al.* (2014)
$P_{S_{max}}$	0.90	dimensionless	Weekes *et al.* (2014)
A_{in}	2–20	dimensionless	
δ_S	$1.5\ \alpha_S P^*_{S_{min}}$	$\frac{1}{day}$	
δ_D	0.0612	$\frac{1}{day}$	Molina-Peña and Álvarez (2012)
δ_E	0.2	$\frac{1}{day}$	
P_{Ns}	800000	dimensionless	
n	3	dimensionless	

2.4.2 Simulations

The model 2.1.5 is simulated using the parameter values given in Table 2.2 (unless otherwise stated). To initiate tumor growth, we begin with one thousand CSCs, which corresponds to (S(0)=1000, E(0)=0, D(0)=0) being used as the initial condition for our simulations. Figure 2.4 depicts tumor volume over time for various values of the number of TA divisions, A_{in}, and the division rate of CSCs, α_S. It is evident from Figure 2.4 that both A_{in} and α_S can considerably impact the rate of tumor growth and the percentage of CSCs.

Numerical simulations suggest that higher values of both of the number of TA division, A_{in}, and the division rate of CSCs increase the rate of tumor growth. Figures 2.4-A and 2.4-C show the tumor volume dynamic over time for various values of A_{in} and α_S. In contrast, as depicted in Figures 2.4-B and 2.4-D (dashed lines), the higher values of A_{in} and α_S result in the smaller percentage of CSCs at the equilibrium level. For instance, increasing A_{in} from 2 to 20 causes approximately 88% reduction in the percentage of CSCs at day 100. Interestingly, the changes in the percentage of CSCs also change the percentage of PCs (Figures 2.4-B and 2.4-D) All together, these results suggest that depending on the parameter values tumor composition, specifically the percentage of CSC%, can be different in various tumors. This is fairly reasonable, since the probability of CSC self-renewal and death can be influenced by microenvironmental factors, which can vary among different tumor types.

To emphasize the above results further, Figure 2.5 depicts the dependence of the fraction of CSCs at steady state on some of the key parameters of the model. The percentage of CSCs is negatively correlated to the increasing values of the division rates of CSCs, α_S, and also A_{in}, whereas it is positively correlated to the death rate

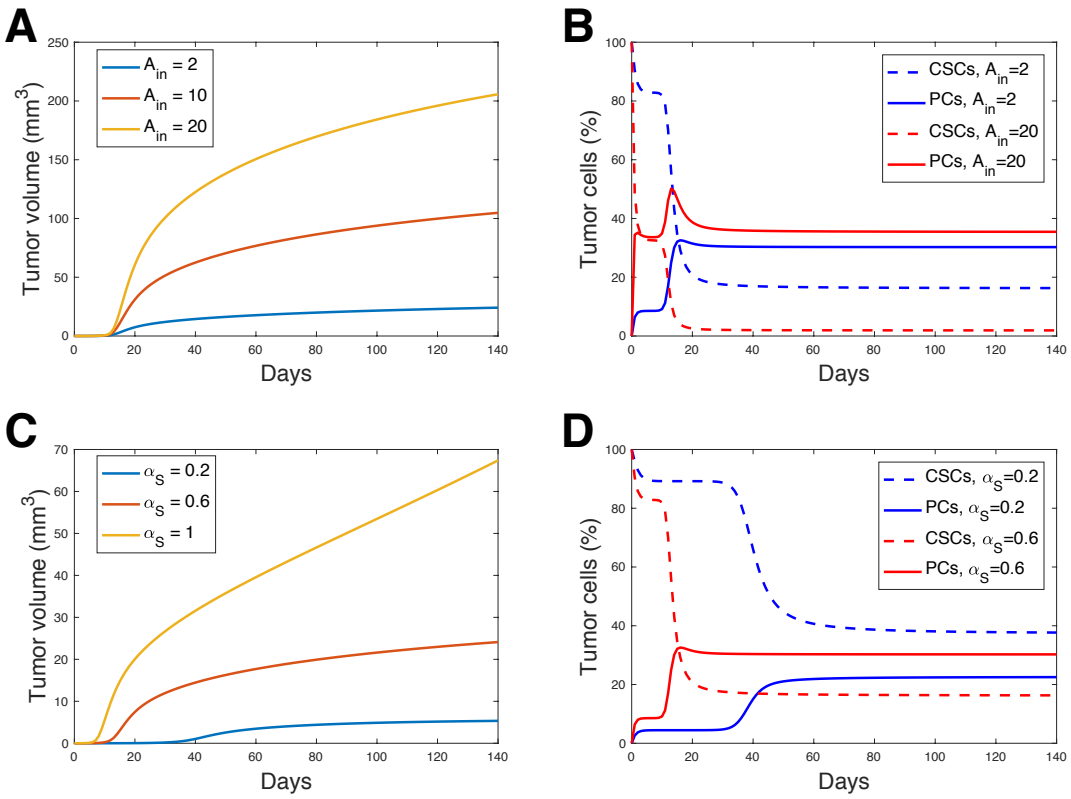

Figure 2.4: Simulations of the model 2.1.5, showing (A) the tumor volume for $A_{in} = 2, 10$ and 20, (B) the percentage of CSCs (dashed lines) and PCs (solid lines) for $A_{in} = 2$ and 20, (C) the tumor volume for $\alpha = 0.2, 0.6$ and 1, (D) the percentage of CSCs (dashed lines) and PCs (solid lines) for $\alpha_S = 0.2$ and 0.6.

of CSCs. That is, any increase in α_S or A_{in} (δ_S) results in a decrease (an increase) in the final percentage of CSCs (Figures 2.5-A, B and C). Moreover, Figure 2.5-A suggests that a 10-fold increase in the division rate of CSCS, α_S leads to a 15 percent difference in CSC percentage. However, Figure 2.5-B suggests that perturbations in the baseline value of the death rate of CSCs, δ_S, have only moderate impact on the CSC percentage when compared to changes in the CSC division rate. It shows that a 5-fold change in the death rate of CSCs leads to a 0.02 difference in the percentage of CSCs. In addition, Figure 2.5-D numerically illustrates that

depending on the value of $\Delta = \delta_D - 2\alpha_E$, the percentage of CSCs can be either negatively or positively correlated to the division rate of PCS, α_E.

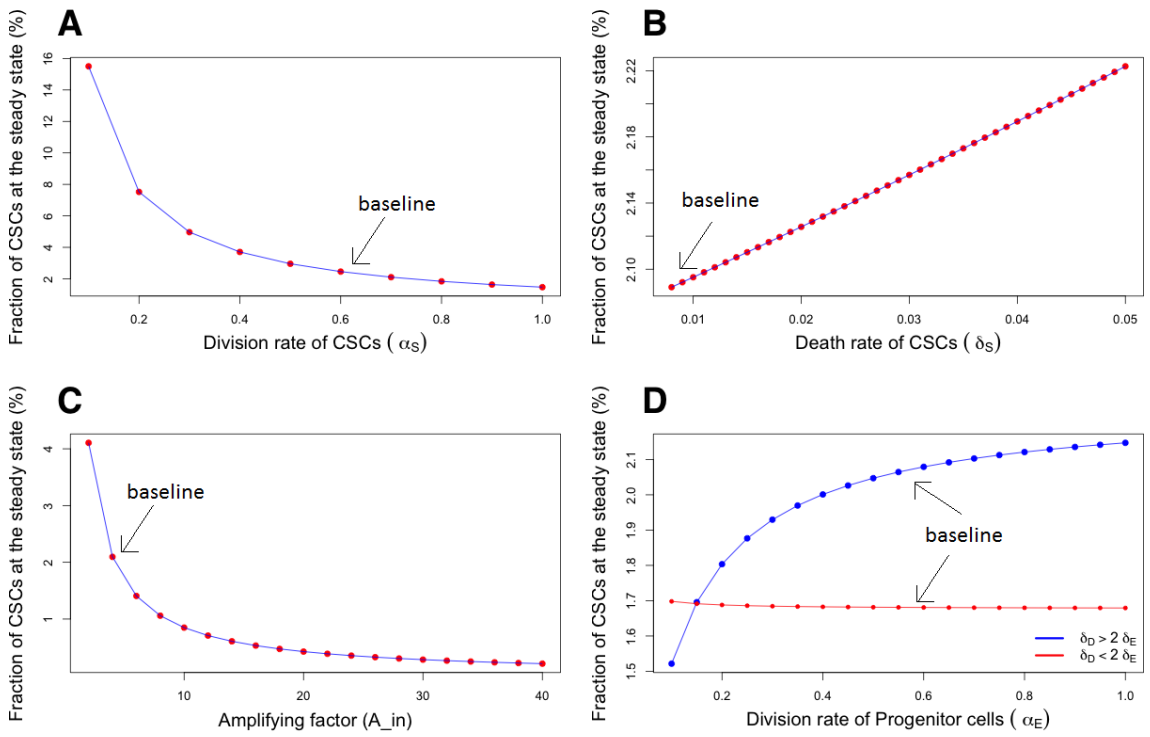

Figure 2.5: Fraction of Stem Cells Within the Tumor; it is shown that at the steady state how the fraction of cancer stem cells depends on the parameter values of the model.

2.5 Summary and Discussion

The discovery of the tumor-initiating cells, so called cancer stem cells (CSCs), that share many features of normal stem cells led to the new hypotheses explaining the origins and progression of cancerous tumors. Among those, CSC hypothesis suggests that malignant growth is driven by a small subpopulation of CSCs Wicha *et al.* (2006) and that those cells are responsible for tumor growth, resistance, and recurrence. In addition, the bulk tumor consists of cells lacking stemness (non-CSC)

which are not able to not capable of initiating and sustaining, and re-initiating tumor growth, regardless of their differentiation status or proliferative capacity Enderling *et al.* (2013). These cells are generated from CSCs through their differentiation. While numerous studies support that CSCs are a rare population within a tumor, there are newly emerging evidence suggesting a large variation in CSC fractions within and among tumors Enderling *et al.* (2013); Reya *et al.* (2001). Cancer stem cells have now been identified in tumors of the breast, brain, head and neck, and blood, among others Al-Hajj *et al.* (2003); Gentry and Jackson (2013); Krishnamurthy *et al.* (2014); Singh *et al.* (2003). Emerging evidence suggests that CSCs exhibit resistance to chemotherapy and radiotherapy and are involved in the establishment of metastasis Krishnamurthy *et al.* (2014); Molina-Peña and Álvarez (2012). Taken together, all these findings suggest that curative therapy will require the complete ablation of CSCs.

Due to the difficulty of isolating and studying stem cells experimentally, mathematical modeling can provide further insight into the fundamental issues underlying CSC biology and can shed light on the potential of stem cell targeted treatments. Several mathematical and computational models has been developed to investigate the growth dynamics involved during tumorigenesis in hierarchical tissue and have increasingly been applied to the biological system that arises from CSC/non-CSC dynamics Kapitanov (2012); Michor *et al.* (2005); Sottoriva *et al.* (2010); Tomasetti and Levy (2010); Turner *et al.* (2009); Youssefpour *et al.* (2012) (also see Weekes *et al.* (2014) for a review). Ganguly et al. (2006) developed a mathematical based on a cell compartments method to pose and validate nonintuitive scenarios arising from the cancer stem cell hypothesis. This model describes formation of CSCs/PCs from normal stem/progenitor cells. They showed that CSC

and PC populations reach a steady population and maintain a constant mature cell population. The model is compartmentalized into norma/abnorma stem cells, early and late progenitor and differentiated cells and it assumed that the oncogenic mutations in normal stem and/or progenitor cells produces the cancerous stem/progenitor cells. It is also assumed that each late progenitor cells undergoes a limited number of cell division stages (ω) and once divides enters to a new progeny compartment with a less capacity of cell division. They showed that mutations in stem cells lead to faster growth of the abnormal progeny when compared to mutations in progenitor cells. Following the modeling technique in Ganguly and Puri (2006) and also Gentry and Jackson (2013), we designed a simple mathematical model based on the CSC hypothesis to study cancer stem cell-driven tumor growth and to evaluate its ability to estimate the stem cell proportion in a tumor at steady state and during exponential growth. However, in our model we just track the tumor cell population and instead of adding ω number of sub-compartment of progenitor cells, it is assumed that each stem cell is amplified on upon entry into the progenitor cell pool, whereas there is no amplification upon exit to the terminally differentiated cell pool. A thorough mathematical analysis of the model 2.1.5 was carried out and the condition required for tumor initiation, bounded progression and/or exponential growth was introduced. Numerical simulations further illustrated the impact of the various parameters on the tumor growth dynamics and the fraction of CSCs in the tumor.

Depending of the balance between the division rate of CSCs, α_S, and the death rate of CSCs, δ_S, the qualitative behavior of the model (tumor) changes. For the values of α_S and δ_S which satisfy in $\alpha_S P_{S_{min}} < \delta_S < \alpha_S P_{S_{max}}$, tumor growth is bounded and reaches to a steady population whereas $\delta_S < \alpha_S P_{S_{min}}$ causes an ex-

ponential growth of CSCs which can results in unbounded exponential growth of tumor. In addition, numerical simulations suggested that the tumor growth rate is extremely sensitive to the small changes in the parameter values involved in the CSC self-renewal probability (n and P_{N_S}) and also the amplifying factor A_{in}. Both n and P_{N_S} can be regulated by the tumor microenvironmental factors suggesting that the tumor mircoenvironment can induce pathways that provide better conditions for cell division and survival such as recruiting additional microvessels into stem cell niche, which provides additional sources of nutrition and oxygen for tumor cells to grow and survive. Furthermore, there are other studies that emphasizes the potential influences of the A_{in}. Sottoriva et al. (2010) and Enderling et al. (2013) used an agent-based model and cellular automaton approaches and shown that in addition to cancer stem cell self-renewal the number of amplifications of progenitor cells is one of the most pivotal modulators of overall tumor dynamics.

Considering the important role of CSCs in tumor initiation, progression and in developing targeted therapies, one of the central objectives of this chapter is to predict the fraction of CSCs in various stages of tumor growth. Interestingly, a growing line of biological evidence suggests that depending on the tissue of origin, cancer type, individual physiology, the fraction of CSCs can vary from a very small proportion (close to zero) to almost the whole proportion of the tumor (close to one). Therefore, we used our model 2.1.5 to not only estimate the fraction of cancer stem cells, but also to find possible explanations for the wide variation in percentages of CSCs that has been reported Enderling *et al.* (2013); Reya *et al.* (2001). Our results suggest that the fraction of CSCs depends on the balance between the influx rate of stem cells into the progenitor compartment, $(\alpha_S - \delta_S)A_{in}$, and the efflux rate of progenitor cells into the terminally differentiated caner cells

compartment, $\alpha_E + \delta_E$. It further depends on the balance between the division rate of the progenitor cells, α_E and the death rate of differentiated cancer cells, δ_D. Moreover, the model predictions suggested that the fraction of cancer stem cells is significantly influenced by relatively small changes in the value of amplification factor A_{in}. Recall that $A_{in} \times 2 = 2^w$, where w is "the number of successive stages of cell division before transforming into differentiated mature cell". So, higher value of A_{in} could result in a higher fraction of non-CSCs and a lower fraction of CSCs. In fact, amplification factor may vary in response to tumor niche signaling. To support our claim, for instance, in Foley and Mackey (2009) it is assumed that the amplification factor, $A(G)$, depends on Granulocyte-colony stimulating factor (G-CSF), which they modeled as $A(G) = (A_{max} - A_{min})\frac{G(t)}{G(t)+b_A} + A_{min}$. G(t) is the concentration of G-CSF at time, A_{max}, A_{min} are the maximum and minimum of amplification factors, respectively, and b_A controls the steepness of the function. The functional form of $A(G)$ suggests that the amplification factor is low whenever there is no G-CSF-induced signal, but when there is plentiful signal. the amplification factor is high. So, in line with these assumptions in Foley and Mackey (2009), our numerical simulations suggest that under the influences of the tumor micro-environmental factors, CSC fraction can almost get any value between 0 and 1.

This is well documented that CSCs reside in perivascular niches and depend on crosstalk with tumor-associated endothelial cells for their survival and maintenance of an undifferentiated state Krishnamurthy *et al.* (2014). These discoveries suggest the essence of developing the new therapeutic methods that targets that blocks signaling pathways initiated by endothelial cells and that contribute to CSC survival and self-renewal. However, the mechanisms involving the crosstalk between endothelial cells and CSC are unknown. However, mathematical mod-

els along with experimental methods are providing strong tools to explore those mechanisms. In the next chapters we extend our model to include the impacts of some of the tumor microenvironmental factors, endothelial cells and investigate the significant role of the cross-talk between endothelial and tumor cells. The extended models also are used to study the responses of tumor cells to both targeted-therapy alone or in combination with chemotherapy.

Chapter 3

A MATHEMATICAL MODEL FOR IL-6-MEDIATED, STEM CELL DRIVEN TUMOR GROWTH AND TARGETED TREATMENT

In this chapter, we develop a preliminary mathematical model for cancer stem cell-driven tumor growth that includes the molecular level details of tumor cell-secreted IL-6 signaling. Our immediate goal is to gain insight into the impact of IL-6 on tumor growth and CSC self-renewal. The platform we model is the *in vivo* growth of human tumor xengrafts that originate from a small population of CSCs in a mouse model system. Krishnamurthy et al. Krishnamurthy *et al.* (2014) transplanted primary human CSCs into IL-6+/+ immunodeficient/athymic mice and recorded the volume of generated tumors at 24 time-points over 121 days after implantation. Using IL6 +/+ mice data as our experimental baseline, we preform rigorous parameter estimation and sensitivity analysis in order to fully calibrate our model. Furthermore, in order to quantify the influence of host (murine) stromal IL-6 on tumor growth and the survival of CSCs, they transplanted the same number of CSCs in IL-6-/- immunodeficient mice and showed that tumor xenografts generated in the IL-6+/+ mice produced a greater number of tumors that were larger in size than in the IL-6 -/- mice. In addition, they reported that the fraction of CSCs in the IL-6+/+ mice tumor xenografts was approximately 10-fold larger than in the IL-6-/- mice. Therefore, to further validate and test the predictive power of our modeling framework we use it, and the IL-6-/- mice data, to explore the effects of murine stromal IL-6 secretion on human cancer cell growth. This is the first step in our larger goal of quantifying the impact of human stromal IL-6 secretion on cancer stem cell percentage and tumor growth dynamics and assessing its

potential as a therapeutic target.

3.1 Modeling Cancer Stem Cell Driven Tumor Growth Pre-treatment

In this section we develop a mathematical model for cancer stem cell-driven tumor growth that is designed to quantify the influence of *tumor cell-secreted* IL-6 signaling on tumor growth and cellular composition. The model is then extended to include therapeutic intervention with the anti-IL-6R antibody, Tocilizumab (TCZ). This model formulation only considers IL-6 produced by the human cancer stem and non-stem (bulk) cells. It is important to note that host (murine) stromal cells are also capable of producing a form of IL-6, however, murine IL-6 does not directly bind to human IL-6R and therefore, murine IL-6 cannot directly (only indirectly) impact tumor growth. The pre-treatment model tracks the temporal evolution of three cancer cell types (stem, progenitor, and terminally differentiated) as well as IL-6 and membrane bound IL-6 receptors (IL-6R) in their free and bound forms as depicted in Figure 3.1. Although a soluble form of IL-6R (sIL-6R) exists and can bind IL-6 with a similar affinity as membrane bound IL-6R, we choose to simplify our modeling approach by not including sIl-6R because there is evidence that its role is most important during *trans* signaling when cells lack IL-6R.

Table 1 lists each model variable along with its units.

Cancer Cell Equations

The proposed model is an extension of the model developed in Chapter 1. That is, the total cellular composition of an HNSCC tumor at time t is divided into HNSCC cancer stem cells $S(t)$, HNSCC transient amplifying/progenitor tumor cells

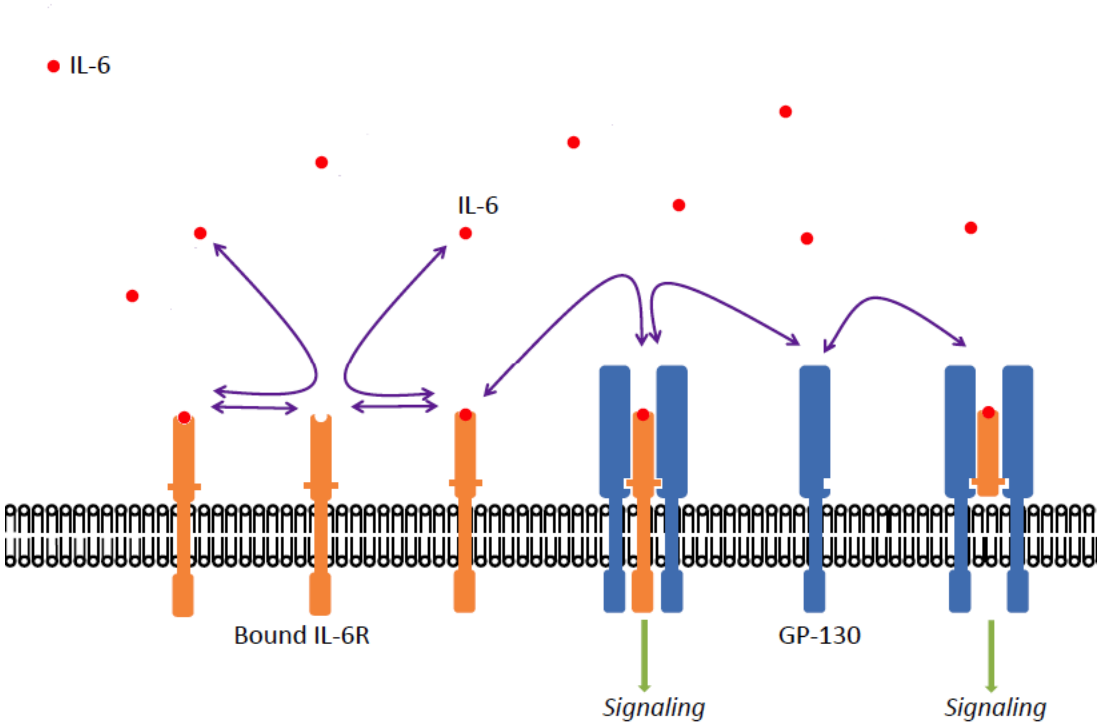

Figure 3.1: Schematic Diagram of the Molecular Processes Considered in the Mathematical Model: IL-6 Binding Dynamics.

$E(t)$ and HNSCC terminally differentiated tumor cells $D(t)$. Tumor cell secreted-IL-6, denoted by $L(t)$, binds to unoccupied (free) IL-6 receptors (IL-6R) on the surface of stem, progenitor and differentiated cells denoted by R_S, R_E, and R_D; respectively. Association of IL-6 to IL-6R results in the formation of IL-6/IL-6R complexes, which are represented by $C_S(t)$, $C_E(t)$ and $C_D(t)$, respectively, for each cell type.

The probability of cancer stem cell self-renewal

In the absence of tumor cell-secreted IL-6, the probability of CSC self-renewal, P_S, is given by

Table 3.1: List of Model Variables

Variable	Description	Units
S	HNSCC stem cells	# of cells
E	HNSCC progenitor tumor cells	# of cells
D	HNSCC differentiated tumor cells	# of cells
L	IL-6	fmol
R_S	IL-6R on stem cells	fmol
C_S	IL-6, cell bound IL-6R complex on stem cells	fmol
R_E	IL-6R on progenitor cells	fmol
C_E	IL-6, cell bound IL-6R complex on progenitor cells	fmol
R_D	IL-6R on differentiated cells	fmol
C_D	IL-6, cell bound IL-6R complex on differentiated cells	fmol

$$P_S(S) = \frac{(P_{S_{max}} - P_{S_{min}})P_{N_s}^n}{P_{N_s}^n + S^n} + P_{S_{min}}. \tag{3.1.1}$$

There is experimental evidence supporting the fact IL-6 impacts cancer stem cell self-renewal and that the proportion of CSCs increases due to the presence of IL-6 Krishnamurthy *et al.* (2014). Therefore, in the presence of tumor cell-secreted IL-6, we modify the functional form of P_S given by (3.1.1) so that it still decreases as S increases, but also increase as the fraction of bound receptors per cell $\phi_S = \frac{C_S}{R_{T_S}S}$ increases. There are many assumptions we could make for these modifications. For now we assume that $P_{S_{max}}$ remains unchanged (and constant), but $P_{S_{min}}$ increases as the amount of bound IL-6 receptors increases. This helps to ensure that IL-6 will impact stem cell fate when the tumor is large. Together, these assumptions yield:

$$
\begin{aligned}
P_S(S,\phi_S) &= \frac{(P_{S_{max}} - P_{S_{min}}(\phi_S))P_{N_s}^n}{P_{N_s}^n + S^n} + P_{S_{min}}(\phi_S), \\
P_{S_{min}}(\phi_S) &= \mu_S \left(P_{S_{max}} - P^*_{S_{min}}\right)\phi_S + P^*_{S_{min}}
\end{aligned}
\tag{3.1.2}
$$

Remark 1: The first equation in 3.1.2 ensures that even if there is no IL-6 present, the probability of self-renewal will decrease with population size. When IL-6 is present, the minimum probability for self-renewal, $P_{S_{min}}$, will increase to a fraction, μ_S, of its maximum value as the fractional occupancy of bound receptors per cell, ϕ_S, increases.

IL-6-Related Equations

Equation 3.1.3 describes the association at rate k_f and dissociation at rate k_r of IL-6 (L) to its cell-bound receptors (R_S, R_E and R_D) on stem, progenitor and differentiated cells, respectively (Figure 3.1). An underlying assumption in this equation is that the binding rates are the same, independent of cell type. IL-6 is removed via natural decay at rate λ_L and is produced by tumor cells at rate ρ.

$$
\begin{aligned}
\frac{dL}{dt} = &- \underbrace{k_f L R_S}_{\substack{\text{IL6 binding to} \\ \text{stem cells}}} + \underbrace{k_r C_S}_{\substack{\text{IL6 dissociation} \\ \text{from stem cells}}} - \underbrace{k_f L R_E}_{\substack{\text{IL6 binding to} \\ \text{progenitor cells}}} + \underbrace{k_r C_E}_{\substack{\text{IL6 dissociation} \\ \text{from progenitor cells}}} \\
&- \underbrace{k_f L R_D}_{\substack{\text{IL6 binding to} \\ \text{differentiated cells}}} + \underbrace{k_r C_D}_{\substack{\text{IL6 dissociation} \\ \text{from differentiated cells}}} - \underbrace{\lambda_L L}_{\text{IL6 natural decay}} + \underbrace{\rho(S+E+D)}_{\substack{\text{IL-6 Production} \\ \text{by tumor cells}}}
\end{aligned}
\tag{3.1.3}
$$

Equations 3.1.4, 3.1.5 and 3.1.6 describe the temporal changes in free IL-6 receptors on each of the cell types that we are considering. The first two terms in each

equation are the association and dissociation of IL-6 to IL-6R. The recycling terms describe the reactions by which IL-6 is used up in the processes of mediating its cellular response, and the free receptors are recycled back to the cell surface. Following the formulation in, the last two terms in each equation describe the production of new free receptors as new cells are generated and the loss of these receptors as cells die. Definitions of $\mathscr{P}(\cdot)$ and $\mathscr{D}(\cdot)$ are provided in the following section. We note that when IL-6 binds to IL-6R, it subsequently recruits a GP130 molecule to form a ternary complex (IL- 6/IL-6R/GP130) Hirabayashi and Lemmey (2012). However, we do not model GP130 explicitly here, instead, we indirectly account for its role in the binding parameters and recycling parameters.

$$\begin{aligned}\frac{dR_S}{dt} = &- \underbrace{k_f L R_S}_{\substack{\text{IL6 binding to}\\ \text{stem cells}}} + \underbrace{k_r C_S}_{\substack{\text{IL6 dissociation}\\ \text{from stem cells}}} + \underbrace{k_p C_S}_{\text{Recycling}} \\ &+ \underbrace{R_{T_S}\mathscr{P}_{\mathscr{S}}(S,\phi_S)}_{\substack{\text{Generation of new } R_S\\ \text{via cell proliferation}}} - \underbrace{\frac{R_S}{R_S+C_S}R_{T_S}\mathscr{D}_{\mathscr{S}}(S,\phi_S)}_{\substack{\text{Loss of } R_S\\ \text{via cell death}}}\end{aligned} \tag{3.1.4}$$

$$\begin{aligned}\frac{dR_E}{dt} = &- \underbrace{k_f L R_E}_{\substack{\text{IL6 binding to}\\ \text{progenitor cells}}} + \underbrace{k_r C_E}_{\substack{\text{IL6 dissociation}\\ \text{from progenitor cells}}} + \underbrace{k_p C_E}_{\text{Recycling}} \\ &+ \underbrace{R_{T_E}\mathscr{P}_{\mathscr{E}}(E,\phi_E)}_{\substack{\text{Generation of new } R_E\\ \text{via cell proliferation}}} - \underbrace{\frac{R_E}{R_E+C_E}R_{T_E}\mathscr{D}_{\mathscr{E}}(E,\phi_E)}_{\substack{\text{Loss of } R_E\\ \text{via cell death}}}\end{aligned} \tag{3.1.5}$$

$$\frac{dR_D}{dt} = - \underbrace{k_f L R_D}_{\substack{\text{IL6 binding to} \\ \text{differentiated cells}}} + \underbrace{k_r C_D}_{\substack{\text{IL6 dissociation} \\ \text{from differentiated cells}}} + \underbrace{k_p C_D}_{\text{Recycling}} + \underbrace{R_{T_D} \mathscr{P}_{\mathscr{D}}(D, \phi_D)}_{\substack{\text{Generation of new } R_D \\ \text{via cell proliferation}}} - \underbrace{\frac{R_D}{R_D + C_D} R_{T_D} \mathscr{D}_{\mathscr{D}}(D, \phi_D)}_{\substack{\text{Loss of } R_D \\ \text{via cell death}}} \tag{3.1.6}$$

Equations 3.1.7, 3.1.8 and 3.1.9, are analogous to the ones above as they describe changes in receptor-ligand complexes on each cell type. Similarly in these equations, the internalization term describes the reactions by which the complex is internalized and the free receptors are recycled to the cell surface. The last term in each equation describes the loss of these receptor complexes due to cell death.

$$\frac{dC_S}{dt} = \underbrace{k_f L R_S}_{\text{IL6 binding to } R_S} - \underbrace{k_r C_S}_{\substack{\text{IL6 dissociation} \\ \text{from } R_S}} - \underbrace{k_p C_S}_{\text{Internalization}} - \underbrace{\frac{C_S}{R_S + C_S} R_{T_S} \mathscr{D}_{\mathscr{S}}(S, \phi_S)}_{\substack{\text{Loss of } C_S \\ \text{via cell death}}} \tag{3.1.7}$$

$$\frac{dC_E}{dt} = \underbrace{k_f L R_E}_{\text{IL6 binding to } R_E} - \underbrace{k_r C_E}_{\substack{\text{IL6 dissociation} \\ \text{from } R_E}} - \underbrace{k_p C_E}_{\text{Internalization}} - \underbrace{\frac{C_E}{R_E + C_E} R_{T_E} \mathscr{D}_{\mathscr{E}}(E, \phi_E)}_{\substack{\text{Loss of } C_E \\ \text{via cell death}}} \tag{3.1.8}$$

$$\frac{dC_D}{dt} = \underbrace{k_f L R_D}_{\text{IL6 binding to } R_D} - \underbrace{k_r C_D}_{\substack{\text{IL6 dissociation} \\ \text{from } R_D}} - \underbrace{k_p C_D}_{\text{Internalization}} - \underbrace{\frac{C_D}{R_D + C_D} R_{T_D} \mathscr{D}_{\mathscr{D}}(D, \phi_D)}_{\substack{\text{Loss of } C_D \\ \text{via cell death}}} \tag{3.1.9}$$

Proliferation and Death Function Definitions

The functions $\mathscr{P}_{\mathscr{S}}(S,\phi_S)$, $\mathscr{P}_{\mathscr{E}}(E,\phi_E)$ and $\mathscr{P}_{\mathscr{D}}(D,\phi_D)$ are the rates at which new stem cells, progenitor and differentiated cells are generated, respectively. These relationships are taken directly from equations 2.1.1, 2.1.2 and 2.1.3 and are therefore given by:

$$\mathscr{P}_{\mathscr{S}}(S,\phi_S) = \alpha_S P_S(S,\phi_S)S \tag{3.1.10}$$

$$\mathscr{P}_{\mathscr{E}}(E,\phi_E) = A_{in}\alpha_S(1-P_S(S))S - \alpha_E E \tag{3.1.11}$$

$$\mathscr{P}_{\mathscr{D}}(D,\phi_D) = 2\alpha_E E \tag{3.1.12}$$

The second to last terms in equations 3.1.4, 3.1.5 and 3.1.6 assume that a total of R_{T_S}, R_{T_E}, and R_{T_D}, new free receptors are generated at the proliferation rates defined in equations (2.1.13) - (2.1.15); respectively.

The functions $\mathscr{D}_{\mathscr{S}}(S,\phi_S)$, $\mathscr{D}_{\mathscr{E}}(E,\phi_E)$ and $\mathscr{D}_{\mathscr{D}}(D,\phi_D)$ are the death rates of stem cells, progenitor and differentiated cells; respectively. These relationships are taken directly from equations 2.1.1, 2.1.2 and 2.1.3 and are therefore given by:

$$\mathscr{D}_{\mathscr{S}}(S,\phi_S) = \frac{\delta_S}{1+\gamma_1\phi_S}S \tag{3.1.13}$$

$$\mathscr{D}_{\mathscr{E}}(E,\phi_E) = \frac{\delta_E}{1+\gamma_E\phi_E}E \tag{3.1.14}$$

$$\mathscr{D}_{\mathscr{D}}(D,\phi_D) = \frac{\delta_D}{1+\gamma_D\phi_D}D \tag{3.1.15}$$

The last terms in equations 3.1.4 - 3.1.6 and in equations 3.1.7 - 3.1.9 assume that the fraction of the total number of receptors that are either free or bound, respec-

tively, are removed at the death rates defined in equations (2.1.16) - (2.1.18).

Notes on the Model Formulation

This formulation assumes that the total number (converted to fmol using molecular weight) of receptors per cell (R_{T_S}, R_{T_E} and R_{T_D}) remains constant. This means that the total amount of IL-6R in the system should be conserved. In other words: Total IL-6R in the system that is associated with stem cells = IL-6R/cell $\times$ the number of stem cells. In terms of our variables, for stem cells this equations reduces to R_S(unoccupied IL-6R) + C_S(occupied IL-6R) $= R_{T_S} \times S$. We can ensure that the model equations do in fact conserve IL-6R by considering the sum

$$\frac{dR_S}{dt} + \frac{dC_S}{dt} = R_{T_S}\left(\mathscr{P}_{\mathscr{S}}(S, \phi_S) - \mathscr{D}_{\mathscr{S}}(S, \phi_S)\right) = R_{T_S}\frac{dS}{dt}$$

Therefore, upon integration, we have

$$R_S + C_S = R_{T_S} S. \tag{3.1.16}$$

Similarly, for progenitor and differentiated cells we have

$$R_E + C_E = R_{T_E} E, \tag{3.1.17}$$

$$R_D + C_D = R_{T_D} D. \tag{3.1.18}$$

Using Eqs. (3.1.16-3.1.18) we have, $R_S = R_{T_S}S - C_S$, $R_E = R_{T_E}E - C_E$ and $R_D = R_{T_D}D - C_D$, so we can remove three equations $\frac{dR_S}{dt}$, $\frac{dR_E}{dt}$ and $\frac{dR_D}{dt}$ from the model and replace R_S, R_E and R_D by $R_{T_S}S - C_S$, $R_{T_E}E - C_E$ and $R_{T_D}D - C_D$, respectively. These changes result in following model system with a reduced number of equations:

Model (1): IL-6 Model with Amplification Factor

$$
\begin{aligned}
\frac{dS}{dt} &= \alpha_S P_S(S,\phi_S)S - \frac{\delta_S}{1+\gamma_S\phi_S}S \\
\frac{dE}{dt} &= A_{in}\alpha_S(1-P_S(S,\phi_S))S - \alpha_E E - \frac{\delta_E}{1+\gamma_E\phi_E}E \\
\frac{dD}{dt} &= 2\alpha_E E - \frac{\delta_D}{1+\gamma_D\phi_D}D \\
\frac{dL}{dt} &= -k_f L(R_{T_S}S - C_S) + k_r C_S - k_f L(R_{T_E}E - C_E) + k_r C_E \\
&\quad - k_f L(R_{T_D}D - C_D) + k_r C_D - \lambda_L L + \rho_T(S+E+D) \\
\frac{dC_S}{dt} &= k_f L(R_{T_S}S - C_S) - k_r C_S - k_p C_S - \frac{\delta_S}{1+\gamma_S\phi_S}C_S \\
\frac{dC_E}{dt} &= k_f L(R_{T_E}E - C_E) - k_r C_E - k_p C_E - \frac{\delta_E}{1+\gamma_E\phi_E}C_E \\
\frac{dC_D}{dt} &= k_f L(R_{T_D}D - C_D) - k_r C_D - k_p C_D - \frac{\delta_D}{1+\gamma_D\phi_D}C_D
\end{aligned}
\tag{3.1.19}
$$

$\frac{dS}{dt}$, $\frac{dE}{dt}$ and $\frac{dD}{dt}$ in Model (1) describe the tumor growth at the tissue level whereas $\frac{dL}{dt}$, $\frac{dC_S}{dt}$, $\frac{dC_E}{dt}$ and $\frac{dC_D}{dt}$ represent the cell surface dynamics of receptor-ligand bindings. Binding IL-6 to IL-6R activates the receptors on the cell membrane which leads to intracellular signal transduction cascade which by itself enhances the self-renewal probability of CSCs and survival of tumor cells. Tracking the temporal changes of the number of IL-6-IL-6R complex molecules (ϕ_S, ϕ_E and ϕ_D) at the intracellular level allows us to quantify the impacts of IL-6 mediated pathways on CSC self-renewal potentials and tumor cell death. A schematic representation of the incorporated scales in Model (1) is given in Figure 3.2.

It is worth mentioning that in addition to the aforementioned levels, this model is running in two different time scales. While the changes at molecular level hap-

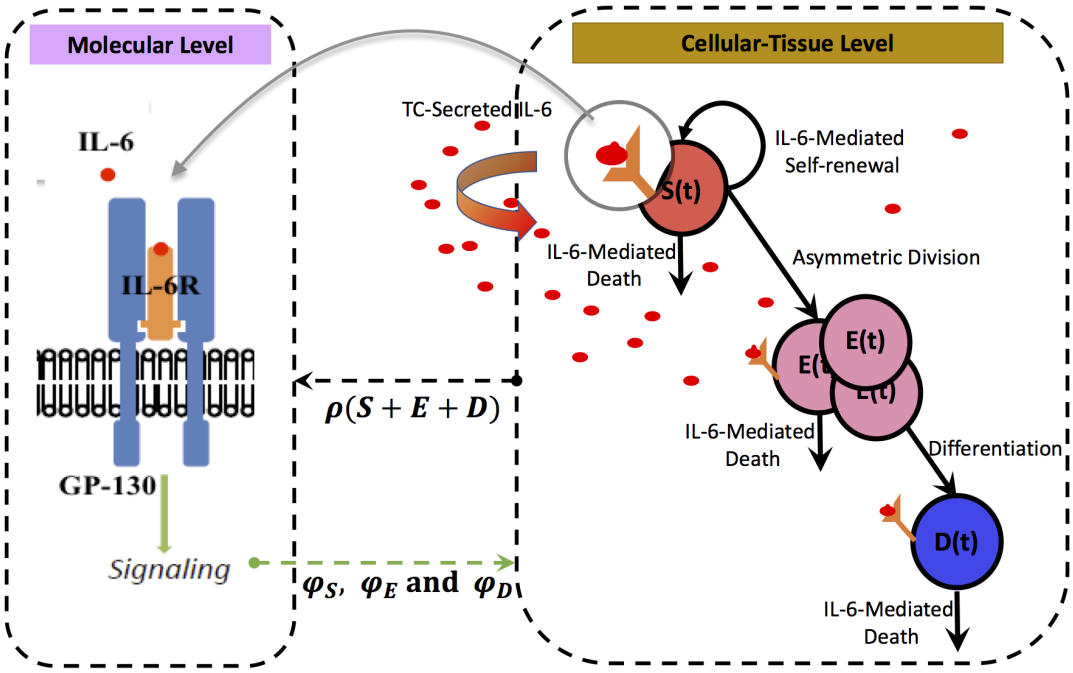

Figure 3.2: Schematic Illustration of the Interaction Between IL-6 and Tumor Cells; The left panel represents a closer look to the IL-6-IL-6R complex molecules on the tumor cell membrane. Tumor secreted IL-6 binds to unoccupied IL-6 receptors on tumor cells (CSCs, PCs and DCs) and initiate signaling pathways which promote the self-renewal probability of CSCs and enhance survival of tumor cells. Tracking the temporal changes of the fractional occupancies of IL-6R (ϕ_S, ϕ_E and ϕ_D) allows us to quantify the impacts of IL-6 on tumor growth dynamics.

pens in seconds, the events related to tumor cell division, differentiation and death occur at the scale of days and even weeks.

We will use this model as a foundation for extensions designed to study the effects of *human stromal cell-secreted* IL-6 on the tumor growth dynamics and further to investigate the response of CSCs to combination therapy using a Cisplatin and Tocilizumab (TCZ).

3.2 Numerical Analysis

In this section, we first introduce the parameter values that we can find from the literature. For parameters which there is no information, we estimate them by performing a best-fit to experimental data, particularly, to IL-6+/+ mice data with initial condition $(S_0, E_0, D_0, L_0, C_{S_0}, C_{E_0}, C_{D_0}) = (1000, 0, 0, 0, 0, 0, 0)$. Furthermore, we will perform uncertainty and sensitivity analysis to find the most influential parameters on the tumor growth, percentage of CSCs and the fractional occupancies of bound IL-6 receptors on CSCs.

3.2.1 Parameter values

The parameter values obtained from the literature are tabulated in Table 3.2.

Table 3.2: Parameter Values Taken from the Literature and Their Sources

Parameters	**Baseline Values**	**Units**	**Reference**
A_{out}	2	dimensionless	Ganguly and Puri (2006)
α_S	0.6	day^{-1}	Driessens *et al.* (2012) Gao *et al.* (2013)
α_E	$\frac{log(2)}{1.04}$	day^{-1}	Driessens *et al.* (2012) Gao *et al.* (2013)
$P^*_{S_{min}}$	0.014	dimensionless	Weekes *et al.* (2014)
$P_{S_{max}}$	0.90	dimensionless	Weekes *et al.* (2014)
k_f	2.35	$\text{fmol}^{-1}\text{day}^{-1}$	Özbek *et al.* (1998)
k_r	2.24	day^{-1}	Hirabayashi and Lemmey (2012) Özbek *et al.* (1998)
λ	0.4152	day^{-1}	Lindmark *et al.* (2001)
ρ	7×10^{-7}	$\text{fmol}^{-1}\text{per cell}\text{day}^{-1}$	Bran *et al.* (2011) Nilsson *et al.* (2005) PRIES *et al.* (2006)
R_{T_S}	1.66×10^{-6}	fmol^{-1}per cell	Boayue *et al.* (1998) Shkeir *et al.* (2013) Snyers and De Wit (1990) Takizawa *et al.* (1993)
R_{T_E}	$\frac{1}{8}R_{T_S}$	fmol^{-1}per cell	Krishnamurthy *et al.* (2014)
R_{T_D}	$\frac{1}{8}R_{T_S}$	fmol^{-1}per cell	Krishnamurthy *et al.* (2014)

For those parameters which there was little or no published information, we compute a best fit to experimental data to obtain reasonable estimates. In section 2.2.4, we also perform uncertainty and sensitivity analysis to find the most influential parameters on the tumor growth, percentage of CSCs and the fractional occupancies of bound IL-6 receptors on CSCs.

3.2.2 *Experimental data*

To begin to understand the impact of stromal IL-6 on the survival of CSCs, Krishnamurthy et al. Krishnamurthy *et al.* (2014) generated tumor xenografts by transplanting primary human cancer stem-like cells in severe combined immunodeficient mice. Specically, immediately after surgical removal of the primary tumor from patients with HNSCC, $ALDH^{HIGH}CD44^{HIGH}$ cells were sorted and transplanted into IL-6 +/+ or IL-6 -/- immunodeficient mice. This approach differs from scaffold experiments where xenograft tumors vascularized with functional human microvessels are generated in SCID mice. In that experimental setup, human tumor cells are seeded along with human dermal microvascular endothelial cells (HDMECs) in poly(L-lactic) acid biodegradable scaffolds, resulting in the growth of human tumors with human vasculature and an additional source of human IL-6 (the HDMECs). In the experimental setup modeled here, no human endothelial cells are implanted and the only source of human IL-6 are the tumor cells themselves. Another difference between the experimental approach modeled here and others in the literature, is the use of primary tumor cells and not immortalized tumor cell lines. Figure 3.3 shows the relevant data taken from Krishnamurthy *et al.* (2014) . When 1,000 $ALDH^{HIGH}CD44^{HIGH}$ were cells transplanted into the IL-6 +/+ mice, the result was more and larger tumors as compared to the transplantation of 1000 $(ALDH^{HIGH}CD44^{HIGH})$ into IL-6 -/- deficient litter mates.

3.2.3 *Estimating baseline parameter values using IL6+/+ mice data*

We fit the mathematical model to the IL-6+/+ mice data in Krishnamurthy *et al.* (2014) in oder to estimate the baseline parameter values for those that we could not obtain in the current literature (A_{in}, P_{N_s}, k_p, γ_i and μ). Data for tumor volume

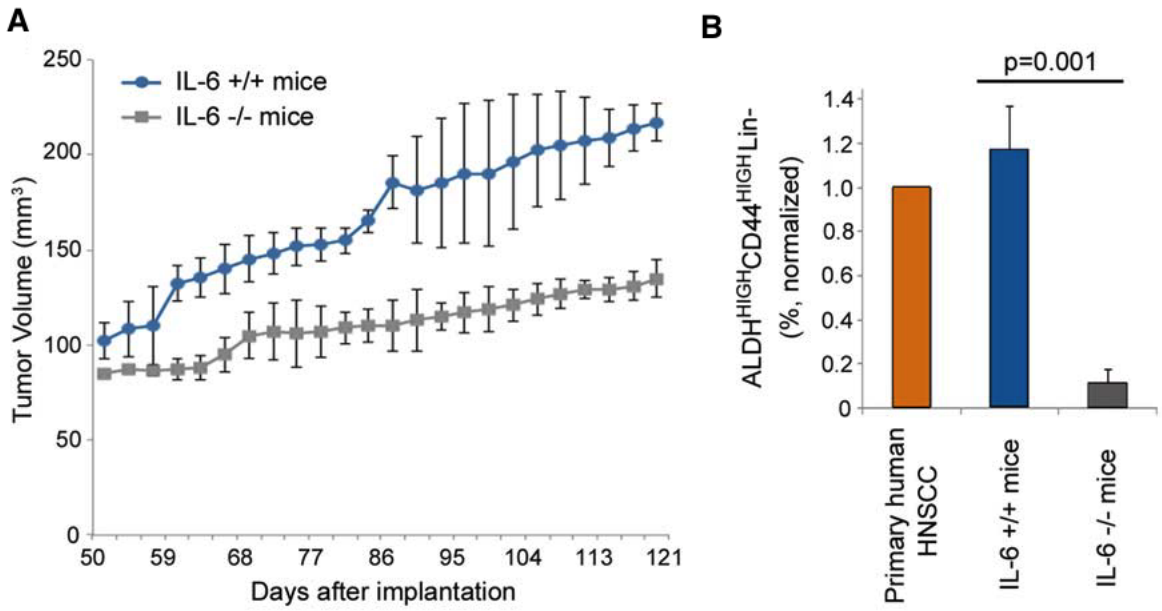

Figure 3.3: Data for Tumor Growth (A) and Stem Cell Percentage (B) Taken Directly from Krishnamurthy *et al.* (2014).

over time (day 50 through day 121) is given in Figure 3.3. We use GraphClick software to extract the data for the tumor volume at each time point in Figure 3.3. The data fitting process uses R lsoda solver with a time-step of one day to predict the volume of the tumor over time. The *Monte Carlo parameter sweep method* Cowan (1998) is used to minimize the Pearson χ^2 statistic by comparing extracted tumor volume from data in Figure 3.3 and the tumor volume predicted by the mathematical model, over 24 data time-points. **Remark:** In order to normalize the percentage of cancer stem cells by the primary human tumor stem cell percentage, it is assumed that the primary human HNSCC tumor is contained 2.1% tumor stem cells, which is normalized to 1%. The parameter values obtained via this fitting process are tabulated in Table 3.3.

As we mentioned earlier, the long-term goal of this study is to evaluate the impact of human endothelial cell-secreted IL-6 (EC-IL-6) on the tumorigenic potential

Table 3.3: List of Estimated Parameter Values for Model (1) Using IL-6+/+ Mice Data.

Parameters	**Baseline Values**	**Units**	**Reference**
A_{in}	2	dimensionless	Fitted to data
δ_S	$1.5\alpha_S P^*_{S_{min}}$	$\frac{1}{day}$	Assumed
δ_E	0.0612	$\frac{1}{day}$	Assumed
δ_D	0.0612	$\frac{1}{day}$	Assumed
P_{Ns}	728455	dimensionless	Fitted to data
n	2.6	dimensionless	Assumed
k_p	24.95	$\frac{1}{day}$	Fitted to data
μ	0.04	dimensionless	Fitted to data
γ_i	2.38	dimensionless	Fitted to data

of CSCs. The rationale is that the IL-6 expression is higher in the endothelial cells than in the HNSCC tumor cells Krishnamurthy *et al.* (2014). To do so, we will use an extended version of Model (1) developed in Chapter 3 along with data from an experiment in which human tumor cells and human endothelial cells are transplanted into immunodeficient mice Krishnamurthy *et al.* (2014). Therefore, we will use the model developed here, Model (1), to estimate baseline parameter values that we will later use in the extended model presented in Chapter 3.

3.2.4 Characterizing IL-6 dependent tumor growth

We fit Model (1) to the IL-6+/+ mice data (given in Figure 3.3) to estimate the baseline parameter values for those that we could not find any information in the literature (A_{in}, P_{N_s}, k_p, γ_i and μ). The best-fit parameter values are tabulated in Table 3.3 and results of the numerical simulations are depicted in Figure 3.4-A. There is a strong correlation between the model output (red) and the experimental data

in Krishnamurthy *et al.* (2014) (blue). The green line in Figure 3.4-A represents the tumor volume over time when no IL-6 is produced by tumor cells, thereby showing how much even low secretion rates of IL-6 ($\rho = 7^{-7}\frac{\text{fmol}}{\text{cell}\times\text{day}}$) influence tumor growth. In addition, we use the best-fit parameter values to predict the percentage of CSCs on the last day of the experiment. Figure 3-B shows the experimentally measured percentage of CSCs in primary tumors (brown), the experimentally measured percentage of CSCs on day 121 for tumors grown in IL-6 +/+ mice (blue), along with our mathematical model prediction (red). The model is able to accurately capture the correct proportion of stem cells and Figure 3-D shows how the stem cell percentage evolves over time.

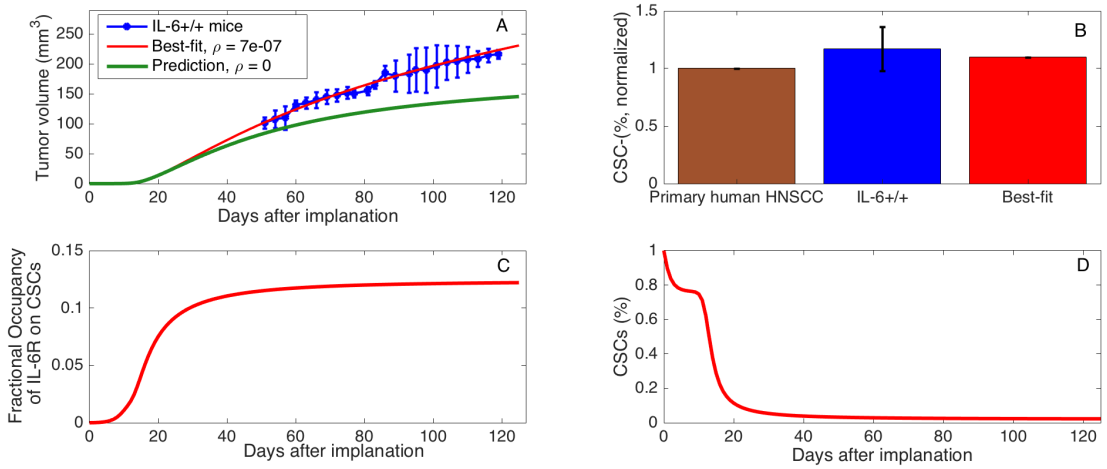

Figure 3.4: (A) Best Fit of the Model Prediction of Tumor Volume Over Time to the IL-6+/+ Data in Krishnamurthy *et al.* (2014). The green line in (A) shows the special case in which the tumor cells are not producing IL-6, $\rho = 0$. (B) Comparison of the experimentally measured percentage of CSCs in primary tumors (brown), the experimentally measured percentage of CSCs on day 121 for tumors grown in IL-6 +/+ mice (blue), and the mathematical model prediction percentage of CSCs on day 121 (red). (C) Model prediction of the temporal changes in the factional occupancy of IL-6 receptors on CSCs, ϕ_S. (D) Model prediction of the stem cell percentage over time.

Recall that the first step in the IL-6 signal transduction pathway is to binding

to IL-6R. The IL-6-IL-6R complex then recruits GP130. The triple complex of IL-6-IL-6R-GP130 activates signaling pathways (such as STAT3) Garbers *et al.* (2015); Zhang *et al.* (2006) that play a critical role in the self-renewal and survival of CSCs. Therefore, the fractional occupancies of bound receptors can provide a useful tool for quantifying the influence of tumor cell-secreted IL-6 on the tumorigenic potential of CSCs and subsequently on tumor growth dynamics. Figure 3.4-C plots the fractional occupancy of IL-6R on CSCs over time for our baseline level of tumor secretion of IL6. The model suggests that a fractional occupancy of 12% on CSCs is sufficient to result in the experimentally observed tumor growth rate. In fact, because endothelial cells can secrete higher levels of IL-6 than tumor cells Krishnamurthy *et al.* (2014), if we were to add endothelial cells to our model then we would expect even greater interdependencies among IL-6, tumor growth dynamics and the tumorigenic potential of CSCs.

Figure 3.5 shows that if we fix all the other parameters while varying the secretion rate of tumor IL-6, ρ, then relatively small changes in this value (from $\rho = 7e-7$ to $5.35e-6$ fmol/cell/day) lead to 90% fractional occupancy. This supports the idea that an IL-6 agonist could temper the effects of IL-6-induced pathways, thereby impeding tumor growth.

Sensitivity analysis

We use sensitivity analysis to determine which parameters are the most influential on the tumor volume, $TV = \frac{S(t)+E(t)+D(t)}{10^6}$, percentage of cancer stem cells, $\Omega = \frac{S(t)}{S(t)+E(t)+D(t)} \times \frac{100}{2.1}$ and the fraction of occupied bound receptors on the CSCs, $\phi_S = \frac{C_S}{R_{T_S} S}$, at days $= 15, 50, 90$ and 120. The uncertainty quantification method we use is a global sensitivity analysis that uses Latin Hypercube Sampling (LHS)

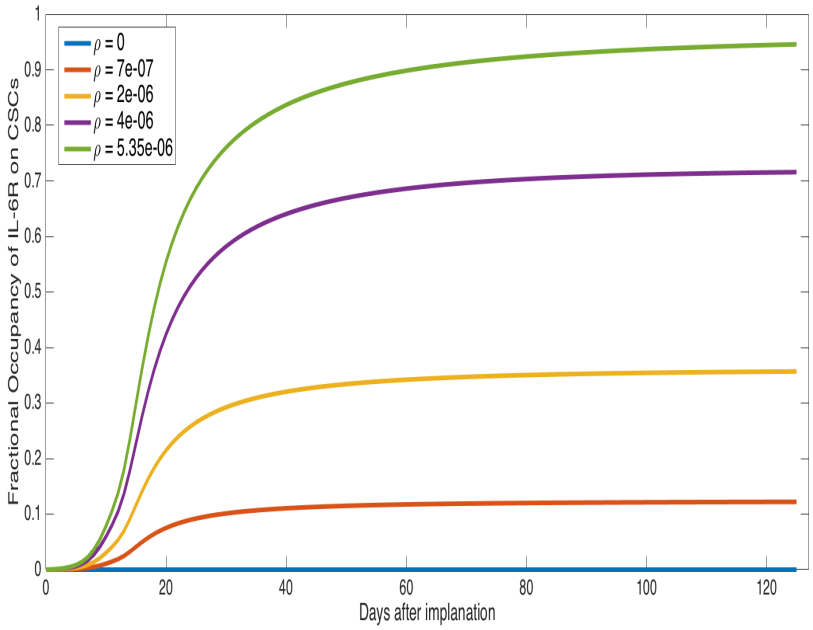

Figure 3.5: The Fractional Occupancies of IL-6R on CSCs, ϕ_S, Highly Depends on Secretion of IL-6 by Human Tumor Cells, ρ

along with Partial Rank Correlation Coefficient (PRCC) [1] to assess the sensitivity of the output of interest (tumor volume, percentage of cancer stem cells, and the fraction of occupied bound receptors) to each of the parameters at the given time-pointsBlower and Dowlatabadi (1994); Marino *et al.* (2008); Sanchez and Blower (1997). The LHS method involves defining baseline values and ranges for each of the parameters, assuming they obey a uniform distribution, and carrying out multiple runs (number of runs = 1000) of the sampled values for the response output (TV, Ω, and ϕ_S in this case) Blower and Dowlatabadi (1994); Marino *et al.* (2008); Sanchez and Blower (1997). We use the best-fit parameter values as the baseline parameter values to calculate LHS PRCC values and $\pm 10\%$ of the best-fit parameter values as the range.

[1] More information about LHS & PRCC can be found in Appenidx

As depicted in Figures (3.6-3.8), sensitivity analysis reveals that in some cases, parameter sensitivity varies as the tumor grows. For example, since $|PRCC(TV, A_{in})| \approx 1$ and $|PRCC(TV, \alpha_S)| \approx 1$ (Figure 3.6), tumor volume is highly sensitive to the relatively small changes in both the amplification factor, A_{in}, and the stem cell proliferation rate, α_S, at all the times. However, the tumor volume becomes less and less sensitive to the parameter $P_{S_{max}}$ as tumor volume increases. Other parameters with a large influence on the tumor volume are the death rate of the terminally differentiated cancer cells, δ_D; the minimum probability of CSC self-renewal, $P^*_{S_{min}}$; the production rate of IL-6 by tumor cells, ρ; and the total number of IL-6 receptors on CSCS, R_{T_S}. These results highlight how critically important CSC dynamics are for driving tumor growth. Interestingly, the only influential parameter not related to CSCs and IL-6 is the maximum death rate of the terminally differentiated cancer cells.

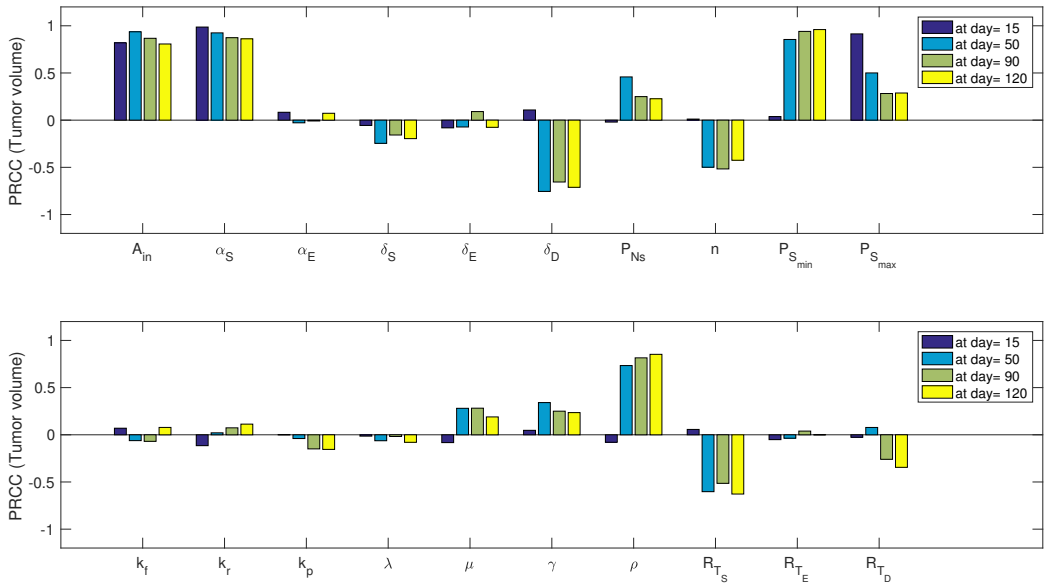

Figure 3.6: PRCC Values for the Parameters of Model (1) Using the Tumor Volume as the Output of Interest

PRCC values given in Figure 3.7 shows that percentage of CSCs within the tumor is also highly influenced by the amplification factor, A_{in}, at all times. The death rate of the terminally differentiated cancer cells, δ_D and the minimum probability of CSC self-renewal, $P^*_{S_{min}}$, are most influential at later times, while the stem cell proliferation rate, α_S becomes less influential as the tumor grows larger.

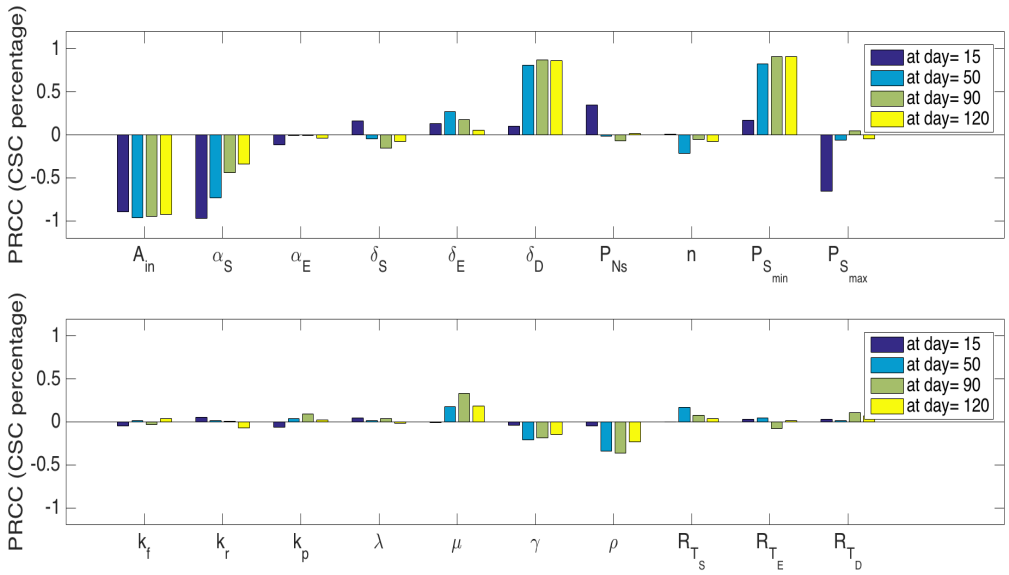

Figure 3.7: PRCC Values for the Parameters of Model (1) Using the Percentage of Caner Stem Cells as the Output of Interest

Finally, PRCC values for parameters using the fractional occupancy, ϕ_S, as the output of interest (Figure 3.8) reveals that A_{in}, ρ, and R_{T_S} are consistently the most influential parameters. Again, α_S is influential early in tumor growth, but loses its impact for later times.

We used IL-6+/+ mice data to estimate the baseline parameter values (Tables 3.2 and 3.3) that will be used in the extended version of Model (1) to study the impacts of EC-IL-6 and treatment on tumor growth. We further used these base-

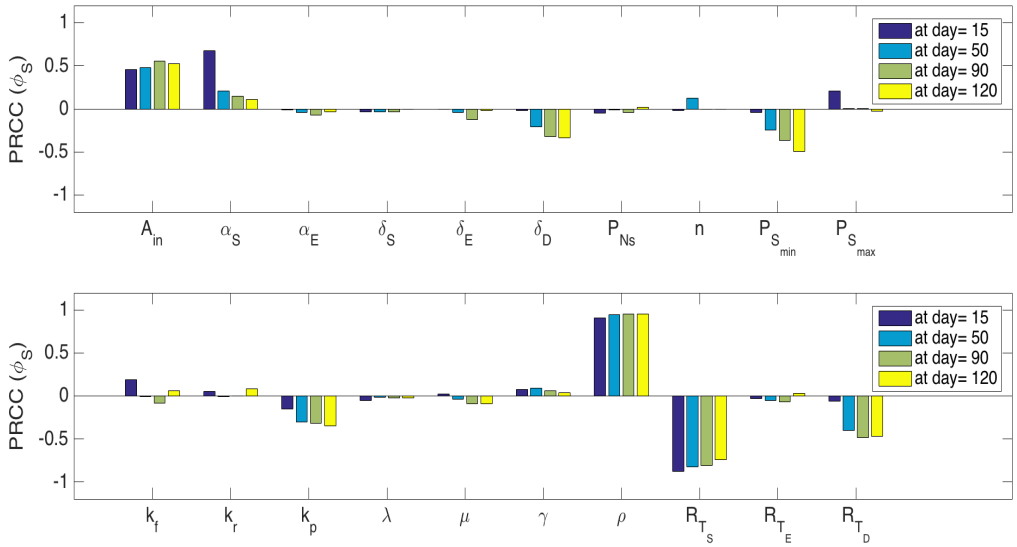

Figure 3.8: PRCC Values for the Parameters of Model (1) Using Fraction of Occupied Bound Receptors as the Output of Interest

line parameter values to run a global sensitivity analysis on Model (1) in order to determine the most influential parameters on the tumor growth dynamics including changes in the tumor volume, percentage of CSCs and fractional occupancies of IL-6 bound receptors over time. We observed that some of the parameters are influential at all the time-points; whereas, some of the others are more influential at the early stages of tumor growth but their significance is reduced as the tumor grows larger. This might be due to the tendency of the system to reach to a stable state relatively quickly. Numerical simulations suggests that soon after tumor starts to grow, both the fractional occupancies of bound receptors and CSC percentage rapidly reach equilibrium and remain fixed for all the future time points (Figures 3.4-C and 3.4-D).

3.2.5 Impacts of Murine stromal cell-secreted IL-6 on tumor growth

In addition to IL-6+/+ mice, Krishnamurthy *et al.* (2014) used the same approach to generate tumor genografts in IL-6-/- mice, which are unable to produce murine stromal IL-6 (gray data points in Figure 3.3-B). Despite the fact that murine IL-6 can not directly impact human tumor cell proliferation (since it can not bind to IL-6 receptors on the tumor cells Coulie *et al.* (1989)), they reported that tumor xenografts generated in the presence of murine IL-6 (in IL-6+/+ mice) produced a greater number of tumors that were larger in size than in the IL-6 -/- mice Krishnamurthy *et al.* (2014). On the other hand, it is known that both human and murine IL-6 do react with the murine stromal IL-6-receptor Coulie *et al.* (1989). Thus, one potential interpretation of this data is that murine IL-6 secreted by stromal cells of the host in IL-6+/+ mice is affecting the mouse endothelial cells leading to increased angiogenesis and survival potential for the tumor cells Krishnamurthy *et al.* (2014). So we would like to test the ability of Model (1) to fit and explain this idea as further validation. Also, insights gained may be viewed as a useful first step in our overarching goal of understanding the role of human endothelial (stromal) cell secreted IL-6, which directly impacts cancer growth.

Method description

Knowing the most influential parameters from the previous section, in order to explore the effects of murine IL-6 on the dynamics of tumor growth, we need to address the following question:

"which of the influential parameters should be altered in response to the absence of Murine stromal IL-6?". In fact, the interaction between CSCs and their surrounding microenvironment is poorly understood Lu *et al.* (2014); Noll *et al.*

(2014); O'Brien *et al.* (2010); Plaks *et al.* (2015). However, what is well-understood is that tumor microenvironment plays a crucial role in regulating proliferation and survival of tumor cells as well as mediating a potential protective environment for stem cells to grow and divide without interruption Lu *et al.* (2014); Noll *et al.* (2014); O'Brien *et al.* (2010); Plaks *et al.* (2015); Sujata and Chaudhuri (2008). In particular, IL-6 secreted by endothelial cells within tumor niche directly regulates CSC growth and behavior through binding to their receptors on the CSCs Noll *et al.* (2014). Despite the fact that murine IL-6 can not bind to IL-6 receptors on the human tumor cells, it still has indirect impacts on the tumor niche. In fact, it has been shown that IL-6 function is not just limited to modulating the CSC self-renewal, rather IL-6 has an indirect impact on CSC growth through recruiting mesenchymal stem cells (MSCs), which results in angiogenesis as well as providing nutrition and oxygen for the tumor cells Noll *et al.* (2014). Therefore, among the most influential parameters obtained via sensitivity analysis, we need to choose those that can be altered in response to the absence of murine IL-6 in tumor microenvironment. Thus, the potential parameter candidates are A_{in}, n and P_{N_S} since the rest can only be changed through IL-6-IL-6R binding signals. To support our claim, we provide some biological evidence below.

The balance between self-renewal and differentiation, as well as, the number of TA divisions of progenitor cells is regulated by the tumor niche in order to maintain the cancer stem cell function and protection against chemotherapeutic agents Clarke and Fuller (2006); Noll *et al.* (2014). As a result, the number of stem cells within a particular tissue can be regulated by controlling the number of composition of existing niches Clarke and Fuller (2006). The number of TA divisions is flexible in various tissues and can respond to extracellular signals Insco *et al.* (2009); Monk *et al.* (2010). However, little is currently known about the mechanism that

regulates and/or determines the number of TA division Clarke and Fuller (2006); Insco *et al.* (2009); Monk *et al.* (2010). In addition, mutations may allow transit amplifying progenitor cells to escape the controls that normally regulate the number of TA divisions leading to continued proliferation rather than terminal differentiation Clarke and Fuller (2006). Alternatively, oncogenic mutations arising in transit-amplifying progenitor cells may imbue them with stem cell properties of self-renewal resulting in a pool of cancer stem cells in a fully neoplastic state Clarke and Fuller (2006).

In Model (1), parameter A_{in} reflects the controlling effects of the "regulatory feedback signaling" of transit-amplifying progenitor cell division Ganguly and Puri (2006). Therefore, it is reasonable to assume that the number of TA divisions (which corresponds to the value of A_{in}) might vary in response to the absence and/or presence of murine IL-6. Along with that, PRCC values show A_{in} has the largest impact on both tumor growth and CSC percentage. However, tumor volume is positively correlated to A_{in} while CSC percentage is negatively correlated to it. So, our challenge is to numerically find a balanced value of A_{in} which favors both of the changes in IL-6-/-mice data.

Both P_{N_S} and n are parameters that represent effects of micro-environmental influences on tumor growth (including murine IL-6) in Model (1). For larger values of n, tumor microenvironmental factors have more regulatory control on tumor growth and CSC self-renewal. So in the absence of IL-6 we would expect a larger value of n since comparing IL-6-/-mice and IL-6+/+mice data suggests that murine IL-6 enhances CSCs growth and survival Krishnamurthy *et al.* (2014). P_{N_S} measures the time it takes to reduce the probability of CSC self-renewal to halfway between $P_{S_{max}}$ and $P^*_{S_{min}}$. Numerical simulations reveal that it takes almost 14 days for a 50% decrease in the probability of CSC's self-renewal. So in the absence of

IL-6 we would expect a decrease in the amount of time that it takes to reduce the probability of CSC self-renewal corresponding to a decrease in the IL-6+/+ best-fit parameter value for P_{N_S}.

Now, in order to fit Model (1) to the IL-6-/-mice data, we keep all of the IL-6+/+ best-fit parameter values unchanged except those candidate parameters indicated above. Increasing $A_{in} = 2$ and $n = 2.6$ to $A_{in} = 18.8$ and $n = 4.2$, and also decreasing $P_{N_S} = 728400$ to $P_{N_S} = 77600$, we find the best-fit parameter values for IL-6-/-mice data as depicted in Figure 3.9-A. With these set of parameter values our model also can capture the experimentally observed percentage of CSCs at day 120 (Figure 3.9-B). Furthermore, Figure 3.9-C shows despite the slower tumor growth dynamics in IL-6-/- mice, the fractional occupancies of IL-6R on CSCs does not change when compared to IL-6+/+ mice data. The IL-6-/- best-fit parameter values are tabulated in Table 3.4.

Table 3.4: List of Estimated Parameter Values for Model (1) Using IL-6-/- Mice Data.

IL-6-/- mice data	**IL-6+/+ mice data**	**Parameter Description**
$A_{in} \approx 18 \longleftarrow \longleftarrow$	$A_{in} \approx 2$	Amplification factor
$P_{Ns} = 77600 \longleftarrow \longleftarrow$	$P_{Ns} = 728400$	Half-max stem cell self-renewal concentration
$n = 4.2 \longleftarrow \longleftarrow$	$n = 2.6$	Steepness parameter for P_S

To summarize, we re-fit Model (1) to the IL-6-/- mice data as further validation of the model and as a way of testing its ability to capture tumor growth dynamics even in the absence of murine IL-6. To do so, among the most influential parameter values we chose the ones that could be altered in response to the absence of Murine IL-6. Then we fixed all the other best-fit IL-6+/+ mice parameter values

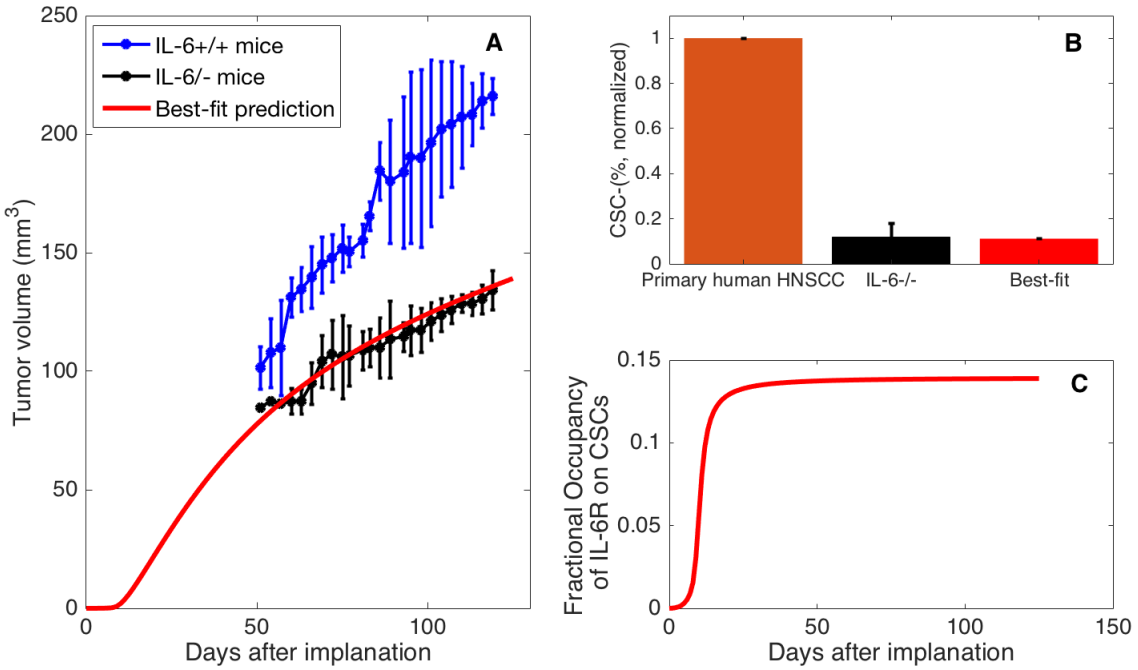

Figure 3.9: Fitting Model (1) to the IL-6-/- Data by Using Parameter Values Given in Tables 3.2, 3.3 and 3.4.

and varied the values of those candidate parameters to find the best-fit of Model 1 to the IL-6-/- mice data. Additionally, we saw that murine IL-6 mostly affects parameters that represent the influence of the tumor micro-environment including A_{in}, P_{N_S} and n. This led us to conclude that the murine IL-6 secreted by host cells can affect the system by impacting the associated tumor microenvironment.

3.3 Treatment of HNSCC Tumors with Anti-IL-6R Antibody, Tocilizumab

We have already shown, in the previous sections, that tumor cell-secreted IL-6 can significantly impact tumor growth. Recall that Figure 3.5 shows how the secretion rate of IL-6 by human tumor cells impacts the fraction of occupied IL-6 receptors. Specifically, we studied the (extreme) case in which there is no secretion

of IL-6 by human tumor cells and saw significant tumor reduction. This motivated us to add treatment with an anti-IL-6R, Tocilizumab (TCZ), to our current model and explore its effects on the growth rate of tumors generated in IL-6+/+ mice. Tocilizumab (TCZ) is a recombinant humanized monoclonal antibody against the IL-6 receptor that has FDA approval for the treatment of moderate to severe RA, however given its efficacy against IL-6R it also has potential as a targeted cancer therapy.

3.3.1 Two-compartment pharmacokinetic model

Experimental evidence suggests a biphasic plasma concentration-time curve for TCZ Igawa *et al.* (2010). Consequently, we proposed the following 2-compartment model to describe TCZ pharmacokinetics. The general two-compartment pharmacokinetic modeling framework consists of a central compartment, denoted by I_s, and peripheral compartment, denoted by I_p. The central compartment is composed of the blood and highly vascularized organs, such as the liver and kidney. The peripheral compartment is made up of slowly perfused tissues and organs.

Table 3.5: Variables Related to TCZ-Therapy Model

Variable	**Description**	**Units**
I_s	Free anti-IL-6R antibody in systemic circulation	fmol
I_p	Free anti-IL-6R antibody in peripheral compartment	fmol

Pharmacokinetic models can be further specified by the type of drug administration. Intravenous injection or i.v. injection is the injection of a substance as a bolus or infusion directly into a blood vessel (intravenous) Turner *et al.* (2011).

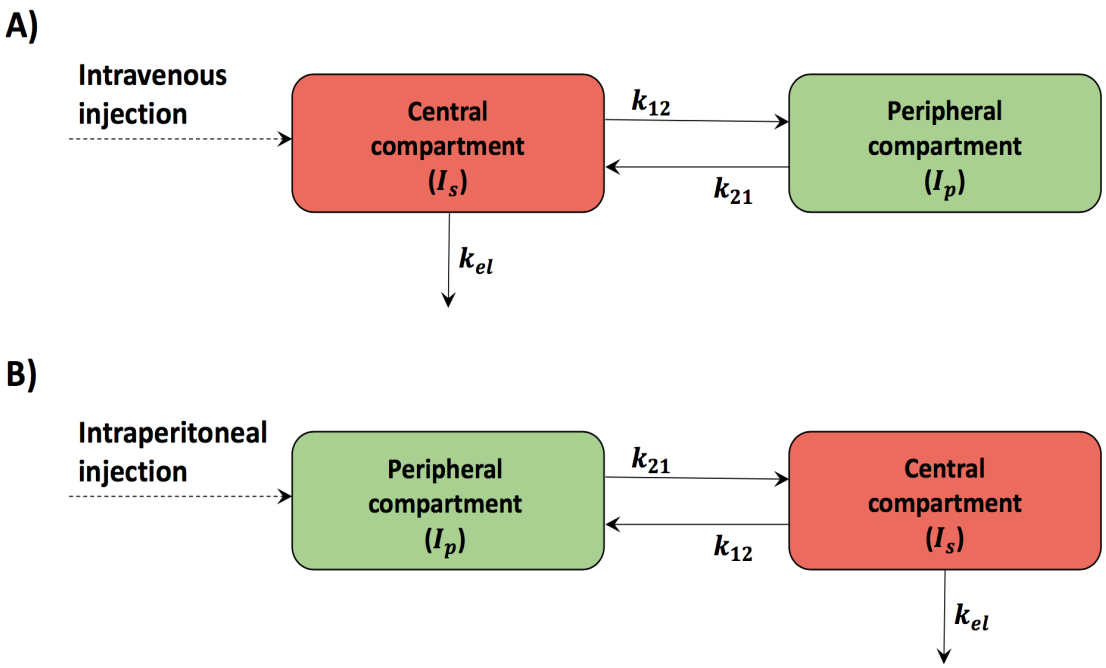

Figure 3.10: General Two-Compartment Pharmacokinetic Model for (A) Intravenous Bolus (i.p.) and (B) Intraperitoneal (i.p.) Injection.

Intraperitoneal injection or i.p. injection is the injection of a substance into the peritoneal cavity. It is more often used in small animals than large mammals and humans. In general, it is preferred when intravenous access is challenging or when large volume of fluids are needed to be injected or when low blood pressure prevents the use of intravenous injection Turner *et al.* (2011). A general schematic representation of the PK-model for both types of injection, i.v. injection and i.p. injection, is given in Figure 3.10.

The corresponding equations for single dose i.v. injection (Figure 3.10-A) are given by:

$$\frac{dI_s}{dt} = -\underbrace{k_{12}Is + k_{21}I_p}_{\text{Pharmacokinetcs}} - k_{el}I_s \tag{3.3.1}$$

$$\frac{dI_p}{dt} = + \underbrace{k_{12}Is - k_{21}I_p}_{\text{Pharmacokinetcs}}$$

where k_{12} and k_{21} are the transfer rate constants between the two compartments and k_{el} is the elimination rate from central compartment.

In prior works several PK-models have been designed differing in generalized assumptions about the number of compartments and/or the path of connectivities. For instance, Charusanti et al. assumed an i.p. injection 3-compartment PK model involving: (1) intraperitoneal cavity, (2) blood and (3) tumor cells. In this model the drug is assumed to be injected to intraperitoneal cavity and then the blood delivers the drug to the tumor cells Charusanti *et al.* (2004). Dedrick and Flessner also designed a PK model for i.p. injection involving two compartments, the peritoneal cavity and a body compartment. They assumed that the drug transfers from the peritoneal cavity into surrounding area via three parallel paths governed by tissue-specific (liver, hollow viscera and parietal tissue) permeabilities Dedrick and Flessner (1997). In other work, Elishmereni et al. designed a PK model under i.p. injection based on data in mice. In this model the drug is injected into the administration site and transported through three tissue compartments to the plasma. Then the drug is transported to the target tissue and/or degraded via three additional compartments Elishmereni *et al.* (2011). The model that we are using is a combination, but simplified version of these models. Instead of multiple number of intraperitoneal cavity compartments, we have one peripheral compartment, which includes the intraperitoneal cavity.

Single dosing via intravenous injection

We assume that at time t_0, a single dose of drug, d_0, is administered by intravenous bolus. Then the pharmacokinetic model with the initial condition $I_s(t_0) = d_0$ and $I_p(t_0) = 0$ can be analytically solved and is given by:

$$I_s(t) = I_s(t_0)\left(Ae^{-\alpha(t-t_0)} + Be^{-\beta(t-t_0)}\right), t \geq t_0 \tag{3.3.2}$$

where,

$$\begin{aligned}
\alpha &= \frac{(k_{12}+k_{21}+k_{el}) + \sqrt{(k_{12}+k_{21}+k_{el})^2 - 4k_{21}k_{el}}}{2} \\
\beta &= \frac{(k_{12}+k_{21}+k_{el}) - \sqrt{(k_{12}+k_{21}+k_{el})^2 - 4k_{21}k_{el}}}{2} \\
A &= \frac{k_{21}-\alpha}{\beta-\alpha} \\
B &= \frac{k_{21}-\beta}{\alpha-\beta}
\end{aligned}$$

A proof of this result is given in Section B of Appendix.

Single dosing via intraperitoneal injection

Using the same approach for intraperitoneal injection we can show that the pharmacokinetic model with the initial condition $I_s(t_0) = 0$ and $I_p(t_0) = d_0$ can be analytically solved and is given by:

$$I_s(t) = I_p(t_0)\left(A_p e^{-\alpha(t-t_0)} + B_p e^{-\beta(t-t_0)}\right), t \geq t_0 \tag{3.3.3}$$

where, α and β are defined above and

$$\begin{aligned} A_p &= \frac{k_{21}}{\beta - \alpha} \\ B_p &= \frac{k_{21}}{\alpha - \beta} \end{aligned}$$

From this point on, we will use the PK-model with i.v. injection given given by Eq. 3.3.2. The pharmacokinetic rate constants (k_{12}, k_{21} and k_{el}) are estimated by fitting the analytical solution of $I_s(t)$ to the experimental data described in Igawa *et al.* (2010). Briefly, in this experiment TCZ and a pH-dependent binding variant of TCZ, PH2, were intravenously injected at single doses of 1 mg/kg in order to calculate and compare the pharmacokinetics of TCZ and PH2 in normal mice. Plasma concentration of TCZ over time and the best fit of $I_s(t)$ to the pharmacokinetic data are shown in Figure 3.11 and the best-fit pharmacokinetic parameter values are tabulated in Table 3.6.

Table 3.6: Pharmacokinetic Parameter Values

Parameters	**Values**	**Units**	**Reference**
k_{12}	14.30	day^{-1}	Estimated
k_{21}	5.55	day^{-1}	Estimated
k_{el}	0.004	day^{-1}	Estimated

Multiple-dosing

We assume that the drug is administered by intravenous bolus injections several times to the body. Now, we need to account for the remaining drug in the body from the previous injections. Firstly, assume that the drug is administered at arbi-

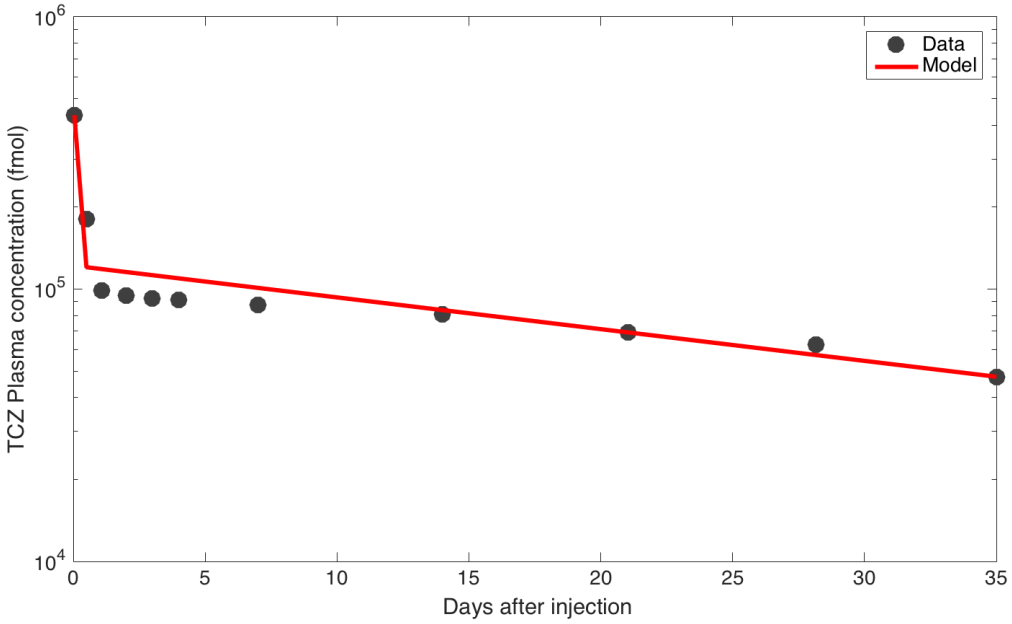

Figure 3.11: Time Profiles of TCZ in Plasma. The best fit of $I_s(t)$ (solid line) defined by Eq. 3.3.1 is plotted together with experimental data (dots) from an in vivo study Igawa *et al.* (2010) of TCZ (and a PH-dependent binding variant of TCZ) in normal mice.

trary dosing time-points denoted by $\tau = (\tau_1, \tau_2, \cdots, \tau_m) \in \mathbb{R}^m$ such that $\tau_j \geq 0$ for $j = 1, \cdots, m$ and $\tau_{j-1} < \tau_j$. That is, τ_j denotes the timing of each dose. $\tau_j - \tau_{j-1}$ denotes the length of the time between the j^{th} and $(j+1)^{th}$ injection and m, accounts for the the total number of injections. Therefore, the concentration of drug in the central compartment right after the j^{th} administration, $I_s^j(t)$, can be given by:

$$I_s^j(t) = \begin{cases} 0, & t < \tau_1 \\ \sum_{i=1}^{j} d_i \left[A e^{-\alpha(t-\tau_i)} + B e^{-\beta(t-\tau_i)} \right], & \tau_j \leq t < \tau_{j+1} \& 1 \leq j \leq m-1 \\ \sum_{i=1}^{m} d_i \left[A e^{-\alpha(t-\tau_i)} + B e^{-\beta(t-\tau_i)} \right], & t \geq \tau_m \end{cases} \tag{3.3.4}$$

where d_i is the dosing concentration at the i^{th} injection.

Special case: equidistance dosing time-points and equal dose of d

Now assume that a fixed concentration of drug, d, is administered to the body at equidistance time-points every π-units of time. Then the concentration of drug in the systemic circulation at time t can be given by:

$$I_s^j(t) = \begin{cases} 0, & t < \tau_1 \\ d\left[A\frac{1-e^{-j\pi\alpha}}{1-e^{-\pi\alpha}}e^{-\alpha(t-\tau_j)} + B\frac{1-e^{-j\pi\beta}}{1-e^{-\pi\beta}}e^{-\beta(t-\tau_j)}\right], & \tau_j \le t < \tau_{j+1} \& 1 \le j \le m-1 \\ d\left[A\frac{1-e^{-m\pi\alpha}}{1-e^{-\pi\alpha}}e^{-\alpha(t-\tau_m)} + B\frac{1-e^{-m\pi\beta}}{1-e^{-\pi\beta}}e^{-\beta(t-\tau_m)}\right], & t \ge \tau_m \end{cases} \tag{3.3.5}$$

A proof is given in Section B of Appendix. Similarly, for i.p. injection we have

$$I_s^j(t) = \begin{cases} 0, & t < \tau_1 \\ d\left[A_p\frac{1-e^{-j\pi\alpha}}{1-e^{-\pi\alpha}}e^{-\alpha(t-\tau_j)} + B_p\frac{1-e^{-j\pi\beta}}{1-e^{-\pi\beta}}e^{-\beta(t-\tau_j)}\right], & \tau_j \le t < \tau_{j+1} \& 1 \le j \le m-1 \\ d\left[A_p\frac{1-e^{-m\pi\alpha}}{1-e^{-\pi\alpha}}e^{-\alpha(t-\tau_m)} + B_p\frac{1-e^{-m\pi\beta}}{1-e^{-\pi\beta}}e^{-\beta(t-\tau_m)}\right], & t \ge \tau_m \end{cases} \tag{3.3.6}$$

In the next section we will add targeted treatment to Model (1) and will use $I_s(t)$ given by Eq. 3.3.5 to add TCZ to the system. We define our dosing schedule based on the experiments described in Mochizuki *et al.* (2015). Briefly, two biodegradable scaffolds seeded with human tumor and endothelial cells were transplanted

in mice. When the xenograft tumors reached 200 mm^3, mice were treated with 5mg/kg tocilizumab weekly. In the experiment that generated the data for our model (shown in Figure 3.3), scaffolds are not used for transplantation of human HNSCC in mice. Therefore, we will administer TCZ when the xenograft tumors reach to 125 mm^3 (the volume without scaffolds). In the experiments described in Mochizuki *et al.* (2015), TCZ is administered as a series of intraperitoneal injections. Here we assume that once injected, the drug rapidly extravasates into the systemic circulation, which approximates injection into the central compartment. Moreover, since we do not have human endothelial cells in our model, there is much less IL-6 present in the tumor environment. Therefore, we will consider TCZ administration for both a high dose of 5mg/kg and a lower dose of drug, 1mg/kg, weekly for 7 weeks.

3.3.2 Model equations related to treatment with anti-IL-6R antibody, Tocilizumab

In this section we modify Model (1) with the equations necessary to describe treatment with TCZ. TCZ is an anti-IL-6R antibody that binds to IL-6R on tumor cells and inhibits formation of IL-6–IL-6R complex molecules. Soon after drug administration, TCZ reaches the tumor environment and binds to IL-6R on tumor cells at a rate k_f^I, and dissociates at a rate k_r^I. The complex of TCZ and IL-6R on stem, progenitor and differentiated cells, denoted by C_S^I, C_E^I and C_D^I, respectively. Equation 3.3.7 describes the association and dissociation of TCZ in the tumor, $I(t)$, to IL-6 cell-bound receptors on tumor cells.

$$\begin{aligned}\frac{dI}{dt} = &- \underbrace{k_f^I I R_S}_{\substack{\text{Anti-IL6R binding to}\\ \text{stem cells}}} + \underbrace{k_r^I C_S^I}_{\substack{\text{Ani-IL6R dissociation}\\ \text{from stem cells}}} - \underbrace{k_f^I I R_E}_{\substack{\text{Anti-IL6R binding to}\\ \text{progenitor cells}}} \\ &+ \underbrace{k_r^I C_E^I}_{\substack{\text{Anti-IL6R dissociation}\\ \text{from progenitor cells}}} - \underbrace{k_f^I I R_D}_{\substack{\text{Anti-IL6R binding to}\\ \text{differentiated cells}}} + \underbrace{k_r^I C_D^I}_{\substack{\text{IL6 dissociation}\\ \text{from differentiated cells}}} \\ &+ \underbrace{k_{12} I_s - k_{21} I}_{\text{Pharmacokinetics}} \end{aligned} \tag{3.3.7}$$

Underlying assumptions for this equations are: (i) the tumor resides in a pharmacokinetic compartment of its own, (ii) the binding rates are the same, independent of cell type; (iii) TCZ is transferred into the tumor from the systemic circulation at the same rate as the peripheral tissue, k_{12}; and (iv) the tumor volume is negligible compared to the volume of mouse; therefore the amount of the drug leaking into blood stream (at the rate k_{21}) will not affect the concentration of free TCZ in the systemic circulation. Thus, the full model after adding treatment with TCZ can be given by:

TCZ-Therapy Model

$$\begin{aligned}\frac{dS}{dt} &= \underbrace{\alpha_S P_S(S,\phi_S) S}_{\text{Stem cell self-renewal}} - \underbrace{\frac{\delta_S}{1+\gamma_S \phi_S} S}_{\text{Stem cell death}} \\ \frac{dE}{dt} &= \underbrace{A_{in}\alpha_S(1-P_S(S,\phi_S))S}_{\substack{\text{Amplified}\\ \text{stem cell differentiation}}} - \underbrace{\alpha_E E}_{\substack{\text{Progenitor cell}\\ \text{differentiation}}} - \underbrace{\frac{\delta_E}{1+\gamma_E\phi_E} E}_{\text{progenitor cell death}} \\ \frac{dD}{dt} &= \underbrace{2\alpha_E E}_{\substack{\text{progenitor cell}\\ \text{differentiation}}} - \underbrace{\frac{\delta_D}{1+\gamma_D\phi_D} D}_{\text{differentiated cell death}}\end{aligned}$$

$$
\begin{aligned}
\frac{dL}{dt} &= -\underbrace{k_f L R_S}_{\substack{\text{IL6 binding to}\\ \text{stem cells}}} + \underbrace{k_r C_S}_{\substack{\text{IL6 dissociation}\\ \text{from stem cells}}} - \underbrace{k_f L R_E}_{\substack{\text{IL6 binding to}\\ \text{progenitor cells}}} + \underbrace{k_r C_E}_{\substack{\text{IL6 dissociation}\\ \text{from progenitor cells}}} \\
&\quad - \underbrace{k_f L R_D}_{\substack{\text{IL6 binding to}\\ \text{differentiated cells}}} + \underbrace{k_r C_D}_{\substack{\text{IL6 dissociation}\\ \text{from differentiated cells}}} - \underbrace{\lambda_L L}_{\text{IL6 natural decay}} + \underbrace{\rho_T (S+E+D)}_{\substack{\text{IL-6 Production}\\ \text{by tumor cells}}} \\
\frac{dI}{dt} &= -\underbrace{k_f^I I R_S}_{\substack{\text{Anti-IL6R binding to}\\ \text{stem cells}}} + \underbrace{k_r^I C_S^I}_{\substack{\text{Ani-IL6R dissociation}\\ \text{from stem cells}}} - \underbrace{k_f^I I R_E}_{\substack{\text{Anti-IL6R binding to}\\ \text{progenitor cells}}} \\
&\quad + \underbrace{k_r^I C_E^I}_{\substack{\text{Anti-IL6R dissociation}\\ \text{from progenitor cells}}} - \underbrace{k_f^I I R_D}_{\substack{\text{Anti-IL6R binding to}\\ \text{differentiated cells}}} + \underbrace{k_r^I C_D^I}_{\substack{\text{IL6 dissociation}\\ \text{from differentiated cells}}} \\
&\quad + \underbrace{k_{12} I_s - k_{21} I}_{\text{Pharmacokinetics}} \\
\frac{dR_S}{dt} &= -\underbrace{k_f L R_S}_{\substack{\text{IL-6 binding to}\\ \text{stem cells}}} + \underbrace{k_r C_S}_{\substack{\text{IL-6 dissociation}\\ \text{from stem cells}}} + \underbrace{k_p C_S}_{\text{Recycling}} - \underbrace{k_f^I I R_S}_{\substack{\text{Anti-IL6R binding to}\\ \text{IL-6R}}} \\
&\quad + \underbrace{k_r^I C_S^I}_{\substack{\text{Anti-IL-6R dissociation}\\ \text{from stem cells}}} + \underbrace{R_{T_S} \mathscr{P}_{\mathscr{S}}(S, \phi_S)}_{\substack{\text{Generation of new } R_S\\ \text{via cell proliferation}}} - \underbrace{\frac{R_S}{R_S + C_S + C_S^I} R_{T_S} \mathscr{D}_{\mathscr{S}}(S, \phi_S)}_{\substack{\text{Loss of } R_S\\ \text{via cell death}}} \\
\frac{dC_S^I}{dt} &= +\underbrace{k_f^I I R_S}_{\substack{\text{Anti-IL6R binding to}\\ \text{IL-6R}}} - \underbrace{k_r^I C_S^I}_{\substack{\text{Ani-IL6R dissociation}\\ \text{from stem cells}}} - \underbrace{\frac{C_S^I}{R_S + C_S + C_S^I} R_{T_S} \mathscr{D}_{\mathscr{S}}(S, \phi_S)}_{\substack{\text{Loss of } C_S^I\\ \text{via cell death}}} \\
\frac{dC_S}{dt} &= +\underbrace{k_f L R_S}_{\text{IL6 binding to } R_S} - \underbrace{k_r C_S}_{\substack{\text{IL6 dissociation}\\ \text{from } R_S}} - \underbrace{k_p C_S}_{\text{Internalization}} - \underbrace{\frac{C_S}{R_S + C_S + C_S^I} R_{T_S} \mathscr{D}_{\mathscr{S}}(S, \phi_S)}_{\substack{\text{Loss of } C_S\\ \text{via cell death}}} \\
\frac{dR_E}{dt} &= -\underbrace{k_f L R_E}_{\substack{\text{IL-6 binding to}\\ \text{progenitor cells}}} + \underbrace{k_r C_E}_{\substack{\text{IL-6 dissociation}\\ \text{from progenitor cells}}} + \underbrace{k_p C_E}_{\text{Recycling}} - \underbrace{k_f^I I R_E}_{\substack{\text{Anti-IL6R binding to}\\ \text{IL-6R}}} \\
&\quad + \underbrace{k_r^I C_E^I}_{\substack{\text{Anti-IL-6R dissociation}\\ \text{from progenitor cells}}} + \underbrace{R_{T_E} \mathscr{P}_{\mathscr{E}}(E, \phi_E)}_{\substack{\text{Generation of new } R_E\\ \text{via cell proliferation}}} - \underbrace{\frac{R_E}{R_E + C_E + C_E^I} R_{T_E} \mathscr{D}_{\mathscr{E}}(E, \phi_E)}_{\substack{\text{Loss of } R_E\\ \text{via cell death}}}
\end{aligned}
$$

$$
\begin{aligned}
\frac{dC_E^I}{dt} &= + \underbrace{k_f^I I R_E}_{\substack{\text{Anti-IL6R binding to}\\ \text{IL-6R}}} - \underbrace{k_r^I C_E^I}_{\substack{\text{Ani-IL6R dissociation}\\ \text{from progenitor cells}}} - \underbrace{\frac{C_E^I}{R_E + C_E + C_E^I} R_{T_E} \mathscr{D}_{\mathscr{E}}(E, \phi_E)}_{\substack{\text{Loss of } C_E^I\\ \text{via cell death}}} \\
\frac{dC_E}{dt} &= + \underbrace{k_f L R_E}_{\text{IL6 binding to } R_E} - \underbrace{k_r C_E}_{\substack{\text{IL6 dissociation}\\ \text{from } R_E}} - \underbrace{k_p C_E}_{\text{Internalization}} - \underbrace{\frac{C_E}{R_E + C_E + C_E^I} R_{T_E} \mathscr{D}_{\mathscr{E}}(E, \phi_E)}_{\substack{\text{Loss of } C_E\\ \text{via cell death}}} \\
\frac{dR_D}{dt} &= - \underbrace{k_f L R_D}_{\substack{\text{IL-6 binding to}\\ \text{differentiated cells}}} + \underbrace{k_r C_D}_{\substack{\text{IL-6 dissociation}\\ \text{from differentiated cells}}} + \underbrace{k_p C_D}_{\text{Recycling}} - \underbrace{k_f^I I R_D}_{\substack{\text{Anti-IL6R binding to}\\ \text{IL-6R}}} \\
&\quad + \underbrace{k_r^I C_D^I}_{\substack{\text{Anti-IL-6R dissociation}\\ \text{from differentiated cells}}} + \underbrace{R_{T_D} \mathscr{P}_{\mathscr{D}}(E, \phi_D)}_{\substack{\text{Generation of new } R_D\\ \text{via cell proliferation}}} - \underbrace{\frac{R_D}{R_D + C_D + C_D^I} R_{T_D} \mathscr{D}_{\mathscr{D}}(E, \phi_D)}_{\substack{\text{Loss of } R_D\\ \text{via cell death}}} \\
\frac{dC_D^I}{dt} &= + \underbrace{k_f^I I R_D}_{\substack{\text{Anti-IL6R binding to}\\ \text{IL-6R}}} - \underbrace{k_r^I C_D^I}_{\substack{\text{Ani-IL6R dissociation}\\ \text{from differentiated cells}}} - \underbrace{\frac{C_D^I}{R_D + C_D + C_D^I} R_{T_D} \mathscr{D}_{\mathscr{D}}(D, \phi_D)}_{\substack{\text{Loss of } C_D^I\\ \text{via cell death}}} \\
\frac{dC_D}{dt} &= + \underbrace{k_f L R_D}_{\text{IL6 binding to } R_D} - \underbrace{k_r C_D}_{\substack{\text{IL6 dissociation}\\ \text{from } R_D}} - \underbrace{k_p C_D}_{\text{Internalization}} - \underbrace{\frac{C_D}{R_D + C_D + C_D^I} R_{T_D} \mathscr{D}_{\mathscr{D}}(D, \phi_D)}_{\substack{\text{Loss of } C_D\\ \text{via cell death}}}
\end{aligned}
$$

It is worth mentioning that similar to our calculations for Model (1), it can be shown that the equations for treatment model satisfy:

$$
\begin{aligned}
R_S &= R_{T_S} S - C_S - C_S^I \\
R_E &= R_{T_E} E - C_E - C_E^I \\
R_D &= R_{T_D} D - C_D - C_D^I
\end{aligned}
$$

Variables and parameter values related to anti-IL-6R treatment are tabulated in Tables 3.7 and 3.8, respectively.

Table 3.7: Variables Related to TCZ-Therapy Model.

Variable	Description	Units
I	Free anti-IL-6R antibody in the tumor	fmol
C_S^I	Anti-IL-6R–cell bound IL-6R complex on stem cells	fmol
C_E^I	Anti-IL-6R–cell bound IL-6R complex on progenitor cells	fmol
C_D^I	Anti-IL-6R–cell bound IL-6R complex on differentiated cells	fmol

Table 3.8: Parameter Values Related to Anti-IL-6R Treatment. $(^*)$ Vol_T is the volume of the tumor in μl and is equal to (volume of 1 million tumor cells) $\times$ (S+E+D), where, the volume of 1 tumor cell is $1 \times 10^{-6} \mu l$ Cunningham *et al.* (1999).

Parameters	Values	Units	Reference
k_f^I	$8.5/\text{Vol}_T$*	$\text{fmol}^{-1}\text{day}^{-1}$	Mihara *et al.* (2005)
k_r^I	21.6	day^{-1}	lens.org/092-218-642-694-833

3.3.3 Predicting the effect of TCZ therapy

We used the treatment model to investigate (predict) tumor response to administration of TCZ for 7 weeks. Once the tumor reached 125mm^3, at each time point $I_s(t)$ (given by Eq. 3.3.5) was calculated assuming that 1mg/kg or 5mg/kg of TCZ was added to the system via i.v. injection, weekly. $I_s(t)$ determined the amount of drug entering the tumor. Figure 3.12-A shows the model predictions for the amount of TCZ within the tumor for the two different doses. Our model predicts a 25% and 28% reduction in the tumor volume as compared with tumor volume without treatment for the two different dosing strategies (Figure 3.12-B). This result is very similar to the experimentally observed tumor reduction shown in Mochizuki *et al.* (2015) for UM-HMC-3B tumor xenografts.

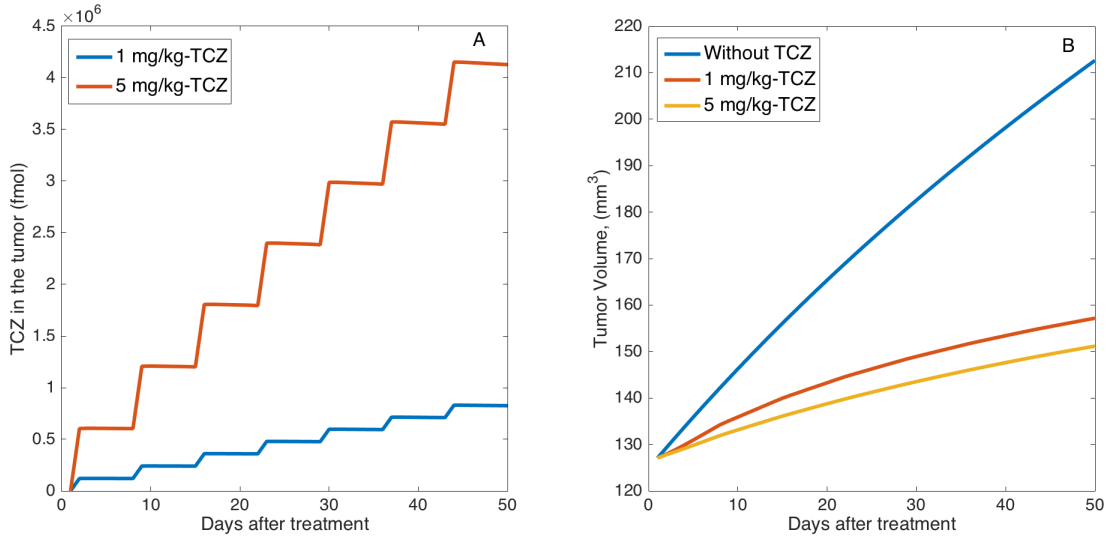

Figure 3.12: (A) The Amount of TCZ Within the Tumor During 7 Weeks of Treatment. (B) Model predictions of tumor volume vs. time after treatment with TCZ. 1mg/kg or 5 mg/kg of TCZ is administered weekly when tumor reaches 125 mm^3.

Small Doses of TCZ Are Sufficient to Outcompete IL-6

The reduction in tumor growth described above is due to the fact that TCZ competes with IL-6 for IL-6R, which results in a sudden decrease in the number of the IL-6–IL-6R signaling complexes. Our modeling framework allows us to quantify these molecular changes caused by administration of TCZ. As shown in Figure 3.13, after treatment there is an 80-90% decrease in the fraction of IL-6R occupied by IL-6 on tumor cells (ϕ_S, ϕ_E and ϕ_D). Figure 3.13 also shows that administration of doses as small as 1mg/kg of TCZ is sufficient for saturating IL-6R with TCZ molecules.

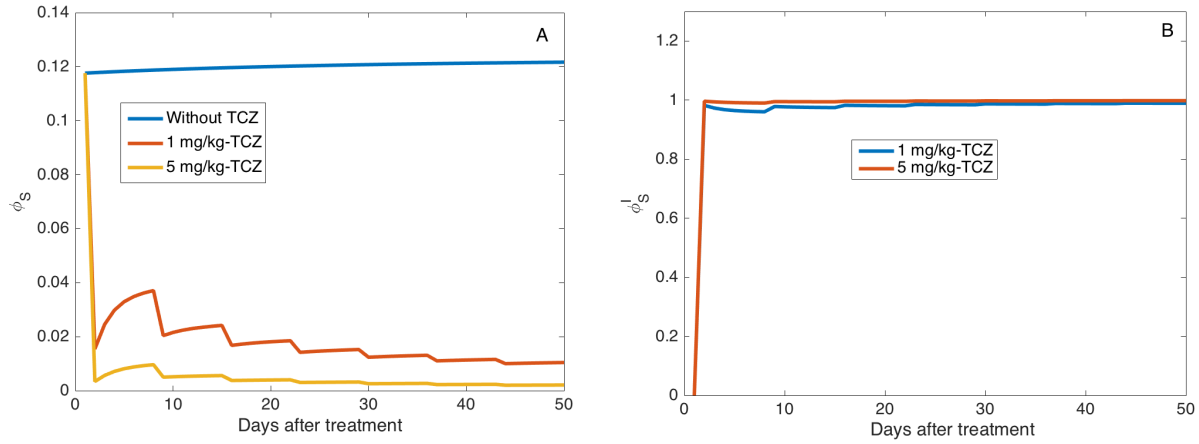

Figure 3.13: Model (1) Predictions after tTCZ-Therapy: (A) Model prediction of the temporal changes in the factional of IL-6 receptors on CSCs that are occupied by IL-6, ϕ_S, for the control case (no treatment, blue), 1 mg/kg TCZ (red), and 5 mg/kg TCZ (yellow). (B) Model prediction of the temporal changes in the factional of IL-6 receptors on CSCs that are occupied by TCZ, ϕ_I, for doses of 1 mg/kg TCZ (blue), and 5 mg/kg TCZ (red).

The Effect TCZ On Tumor Cell Death is More Pronounced Than Its Effect on CSC Self-renewal

Administration of TCZ interferes with the IL-6-mediated pathways that enhance the survival and self-renewal properties of CSCs. Specifically, the TCZ mediated reduction in IL-6-IL-6R signaling complexes decreases the pro-survival effects of IL-6, which results in an increase in the death rates of tumor cells. Our model predicts an increase of approximately 24-27% in the death rates of CSCs (Figure 3.14-A), progenitor cells and terminally differentiated cells. The same mechanism also results in a decrease in the probability of CSC self-renewal. Figure 3.14-B shows that TCZ causes an early reduction of 12-13% in the probability of CSC self-renewal. However, in the later weeks of treatment this difference decreases to 2-4%. This marginal impact of TCZ on the self-renewal probability is likely due to the tendency of CSCs to quickly reach to their equilibrium level (see Figure 3.4-D).

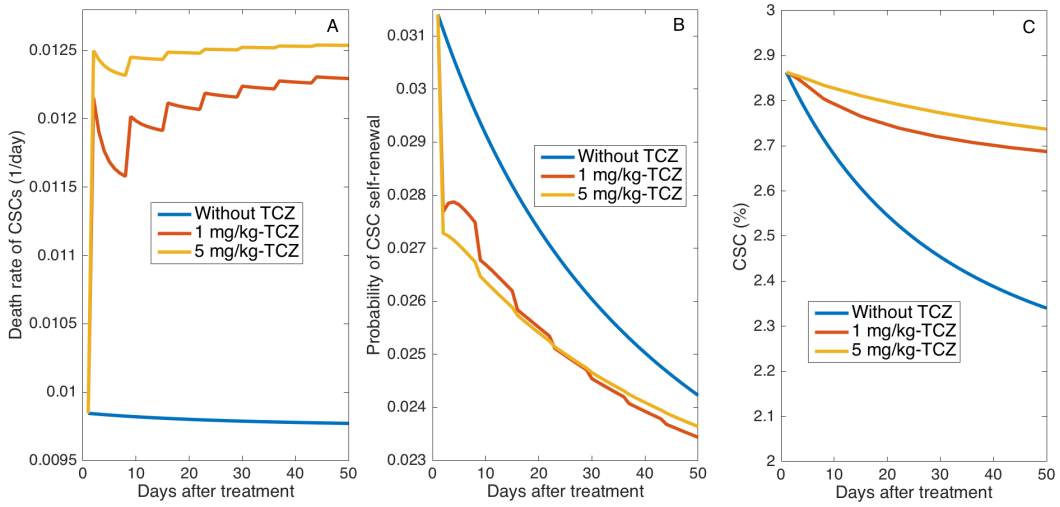

Figure 3.14: Model Predictions of the Temporal Impact of Administering 1mg/kg or 5mg/kg of TCZ on the (A) Death Rate of CSCs, (B) Probability of CSC Self-Renewal and (C) Percentage of CSCs Within the Tumor.

Changes in self-renewal and death rates of CSCs alter the fraction of CSCs post-treatment. Our model predicts that there is a small increase in the percentage of CSCs after treatment with TCZ (Figure 3.14-C). That is, the effect of TCZ on tumor volume is characterized by overall tumor reduction, but a final tumor composition that has a slightly larger proportion of CSCs. This could be due to the fact that stem cell self-renewal is tightly regulated in our model; see equation (5). Because cancer cells can become self-sufficient in growth signals, it is likely that CSCs could escape control from some of cellular regulatory mechanisms that are usually in place Hanahan and Weinberg (2000, 2011a). It has also been suggested that cancer stem cells are not as dependent on the stem cell niche as normal stem cells Li and Neaves (2006); Li and Li (2006). Should either of these situations occur, CSCs self-renewal would be less dependent on regulatory mechanisms and on niche signaling. This would significantly loosen the tightly regulated feedback interactions that dictate

the modes of stem-cell division in our model, resulting in a greater impact on the final stem cell percentage after therapy.

Interestingly, the minor increase in the percentage of CSCs predicted by our model is somewhat comparable to the results reported in Mochizuki *et al.* (2015) where they showed that TCZ has mixed effects on the fraction of CSCs post therapy. Given these varied results for the influence of TCZ on CSC percentage, we repeated the sensitivity analysis described above and considered PRCC values both before and after the first dose of TCZ. The results are shown in Figure 3.15. Comparing the most influential parameters (Figure 3.15) before and after treatment, suggests that administration of the drug does not change the set of parameters to which the percentage of CSCs is most sensitive. The most influential parameters remain A_{in}, δ_D and $P_{S_{min}}$.

Therefore, relaxing the assumptions associated with stem cell self-renewal is not the only possibility for reducing stem cell percentage post therapy. Figure 3.16 shows that even slightly increasing the amplification factor, A_{in}, after treatment begins also reduces the percentage of CSCs post therapy. Decreasing the maximum death rate for the terminally differentiated cancer cells has the same effect on the final percentage of CSCs.

The Frequency of Dosing Does Not Significantly Impact Tumor Response to TCZ

In the simulations above, TCZ was administered in doses of 1 or 5 mg/kg weekly for 7 weeks. Eventually, we will use modified and extended versions of this model to optimize the timing of combination therapies that deliver TCZ along with cy-

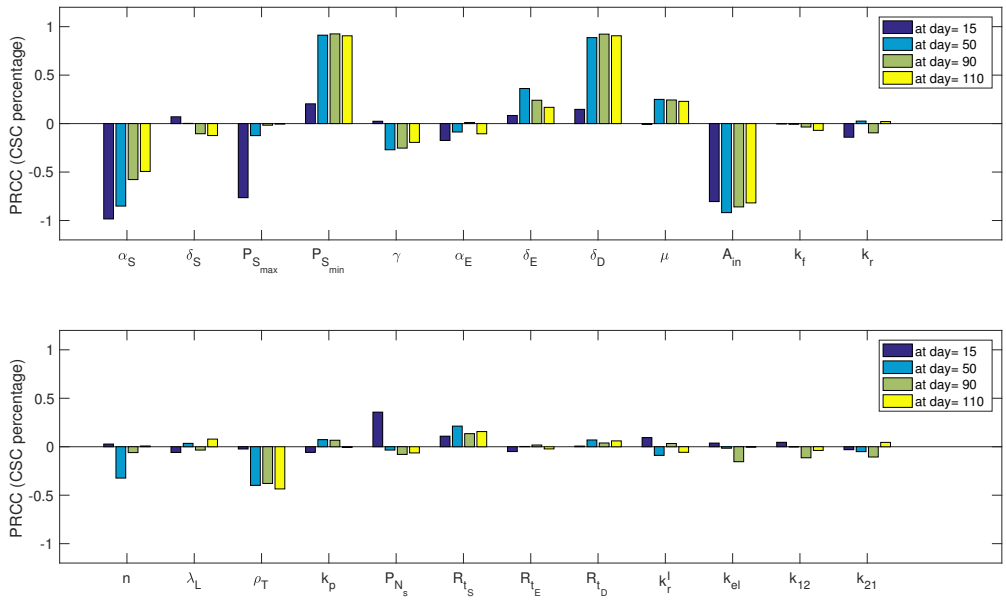

Figure 3.15: PRCC Values for the Parameters of TCZ-Therapy Model Using the Percentage of Caner Stem Cells as the Output of Interest.

totoxic chemotherapeutic agents like cisplatin. However, even for delivery as a single agent, the effect dose frequency has on tumor response is an open question. Furthermore, anti-cancer therapies may be selected based on the convenience of administration to patients, so understanding the differential effect of various dosing schedules is imperative. We therefore used the model to predict the effect of administering TCZ every 14, 21 and 28 days.

Figure 3.17 shows that increasing the time between doses does not lead to large increases in tumor volume. In fact, there little difference in tumor response among all of the dosing schedules tested. Together these results suggest that administering TCZ every 3 o 4 weeks might be preferable to weekly administration as this is clinically more desirable and it leads to only minor changes in tumor volume.

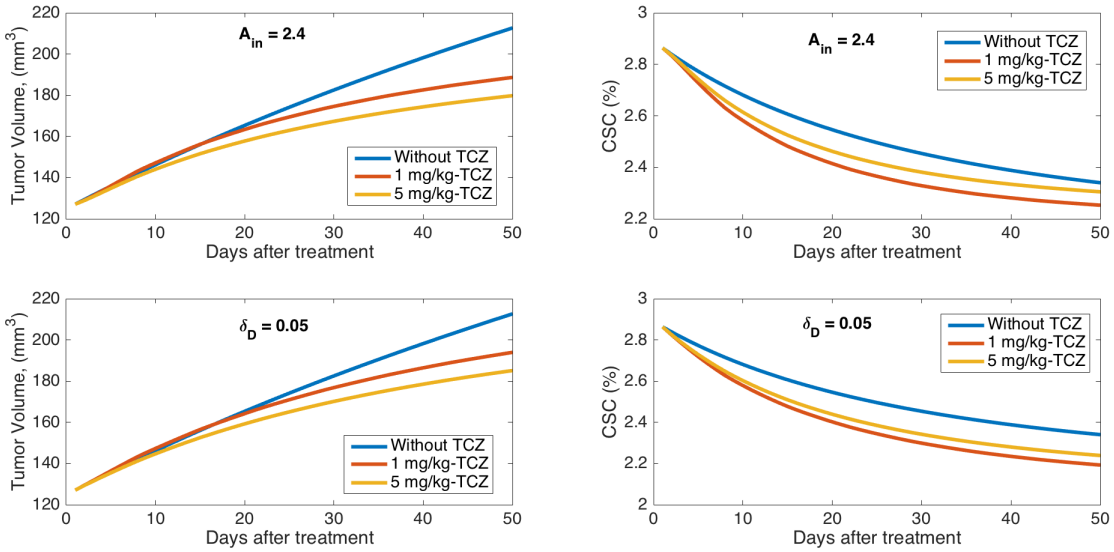

Figure 3.16: Model Predictions of the Tumor Volume Vs. Time for the Control Cases as Well as for Treatment With 1 or 5 mg/kg TCZ When the Amplification factor, A_{in}, is slightly increased from its baseline value (A) and when the differentiated cell death rate, δ_D is slightly decreased from baseline (C). Model predictions of the CSC percentage vs time for the control cases as well as for treatment with 1 or 5 mg/kg TCZ when the amplification factor, A_{in}, is slightly increased (B) and when the differentiated cell death rate, δ_D is slightly decreased (D).

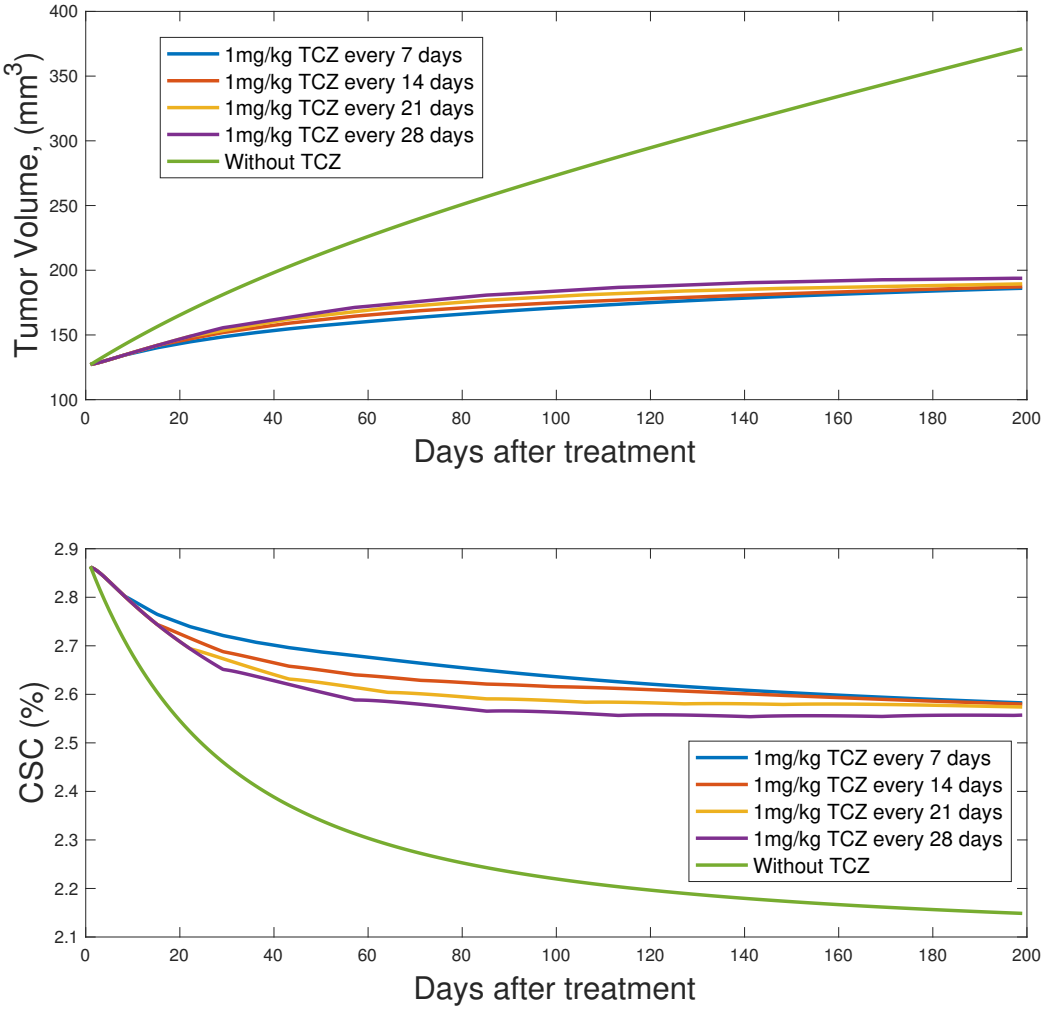

Figure 3.17: Model Predictions of the Tumor Volume vs. Time for the Control Case (no treatment) as well as for Treatment with 1 mg/kg TCZ Administered Every 7, 14, 21 and 28 Days.

3.4 Summary and Discussion

Tumors are often heterogeneous, being composed of multiple cell types with different phenotypic and molecular properties. Numerous studies have demonstrated that a small subset of cancer cells (cancer stem cells) is capable of tumor initiation. In order to improve patient outcomes for stem-cell driven cancers, substantial research is being focused on understanding the molecular biology of cancer stem cell (CSC) self-renewal in an attempt to selectively target pathways that give them their tumorigenic potential. Studies of HNSCC have shown that these cancers express high levels of Interleukin-6 (IL-6), and both autocrine and paracrine signaling have been hypothesized as mechanisms for their IL-6 mediated growth dynamics Krishnamurthy *et al.* (2014); Neiva *et al.* (2014). IL-6 has also been found to play an important role in the inducible formation of CSCs and their dynamic equilibrium with non-stem cells Kim *et al.* (2013). Taken together, this data has prompted investigations of the therapeutic inhibition of the IL-6 pathway by humanized anti-IL-6 antibodies and IL-6 receptor antagonists Mochizuki *et al.* (2015). Recent studies show that Il-6 ligand and receptor targeted therapies can inhibit the survival of cancer stem cells, delay tumor initiation, prevent tumor recurence, and enhance the anti-tumor effect of conventional chemotherapy Krishnamurthy *et al.* (2014); Mochizuki *et al.* (2015).

In this chapter we developed an experimentally based mathematical model for the growth dynamics of HNSCC tumor xenografts, which were generated by transplanting a small number of primary human cancer stem cells ($ALDH^{HIGH}CD44^{HIGH}$) in IL-6+/+ immunodeficient mice. The model includes the effects of human tumor cell-secreted IL-6 signaling on tumor cell survival and proliferation, and also

captures the effect of IL-6 on the probability of self-renewal for cancer stem cells. While numerous models of cancer stem cell driven tumor growth and related treatments have been proposed (see Weekes *et al.* (2014) for a review), few work across the scales proposed here, from signal initiation to tissue level cancer growth. This model is the first of its kind in that it incorporates the molecular details of IL-6 binding to its natural receptor, IL-6R and allows for the quantification of the temporal changes fractional occupancies of bound receptors and their impact on tumor growth dynamics. The model predictions suggest that a fractional occupancy of 12% on CSCs is sufficient to result in the experimentally observed tumor growth rate for these primary tumor xenografts. In the experimental system that is modeled here, the only source of human IL-6 is the cancer cells themselves, as murine IL-6 does not bind to human IL-6R (refs) and cannot directly initiate signals on human cells. We tested the situation where tumors cells were not able to produce IL-6 and found the final tumor sizes to be approximately 45% smaller without direct IL-6 signaling.

There is evidence that human endothelial cells, key players in tumor angiogenesis, can secrete even higher levels of IL-6 than tumor cells [26]. This implies that the 12% fractional occupancies predicted by our model leaves room for increases in proportion of bound IL-6R and more aggressive tumor growth when endothelial cells add to the amount of IL-6 available in the tumor microenvironment. There are several experimental models where human dermal microvascular endothelial cells (HDMECs) are transplanted in mice along with human tumor cells using biodegradable, polymer scaffolds Krishnamurthy *et al.* (2014); Mochizuki *et al.* (2015); Neiva *et al.* (2014); Nör *et al.* (2014). In Chapter 3, we develop a mathematical model of this experimental paradigm and our results show high fractional

occupancies of IL-6R lead to even greater interdependencies among IL-6, tumor growth dynamics and the tumorigenic potential of CSCs.

According to the cancer stem cell hypothesis, only a small minority of cells within the tumor be should tumor-initiating cells. Our model is also able to accurately capture the correct, experimentally observed tumor composition consisting of a very small proportion of cancer stem cells. A simple and general model of the cancer stem cell hypothesis was developed to track cell state transitions. Following Ganguly and Puri (2006); Gentry and Jackson (2013), each non-cancer stem cell is amplified by a factor, A_{in} upon entry into the progenitor cell pool. Interestingly, the best fit to the experimental data was obtained with a value of $A_{in} = 2$, which implies that each progenitor or transient amplifying cell (TAC) only undergoes a one round of amplification before differentiating into a terminally differentiated cell (see derivation in Section 2.1). The fact that our model predicts that little amplification occurs is not surprising because we are using data from human primary tumor cell xenografts, as opposed to cancer cell lines. Also, in the experimental system modeled here that does not include microenvironmental production of IL-6 by endothelial cells, tumors grow relatively slowly, which is consistent with limited amplification. In Chapter 3's extended version of this model that includes human endothelial cells, we are able to show that increased amplification and long with additional IL-6R engagement can predict the faster tumor growth dynamics that are observed with this experimental approach.

It also important to note that although we model the traditional cancer stem cell ideology (CSC $\longrightarrow$ Progenitor cell $\longrightarrow$ Terminal cell), which has been published for several solid tumor types Ganguly and Puri (2006), transient amplify-

ing cells are somewhat challenging to fit into the rubric of HNSCC cancer stem cells due to limitations in the identification of markers for these cells. Here we consider cancer stem cells to be $ALDH^{HIGH}CD44^{HIGH}$. Therefore, our three cellular compartment approach could be envisioned to consist of: $CD44^{HIGH}$ cells as the population of stem cells, various combinations of $ALDH^{HIGH}CD44^{LOW}$ and $ALDH^{LOW}CD44^{HIGH}$ cells as pool mixed cells, and finally $ALDH^{LOW}CD44^{LOW}$ cells. Our model predicts an amplification factor of 2 for the mixed cell pool. In terms of previously mentioned markers for HNSCC, our modeling paradigm can be thought of as each $ALDH^{HIGH}CD44^{HIGH}$ cell (S) asymmetrically dividing (with some probability) to become one $ALDH^{HIGH}CD44^{LOW}$ or one $ALDH^{LOW}CD44^{HIGH}$ (P) cell. That newly generated cell then divides to give rise to 2 new mixed cells. Those two mixed cells then eventually divide to give four terminally differentiated $ALDH^{LOW}CD44^{LOW}$ (D) cells. This limited amount of amplification predicted for primary tumor cells leads to relatively slow tumor growth and a tumor composition that consists of mostly differentiated cells. Interestingly, preliminary simulations of the experimental system that includes SCC cell lines and human endothelial cells shows that increased amplification and IL-6R engagement can lead not only lead to faster tumor growth, but can also change the tumor composition to be dominated by progenitor cells. It is important to note that this is simply one way to interpret the modeling results. Transitions between stem and non stem states have not been established temporally or in response therapy. These are topics that we will tackle in future modeling and experimental studies.

Uncertainty analysis offers a way to investigate the uncertainty in the model output due to the uncertainty in parameter inputs and sensitivity analysis assesses how variations in model outputs can be apportioned to different input sources.

Uncertainty and sensitivity analyses determines an approach to establish what factors and how affect model outputs. Depending on the type of system under study, different techniques should be performed Blower and Dowlatabadi (1994); Marino *et al.* (2008). For nonlinear but monotonic relationships between outputs and inputs (such as our model), partial rank correlation coefficient (PRCC) works well Marino *et al.* (2008). However, it is critical to mention that PRCC values are not accurate when the relationships between inputs and output is non-monotonic. With the sampling-based methods, such as PRCC, scatter plots enable us to graphically examine the nonlinearities, non-monotonicities, and correlations between model inputs and outputs Marino *et al.* (2008); Sanchez and Blower (1997). Therefore, we used scatter plots to determine the monotonicity dependence of the model outputs to its parameters (it is not shown) and then performed uncertainty and sensitivity analysis. The PRCC values revealed that the "most influential" parameters on tumor volume growth dynamics, percentage of cancer stem cells and fractional occupancies of IL-6R may change as tumor volume increases. For instance, our analysis showed that A_{in} is always one of the most influential parameters on tumor volume whereas other parameters are only influential early or late in tumor growth. For example, ρ has more impacts over the later stages rather than the early stage of tumor growth.

We also used the model to predict tumor response to administration of the humanized IL-6R monoclonal antibody, tocilizumab (TCZ), as monotherapy. Although the significance of IL-6 as a conceptual target for cancer treatment is well documented Krishnamurthy *et al.* (2014); Mochizuki *et al.* (2015), we still do not fully understand how anti-IL6 therapies work in vivo. Our simulations predict that as little as 1mg/kg of TCZ administered weekly for 7 weeks is sufficient to

result in tumor reduction and a sustained tumor slowing of tumor growth. The observed effect of TCZ is due to the fact that it competes with IL-6 for the signaling receptor, IL-6R. The model also predicts that administration of doses as small as 1mg/kg of TCZ is sufficient for saturating IL-6R with TCZ molecules. We expect that larger doses of TCZ may be necessary to achieve this same type of interference when xenografts include both human endothelial cells and human tumor cells, as in this case the amount of competing IL-6 in the tumor microenvironment will significantly increase.

We were interested to know if TCZ had greater impact on cell death or on cancer stem cell self-renewal, as changes in self-renewal and death rates of CSCs can alter the final proportion of CSCs post-treatment. The model predicts that effect of TCZ on cell death is more pronounced than its effect on CSC self-renewal, and this leads to an increase in the percentage of CSCs after treatment with TCZ. Therefore, for these primary tumor xenografts that do not include human endothelial cells, TCZ results in overall tumor reduction, but a final tumor composition that has a slightly larger proportion of CSCs. In [33], the effect of TCZ on Mucoepidermoid carcinoma (MEC) cell lines is investigated in an experimental setting that included human endothelial cells. In that study, they showed that TCZ has mixed effects on the fraction of CSCs post therapy. Interestingly, our preliminary model simulations of an experimental system that includes SCC cell lines and human endothelial cells shows that TCZ leads to a decrease in the proportion of cancer stem cells.

It is clear that IL-6 plays a critical role in the pathobiology of cancer, due in part to its impact on cancer stem cells. This has provided strong rationale for developing targeted inhibitors of IL-6. This modeling study not quantifies the influence on

IL-6 on primary tumor xenografts; it also provides some explanations for the various effects of TCZ on tumor growth and CSC percentage. In the next chapter, we will modify this model to describe xenografts that include human endothelial cells that have been demonstrated to produce IL-6 in greater amounts than tumor cells. We will also extend the model to include combination therapies with traditional chemotherapeutic agents, like cisplatin. This extended model can be used to simulate different dose-scheduling regimens in order to investigate synergism between the two therapies. Continued modeling efforts in this direction have the potential to shed light conditions under which TCZ sensitizes cancer cells for treatment with cisplatin and can be used to predict the optimal dose scheduling that will lead to maximal tumor response.

Chapter 4

MODELING IL-6 MEDIATED CROSS-TALK BETWEEN ENDOTHELIAL AND TUMOR CELLS AND ITS IMPACT COMBINATION THERAPIES

In Chapter 2 we showed that even relatively small amounts of tumor cell-secreted IL-6 can greatly enhance both tumor growth and the fraction of CSCs within xenograft tumors. Interestingly, there is experimental evidence that endothelial cells secrete significantly higher levels of IL-6 than HNSCC tumor cells Krishnamurthy *et al.* (2014). Furthermore, it has been shown that HNSCC CSCs reside in perivascular niches and depend on crosstalk with tumor associated endothelial cells for their survival and growth Krishnamurthy *et al.* (2010, 2014). Therefore, all of this motivates us to explore the effects of endothelial cell-secreted IL-6 on the survival, self-renewal and tumorigenic potentials of CSCs within the HNSCC tumor niche, and further leads us to investigate it as a potential therapeutic target against HNSCC tumors. In this chapter we extend the pre-treatment model in the previous chapter to a multi-scale framework to investigate the role of endothelial cell-secreted IL-6 on the bidirectional communication (i.e. crosstalk) between endothelial cells and tumor cells that contributes to and enhances key aspects of tumorigenesis. This model is used to describe tumor angiogenesis, vascular tumor growth, and response to treatment based on a SCID Mouse Model of Human Tumor Angiogenesis.

4.1 The Model for Cross-talk between Endothelial and Tumor Cells

In this section we follow the mathematical framework developed in Jain and Jackson (2017); Jain *et al.* (2008, 2009) to develop a mathematical model to describe

the interaction (crosstalk) between endothelial cells (ECs) and tumor cells (TCs) (Figure 4.1) in an *in vivo* setting, by tracking the cellular and molecular species used in the experiments described in Kaneko *et al.* (2007); Krishnamurthy *et al.* (2014); Neiva *et al.* (2009). The proposed pre-treatment EC-TC model operates at the following levels: (1) Intracellular level: regulation of signaling pathways that are critical to cell proliferation, apoptosis, and migration; (2) Cellular level: cell-surface dynamics of receptor-ligand binding and receptor activation that lead to intracellular signal transduction cascades; and (3) Tissue level: dynamics of signaling chemicals and anti-cancer agents within the tissue, tumor growth dynamics, and tumor and vascular response to treatment.

The pre-treatment model describes the temporal changes in cancer stem cell, progenitor cell and differentiated cell density, free tumor and/or endothelial cell-secreted IL-6 concentration, endothelial cell density, free VEGF concentration and free Bcl-2 mRNA expressed by both tumor and endothelial cells. VEGF can bind to its natural receptors, VEGFR1 and VEGFR2, on endothelial cells to form a signal initiating complex, VEGF–VEGFR2, and a decoy complex, VEGF–VEGFR1 Mac Gabhann and Popel (2007a); Zhang *et al.* (2010). Although VEGF can bind to VEGFR1 expressed on the surface of all tumor cell types, we do not consider it in our model. All of the IL-6 binding dynamics that were previously described in Chapter 2 carry over to this model.

Figure 4.1 is a schematic drawing illustrating the proposed mechanism behind the EC-TC crosstalk model. Under hypoxia tumor cells secrete VEGF. Tumor-cell secreted VEGF binds to its receptors, VEGFR1 and VEGFR2 on endothelial cells initiates a "paracrine" signaling cascade that results in phosphorylation of STAT3, Akt, and ERK in tumor cells. These phosphorylation enhance the expression of Bcl-2 and that Bcl-2 itself enhances the secretion of CXCL8 (IL-8) in both tumor and

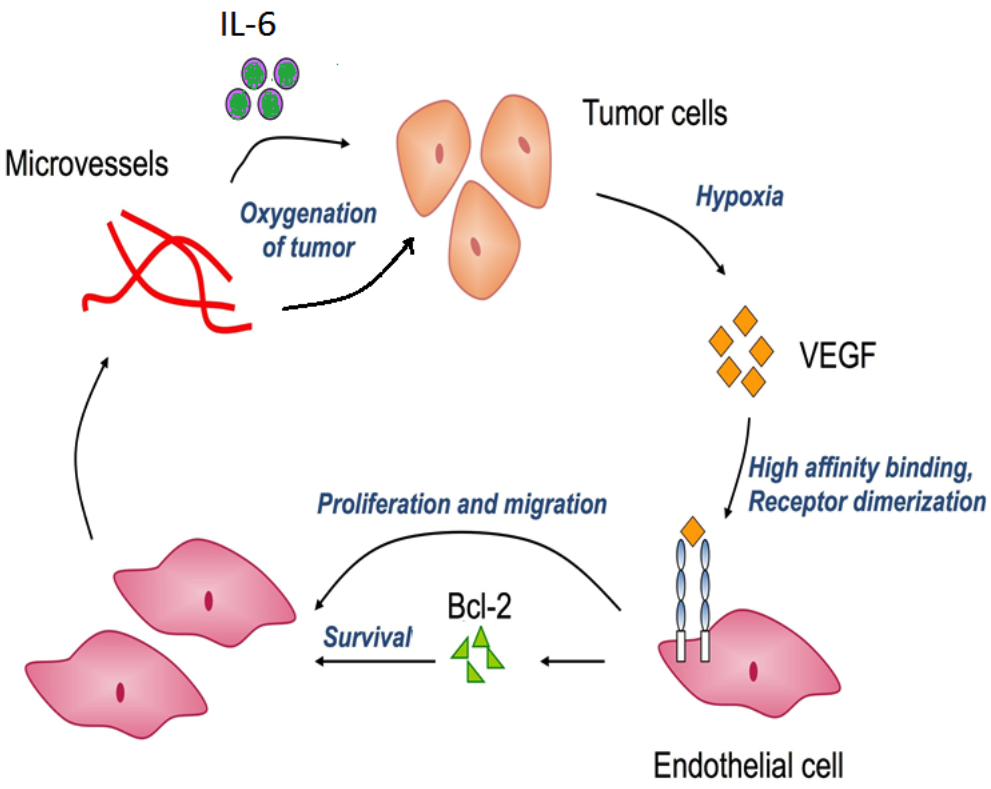

Figure 4.1: A Model for Crosstalk Between Endothelial and Tumor Cells: Tumor cell-secreted VEGF binds to its receptors, VEGFR1 and VEGFR2, to induce Bcl-2 expression. Bcl-2 signaling is sufficient to induce IL-6 secretion by endothelial cells. Kaneko *et al.* (2007); Neiva *et al.* (2009).

endothelial cells. Up-regulation of Bcl-2 is enough to enhance survival, proliferation and migration of endothelial cells. Enhanced proliferation rate of endothelial cells results in more secretion of IL-6 which itself leads to survival and proliferation of tumor cells, particularly CSCs. This bidirectional communication between endothelial cells and tumor cells is centrally regulated by VEGF (Figure 4.2), which would in turn maintain this feedback loop Kaneko *et al.* (2007); Neiva *et al.* (2009).

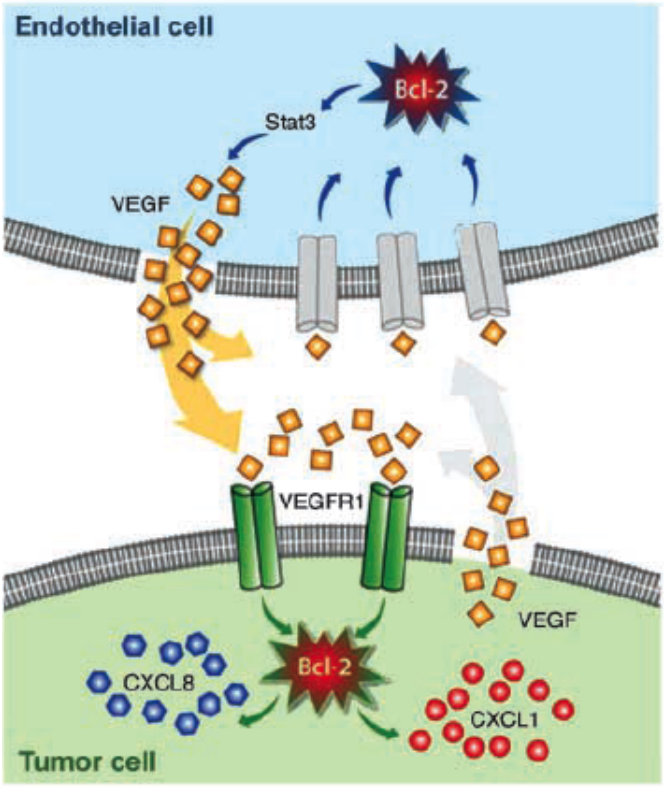

Figure 4.2: Model for Cross-Talk Between Endothelial and Tumor Cells Kaneko *et al.* (2007)

4.1.1 Equations related to the EC-TC model

We begin with a mathematical description of the interaction between endothelial and tumor cells by tracking the temporal changes in the cellular and molecular species listed in Table 3.1 below.

Human dermal microvascular endothelial cell response to VEGF

It has been reported that VEGF and its receptor VEGFR-1/2 are highly expressed in HNSCC and that VEGF-mediated signaling is vital for free ECs' proliferation, survival and migration Jain and Jackson (2017); Kaneko *et al.* (2007); Neiva *et al.*

Table 4.1: Description of Variables of EC-TC Cross-Talk Model

Variables	Description	Units
H	Endothelial cell number	#
S	Cancer stem cell number	#
E	Progenitor cell number	#
D	Differentiated cell number	#
A	Amount of free VEGF	fmol
$R_{H_{A1}}$	Number of free VEGFR1 on endothelial cells	fmol
$R_{H_{A2}}$	Number of free VEGFR2 on endothelial cells	fmol
$R_{S_{A1}}$	Number of free VEGFR1 on tumor stem cells	fmol
$R_{E_{A1}}$	Number of free VEGFR1 on tumor progenitor cells	fmol
$R_{D_{A1}}$	Number of free VEGFR1 on tumor differentiated cells	fmol
$C_{H_{A1}}$	VEGF-VEGFR1 complexes on endothelial cells	fmol
$C_{H_{A2}}$	VEGF-VEGFR2 complexes on endothelial cells	fmol
$C_{S_{A1}}$	VEGF-VEGFR1 complexes on stem cells	fmol
$C_{E_{A1}}$	VEGF-VEGFR1 complexes on progenitor cells	fmol
$C_{D_{A1}}$	VEGF-VEGFR1 complexes on differentiated cells	fmol
L	IL-6 secreted by endothelial & tumor (stem/non-stem) cells	fmol
R_S	IL-6R on tumor stem cells	fmol
R_E	IL-6R on tumor progenitor cells	fmol
R_D	IL-6R on tumor differentiated cells	fmol
C_S	IL-6–IL-6R complex on tumor stem cell	fmol
C_E	IL-6–IL-6R complex on tumor progenitor cell	fmol
C_D	IL-6–IL-6R complex on tumor differentiated cell	fmol
B_H	Bcl-2 mRNA expression level per endothelial cell	dimensionless
B_T	Total Bcl-2 mRNA expression level by tumor cells	dimensionless

(2009); Tarquinio *et al.* (2012). The VEGF induces Bcl-2 expression in ECs and that Bcl-2 expression level in tumor-associated endothelial cells play a direct role in tumor angiogenesis and tumor growth Neiva *et al.* (2009). It is also known that Bcl-2 enhances HNSCC survival, invasiveness and local recurrence Neiva *et al.* (2009). Therefore, the rate of change of the HDMEC population is chosen to be an increasing function of the fractional occupancies of VEGFR2 per cell ($\phi_{E_{A_2}}$). Also the rate of endothelial cell death is assumed to be a decreasing function of intracellular

Bcl-2 expression by ECs (B_H). Thus, we have:

$$\underbrace{\frac{dH}{dt}}_{\text{Endothelial cells}} = \underbrace{\alpha_H \phi_{H_{A2}}^{n_H} H}_{\substack{\text{Activated VEGFR2-mediated} \\ \text{proliferation}}} - \underbrace{\frac{\delta_H}{1+\beta_H B_H} H}_{\substack{\text{Bcl-2-mediated} \\ \text{apoptosis}}}, \tag{4.1.1}$$

where, $\phi_{H_{A2}} = \frac{C_{H_{A2}}}{R^t_{H_{A2}} H}$.

Tumor cells (stem/bulk cells) response to IL-6 and Bcl-2

The equations for the growth dynamics of tumor cells (CSCs, PCs and DCs) are the same as equations given in Chapter 2. However, we are now modeling EC-TC scaffolds, which are initially hypoxic. Because we are now interested in the impact of human ECs and, subsequent functional blood vessels on tumor growth, we modify the cancer cell equations so that cellular proliferation and death are dependent on oxygen concentration, N(t). The effects of oxygen pressure on tumor cell proliferation and survival are denoted by $\mathcal{H}(N - N_p)$ and $1 + \mathcal{H}(N_d - N)$, respectively, where $\mathcal{H}(.)$ is a Heaviside function. That is, when the oxygen level is less than a critical threshold ($N < N_p$), tumor cells stop proliferating and a further decline in oxygen level (below N_d) results in a doubling of the death rate of the tumor cells. Furthermore, the oxygen pressure level is assumed to be proportional to the vascular proportion of the tumor cell numbers defined as the percentage $V = 100H/(H + S + E + D)$, that is, $N(t) = \sigma_F(t)V$ where

$$\sigma_F(t) = \sigma_N \frac{e^{(t-3)}}{1 + e^{(t-3)}}$$

and σ_N denotes the proportionality constant relating the vessel fraction. The function σ_F gradually approaches to its maximum, σ_N. The rationale for choosing "3" in σ_F function is that it takes almost five or six days for human ECs to generate microvessel networks, connect to mouse vessels and begin blood flow. With "3" chosen, σ_F is approximately 0.95 at t=6 and is 1 with at least 8 digits of accuracy at t=13. It also takes three days for the function to reach half of its maximal. Thus, an increase in the proportion of ECs compared to the number of TCs results in an increase in the level of oxygenation within the tumor.

$$\underbrace{\frac{dS}{dt}}_{\text{Tumor stem cells}} = \underbrace{\alpha_S P_S(S,\phi_S) S\mathcal{H}(N-N_p)}_{\text{Stem cell self-renewal}} - \underbrace{\frac{\delta_S}{1+\gamma_S\phi_S} S[1+\mathcal{H}(N_d-N)]}_{\substack{\text{IL-6 \& Bcl-2 mediated} \\ \text{apoptosis}}}, \tag{4.1.2}$$

where,

$$P_S(S,\phi_S) = \frac{(P_{S_{max}} - P_{S_{min}}(\phi_S))P_{N_s}^n}{P_{N_s}^n + S^n} + P_{S_{min}}(\phi_S),$$

$$P_{S_{min}}(\phi_S) = \mu_S \left(P_{S_{max}} - P^*_{S_{min}}\right)\phi_S + P^*_{S_{min}}$$

$$\underbrace{\frac{dE}{dt}}_{\substack{\text{Tumor} \\ \text{progenitor cells}}} = \underbrace{A_{in}\alpha_S\left[1-P_S(S,\phi_S)\right]S\mathcal{H}(N-N_p)}_{\substack{\text{Amplified} \\ \text{stem cell differentiation}}} - \underbrace{\alpha_E E\mathcal{H}(N-N_p)}_{\substack{\text{Progenitor cell} \\ \text{differentiation}}}$$

$$- \underbrace{\frac{\delta_E}{1+\gamma_E\phi_E} E[1+\mathcal{H}(N_d-N)]}_{\substack{\text{IL-6 \& Bcl-2 mediated} \\ \text{apoptosis}}} \tag{4.1.3}$$

$$\underbrace{\frac{dD}{dt}}_{\substack{\text{Tumor} \\ \text{differentiated cells}}} = \underbrace{2\alpha_E E\mathcal{H}(N-N_p)}_{\substack{\text{progenitor cell} \\ \text{differentiation}}} - \underbrace{\frac{\delta_D}{1+\gamma_D\phi_D} D[1+\mathcal{H}(N_d-N)]}_{\substack{\text{IL-6 \& Bcl-2 mediated} \\ \text{apoptosis}}} \tag{4.1.4}$$

IL-6 uptake and binding by tumor cells

Once bound to its receptors, VEGF enhances expression level of Bcl-2 on both endothelial and tumor cells Kaneko *et al.* (2007); Neiva *et al.* (2009). That Bcl-2 signaling induces IL-6 expression in endothelial/tumor cells Neiva *et al.* (2009). Therefore, the last two terms in Eq. 4.1.1 describe the secretion of IL-6 by both endothelial and tumor cells, which are increasing functions of fraction of activated VEGFR1 and VEGFR2 on the tumor and endothelial cells, respectively. All the equations related to IL-6 binding dynamics are the same as previously described in Chapter 2.

$$\underbrace{\frac{dL}{dt}}_{\text{IL-6}} = -\underbrace{k_f L R_S}_{\substack{\text{IL-6 binding to}\\ \text{stem cells}}} + \underbrace{k_r C_S}_{\substack{\text{IL6 dissociation}\\ \text{from stem cells}}} - \underbrace{k_f L R_E}_{\substack{\text{IL-6 binding to}\\ \text{progenitor cells}}} + \underbrace{k_r C_E}_{\substack{\text{IL-6 dissociation}\\ \text{from progenitor cells}}}$$
$$- \underbrace{k_f L R_D}_{\substack{\text{IL-6 binding to}\\ \text{differentiated cells}}} + \underbrace{k_r C_D}_{\substack{\text{IL-6 dissociation}\\ \text{from differentiated cells}}} - \underbrace{\lambda_L L}_{\text{IL-6 natural decay}}$$
$$+ \underbrace{\rho_T (S+E+D)}_{\substack{\text{IL-6 Production}\\ \text{by tumor cells}}} + \underbrace{\rho_H \phi_{H_{A2}}^{n_L} H}_{\substack{\text{Bcl-2-mediated}\\ \text{IL-6 production}\\ \text{by ECs}}} \tag{4.1.5}$$

(4.1.6)

Following Chapter 2, we define:

$$\mathscr{P}_S(S, \phi_S) = \alpha_S P_S(S, \phi_S) S \mathcal{H}(N - N_p) \tag{4.1.7}$$

$$\mathscr{P}_E(E, \phi_S) = A_{in} \alpha_S [1 - P_S(S, \phi_S)] S \mathcal{H}(N - N_p) \tag{4.1.8}$$

$$\mathscr{P}_D(E) = 2\alpha_E E\mathcal{H}(N - N_p), \tag{4.1.9}$$

and,

$$\begin{aligned}
\mathscr{D}_S(\phi_S, B_S) &= \frac{\delta_S}{1+\gamma_S\phi_S} S[1 + \mathcal{H}(N_d - N)] && (4.1.10)\\
\mathscr{D}_E(\phi_E, B_E) &= \frac{\delta_E}{1+\gamma_E\phi_E} E[1 + \mathcal{H}(N_d - N)] + \alpha_E E\mathcal{H}(N - N_p) && (4.1.11)\\
\mathscr{D}_D(\phi_D, B_D) &= \frac{\delta_D}{1+\gamma_D\phi_D} D[1 + \mathcal{H}(N_d - N)] && (4.1.12)
\end{aligned}$$

Then we have:

$$\begin{aligned}
\frac{dR_S}{dt} = &- \underbrace{k_f L R_S}_{\substack{\text{IL-6 binding to}\\ \text{stem cells}}} + \underbrace{k_r C_S}_{\substack{\text{IL-6 dissociation}\\ \text{from stem cells}}} + \underbrace{k_p C_S}_{\text{Recycling}} + \underbrace{R_{T_S}\mathscr{P}_S(S, \phi_S)}_{\substack{\text{Generation of new } R_S\\ \text{via cell proliferation}}}\\
&\underbrace{- \frac{R_S}{R_S + C_S} R_{T_S}\mathscr{D}_S(\phi_S, B_S)}_{\substack{\text{Loss of } R_S\\ \text{via cell death}}} && (4.1.13)\\
\frac{dR_E}{dt} = &- \underbrace{k_f L R_E}_{\substack{\text{IL-6 binding to}\\ \text{progenitor cells}}} + \underbrace{k_r C_E}_{\substack{\text{IL-6 dissociation}\\ \text{from progenitor cells}}} + \underbrace{k_p C_E}_{\text{Recycling}} + \underbrace{R_{T_E}\mathscr{P}_E(E, \phi_S)}_{\substack{\text{Generation of new } R_E\\ \text{via cell proliferation}}}\\
&\underbrace{- \frac{R_E}{R_E + C_E} R_{T_E}\mathscr{D}_E(\phi_E, B_E)}_{\substack{\text{Loss of } R_E\\ \text{via cell death}}} && (4.1.14)\\
\frac{dR_D}{dt} = &- \underbrace{k_f L R_D}_{\substack{\text{IL-6 binding to}\\ \text{differentiated cells}}} + \underbrace{k_r C_D}_{\substack{\text{IL-6 dissociation}\\ \text{from differentiated cells}}} + \underbrace{k_p C_D}_{\text{Recycling}} + \underbrace{R_{T_D}\mathscr{P}_D(E)}_{\substack{\text{Generation of new } R_D\\ \text{via cell proliferation}}}\\
&\underbrace{- \frac{R_D}{R_D + C_D} R_{T_D}\mathscr{D}_D(\phi_S, B_D)}_{\substack{\text{Loss of } R_D\\ \text{via cell death}}} && (4.1.15)
\end{aligned}$$

$$\frac{dC_S}{dt} = \underbrace{k_f L R_S}_{\text{IL-6 binding to } R_S} - \underbrace{k_r C_S}_{\substack{\text{IL-6 dissociation} \\ \text{from } R_S}} - \underbrace{k_p C_S}_{\text{Internalization}} - \underbrace{\frac{C_S}{R_S + C_S} R_{T_S} \mathscr{D}_S(\phi_S, B_S)}_{\substack{\text{Loss of } C_S \\ \text{via cell death}}} \tag{4.1.16}$$

$$\frac{dC_E}{dt} = \underbrace{k_f L R_E}_{\text{IL-6 binding to } R_E} - \underbrace{k_r C_E}_{\substack{\text{IL-6 dissociation} \\ \text{from } R_E}} - \underbrace{k_p C_E}_{\text{Internalization}} - \underbrace{\frac{C_E}{R_E + C_E} R_{T_E} \mathscr{D}_E(\phi_E, B_E)}_{\substack{\text{Loss of } C_E \\ \text{via cell death}}} \tag{4.1.17}$$

$$\frac{dC_D}{dt} = \underbrace{k_f L R_D}_{\text{IL-6 binding to } R_D} - \underbrace{k_r C_D}_{\substack{\text{IL-6 dissociation} \\ \text{from } R_D}} - \underbrace{k_p C_D}_{\text{Internalization}} - \underbrace{\frac{C_D}{R_D + C_D} R_{T_D} \mathscr{D}_D(\phi_D, B_D)}_{\substack{\text{Loss of } C_D \\ \text{via cell death}}} \tag{4.1.18}$$

Tumor and/or endothelial cell-secreted VEGF

$$\underbrace{\frac{dA}{dt}}_{\text{VEGF}} = \underbrace{-k^f_{H1} R_{H_{A1}} A + k^r_{H1} C_{H_{A1}} - k^f_{H2} R_{H_{A2}} A + k^r_{H2} C_{H_{A2}}}_{\text{reaction with VEGFR1/2 on endothelial cells}} - \underbrace{k^f_T R_{S_{A1}} A + k^r_T C_{S_{A1}}}_{\substack{\text{reaction with VEGFR1} \\ \text{on stem cells}}} - \underbrace{k^f_T R_{E_{A1}} A + k^r_T C_{E_{A1}}}_{\substack{\text{reaction with VEGFR1} \\ \text{on progenitor cells}}} - \underbrace{k^f_T R_{D_{A1}} A + k^r_T C_{D_{A1}}}_{\substack{\text{reaction with VEGFR1} \\ \text{on differentiated cells}}} - \underbrace{\lambda_A A}_{\substack{\text{natural} \\ \text{decay}}} + \underbrace{\alpha_A \frac{B_H}{1 + \beta_A B_H} H}_{\substack{\text{Bcl-2-mediated production} \\ \text{by endothelial cells}}} + \underbrace{\frac{\nu_A}{1 + e^{-\kappa_A (N_h - N)}} (S + E + D)}_{\substack{\text{hypoxia-mediated VEGF} \\ \text{production by stem/bulk cells}}} \tag{4.1.19}$$

VEGF uptake and binding by endothelial cells

The equations for VEGFR1 and VEGFR2 binding are given below and they are derived analogously to the equations given for IL-6R binding.

$$\underbrace{\frac{dR_{H_{A1}}}{dt}}_{\substack{\text{free-VEGFR1}\\ \text{receptors}\\ \text{on ECs}}} = \underbrace{-k^f_{H1}R_{H_{A1}}A + k^r_{H1}C_{H_{A1}} + k^p_{H1}C_{H_{A1}}}_{\text{reaction with VEGF}} + \underbrace{R^t_{H_{A1}}\alpha_H\phi^{n_H}_{H_{A2}}H}_{\substack{\text{production due to}\\ \text{endothelial cell proliferation}}}$$
$$\underbrace{-\frac{R_{H_{A1}}}{R_{H_{A1}}+C_{H_{A1}}}R^t_{H_{A1}}\frac{\delta_H}{1+\beta_H B_H}H}_{\substack{\text{loss due to}\\ \text{endothelial cell apoptosis}}} \tag{4.1.20}$$

$$\underbrace{\frac{dR_{H_{A2}}}{dt}}_{\substack{\text{free-VEGFR2}\\ \text{receptors}\\ \text{on ECs}}} = \underbrace{-k^f_{H2}R_{H_{A2}}A + k^r_{H2}C_{H_{A2}} + k^p_{H2}C_{H_{A2}}}_{\text{reaction with VEGF}} + \underbrace{R^t_{H_{A2}}\alpha_H\phi^{n_H}_{H_{A2}}H}_{\substack{\text{production due to}\\ \text{endothelial cell proliferation}}}$$
$$\underbrace{-\frac{R_{H_{A2}}}{R_{H_{A2}}+C_{H_{A2}}}R^t_{H_{A2}}\frac{\delta_H}{1+\beta_H B_H}H,}_{\substack{\text{loss due to}\\ \text{endothelial cell apoptosis}}} \tag{4.1.21}$$

$$\underbrace{\frac{dC_{H_{A1}}}{dt}}_{\substack{\text{VEGF-VEGFR1}\\ \text{complex}\\ \text{on ECs}}} = \underbrace{k^f_{H1}R_{H_{A1}}A - k^r_{H1}C_{H_{A1}} - k^p_{H1}C_{H_{A1}}}_{\substack{\text{VEGFR1 activation by VEGF}\\ \text{on endothelial cells}}} - \underbrace{\frac{C_{H_{A1}}}{R_{H_{A1}}+C_{H_{A1}}}R^t_{H_{A1}}\frac{\delta_H}{1+\beta_H B_H}H}_{\substack{\text{loss due to}\\ \text{endothelial cell apoptosis}}} \tag{4.1.22}$$

$$\underbrace{\frac{dC_{H_{A2}}}{dt}}_{\substack{\text{VEGF-VEGFR2}\\ \text{complex}\\ \text{on ECs}}} = \underbrace{k^f_{H2}R_{H_{A2}}A - k^r_{H2}C_{H_{A2}} - k^p_{H2}C_{H_{A2}}}_{\substack{\text{VEGFR2 activation by VEGF}\\ \text{on endothelial cells}}} - \underbrace{\frac{C_{H_{A2}}}{R_{H_{A2}}+C_{H_{A2}}}R^t_{H_{A2}}\frac{\delta_H}{1+\beta_H B_H}H}_{\substack{\text{loss due to}\\ \text{endothelial cell apoptosis}}} \tag{4.1.23}$$

The Bcl-Family of Proteins

Bcl-2 mRNA is constitutively expressed within ECs, and undergoes natural decay. VEGF signals through VEGFR1 and VEGFR2 on ECs and induces expression of Bcl-2 and the proangiogenic chemokines such as CXCL1 and CXCL8 in ECs. Combining these processes we obtain the following equations for Bcl-2 mRNA expression in ECs.

$$\underbrace{\frac{dB_H}{dt}}_{\substack{\text{Bcl-2 produced}\\ \text{by ECs}}} = \underbrace{\chi_H}_{\substack{\text{Constitutive}\\ \text{expression}\\ \text{by ECs}}} + \underbrace{\eta_H \frac{\phi_{H_{A2}}^{n_B}}{\omega_H^{n_B} + \phi_{H_{A2}}^{n_B}}}_{\substack{\text{Activated VEGFR2-}\\ \text{mediated production}\\ \text{by ECs}}} - \underbrace{\delta_B B_H}_{\substack{\text{natural}\\ \text{decay}}} \tag{4.1.24}$$

4.1.2 Reduced form of EC-TC cross-talk model

EC-TC cross-talk model can be reduced to the following model with five less equations by using the fact that,

$$R_S = R_{T_S} S - CS \tag{4.1.25}$$

$$R_E = R_{T_E} E - CE \tag{4.1.26}$$

$$R_D = R_{T_D} D - CD \tag{4.1.27}$$

$$R_{H_{A1}} = R_{H_{A1}}^t H - C_{H_{A1}} \tag{4.1.28}$$

$$R_{H_{A2}} = R_{H_{A2}}^t H - C_{H_{A2}} \tag{4.1.29}$$

Thus, we have:

$$\frac{dH}{dt} = \underbrace{\alpha_H \phi_{H_{A2}}^{n_H} H}_{\substack{\text{Activated VEGFR2-mediated} \\ \text{proliferation}}} - \underbrace{\frac{\delta_H}{1+\beta_H B_H} H}_{\substack{\text{Bcl-2-mediated} \\ \text{apoptosis}}} \tag{4.1.30}$$

$$\frac{dS}{dt} = \underbrace{\alpha_S P_S(S,\phi_S) S \mathcal{H}(N-N_p)}_{\text{Stem cell self-renewal}} - \underbrace{\frac{\delta_S}{1+\gamma_S \phi_S} S[1+\mathcal{H}(N_d-N)]}_{\substack{\text{IL-6 \& Bcl-2 mediated} \\ \text{apoptosis}}} \tag{4.1.31}$$

$$\begin{aligned}\frac{dE}{dt} = & \underbrace{A_{in}\alpha_S \left[1-P_S(S,\phi_S)\right] S \mathcal{H}(N-N_p)}_{\substack{\text{Amplified} \\ \text{stem cell differentiation}}} - \underbrace{\alpha_E E \mathcal{H}(N-N_p)}_{\substack{\text{Progenitor cell} \\ \text{differentiation}}} \\ & - \underbrace{\frac{\delta_E}{1+\gamma_E \phi_E} E[1+\mathcal{H}(N_d-N)]}_{\substack{\text{IL-6 \& Bcl-2 mediated} \\ \text{apoptosis}}}\end{aligned} \tag{4.1.32}$$

$$\frac{dD}{dt} = \underbrace{2\alpha_E E \mathcal{H}(N-N_p)}_{\substack{\text{progenitor cell} \\ \text{differentiation}}} - \underbrace{\frac{\delta_D}{1+\gamma_D \phi_D} D[1+\mathcal{H}(N_d-N)]}_{\substack{\text{IL-6 \& Bcl-2 mediated} \\ \text{apoptosis}}} \tag{4.1.33}$$

$$\begin{aligned}\underbrace{\frac{dL}{dt}}_{\text{IL-6}} = & - \underbrace{k_f L R_S}_{\substack{\text{IL-6 binding to} \\ \text{stem cells}}} + \underbrace{k_r C_S}_{\substack{\text{IL6 dissociation} \\ \text{from stem cells}}} - \underbrace{k_f L R_E}_{\substack{\text{IL-6 binding to} \\ \text{progenitor cells}}} + \underbrace{k_r C_E}_{\substack{\text{IL-6 dissociation} \\ \text{from progenitor cells}}} \\ & - \underbrace{k_f L R_D}_{\substack{\text{IL-6 binding to} \\ \text{differentiated cells}}} + \underbrace{k_r C_D}_{\substack{\text{IL-6 dissociation} \\ \text{from differentiated cells}}} - \underbrace{\lambda_L L}_{\text{IL-6 natural decay}} \\ & + \underbrace{\rho_T (S+E+D)}_{\substack{\text{IL-6 Production} \\ \text{by tumor cells}}} + \underbrace{\rho_H \phi_{H_{A2}}^{n_L} H}_{\substack{\text{Bcl-2-mediated} \\ \text{IL-6 production} \\ \text{by ECs}}}\end{aligned} \tag{4.1.34}$$

$$\begin{aligned}\frac{dC_S}{dt} = & \underbrace{k_f L R_S}_{\text{IL-6 binding to } R_S} - \underbrace{k_r C_S}_{\substack{\text{IL-6 dissociation} \\ \text{from } R_S}} - \underbrace{k_p C_S}_{\text{Internalization}} \\ & - \underbrace{C_S \mathscr{D}_S(\phi_S, B_S)}_{\substack{\text{Loss of } C_S \\ \text{via cell death}}}\end{aligned} \tag{4.1.35}$$

$$\frac{dC_E}{dt} = \underbrace{k_f L R_E}_{\text{IL-6 binding to } R_E} - \underbrace{k_r C_E}_{\substack{\text{IL-6 dissociation} \\ \text{from } R_E}} - \underbrace{k_p C_E}_{\text{Internalization}} - \underbrace{C_E \mathscr{D}_E(\phi_E, B_E)}_{\substack{\text{Loss of } C_E \\ \text{via cell death}}} \tag{4.1.36}$$

$$\frac{dC_D}{dt} = \underbrace{k_f L R_D}_{\text{IL-6 binding to } R_D} - \underbrace{k_r C_D}_{\substack{\text{IL-6 dissociation} \\ \text{from } R_D}} - \underbrace{k_p C_D}_{\text{Internalization}} - \underbrace{C_D \mathscr{D}_D(\phi_D, B_D)}_{\substack{\text{Loss of } C_D \\ \text{via cell death}}} \tag{4.1.37}$$

$$\frac{dA}{dt} = \underbrace{-k^f_{H1} R_{H_{A1}} A + k^r_{H1} C_{H_{A1}} - k^f_{H2} R_{H_{A2}} A + k^r_{H2} C_{H_{A2}}}_{\text{reaction with VEGFR1/2 on endothelial cells}} - \underbrace{\lambda_A A}_{\substack{\text{natural} \\ \text{decay}}} + \underbrace{\alpha_A \frac{B_H}{1+\beta_A B_H} H}_{\substack{\text{Bcl-2-mediated production} \\ \text{by endothelial cells}}} + \underbrace{\frac{\nu_A}{1+e^{-\kappa_A(N_h - N)}}(S+E+D)}_{\substack{\text{hypoxia-mediated VEGF} \\ \text{production by stem/bulk cells}}} \tag{4.1.38}$$

$$\frac{dC_{H_{A1}}}{dt} = \underbrace{k^f_{H1} R_{H_{A1}} A - k^r_{H1} C_{H_{A1}} - k^p_{H1} C_{H_{A1}}}_{\substack{\text{VEGFR1 activation by VEGF} \\ \text{on endothelial cells}}} - \underbrace{C_{H_{A1}} \frac{\delta_H}{1+\beta_H B_H}}_{\substack{\text{loss due to} \\ \text{endothelial cell apoptosis}}} \tag{4.1.39}$$

$$\frac{dC_{H_{A2}}}{dt} = \underbrace{k^f_{H2} R_{H_{A2}} A - k^r_{H2} C_{H_{A2}} - k^p_{H2} C_{H_{A2}}}_{\substack{\text{VEGFR2 activation by VEGF} \\ \text{on endothelial cells}}} - \underbrace{C_{H_{A2}} \frac{\delta_H}{1+\beta_H B_H}}_{\substack{\text{loss due to} \\ \text{endothelial cell apoptosis}}} \tag{4.1.40}$$

$$\frac{dB_H}{dt} = \underbrace{\chi_H}_{\substack{\text{Constitutive} \\ \text{expression} \\ \text{by ECs}}} + \underbrace{\eta_H \frac{\phi^{n_B}_{H_{A2}}}{\omega^{n_B}_H + \phi^{n_B}_{H_{A2}}}}_{\substack{\text{Activated VEGFR2-} \\ \text{mediated production} \\ \text{by ECs}}} - \underbrace{\delta_B B_H}_{\substack{\text{natural} \\ \text{decay}}} \tag{4.1.41}$$

Similar to model (1) in Chapter 2, the EC-TC crosstalk represents the tumor growth dynamics in three levels: (1) intracellular; (2) cellular/molecular; and (3) tissue level. The equations $\frac{dH}{dt}$, $\frac{dS}{dt}$, $\frac{dE}{dt}$ and $\frac{dD}{dt}$ in the model describe the tumor

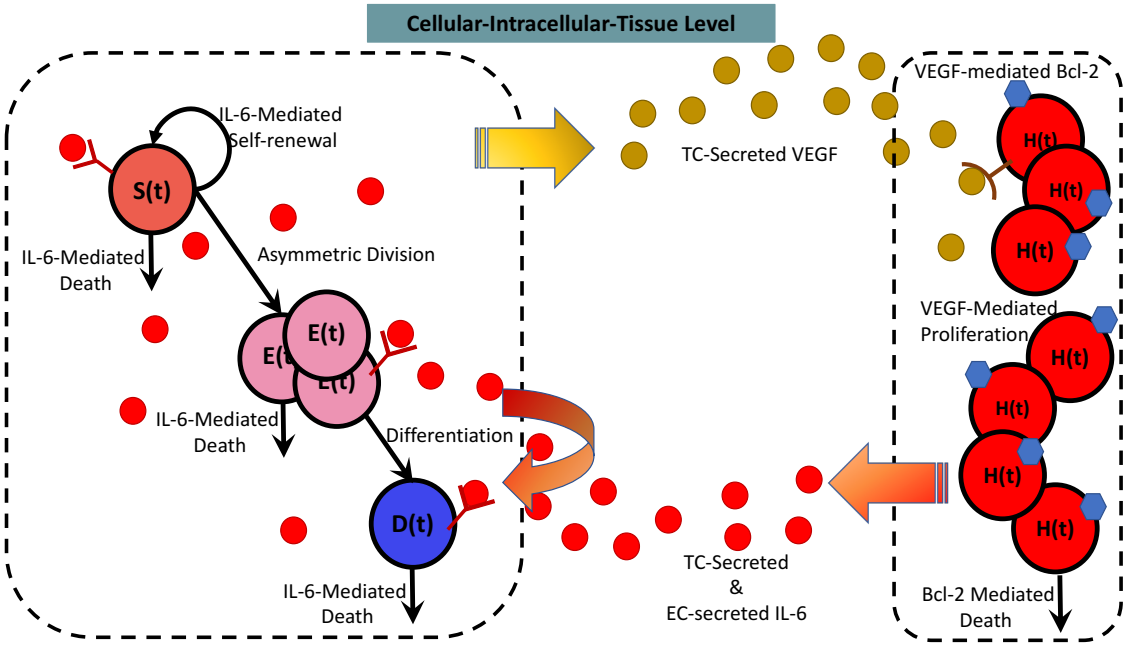

Figure 4.3: Representing the Different Scales Represented in the EC-TC Crosstalk Model.

growth at the tissue level whereas the equations related to IL-6 and VEGF represent the cell surface dynamics of receptor-ligand bindings. Similarly, binding IL-6 to IL-6R on TCs and VEGF to its receptors on ECs activates the receptors on the cells' membrane which leads to intracellular signal transduction cascade which by itself impacts the tumor growth dynamics. Tracking the temporal changes of the number of IL-6-IL-6R and VEGF-VEGFR1/2 complex molecules at the intracellular level allows us to quantify the impacts of IL-6 mediated pathways on CSC self-renewal potentials and tumor cell death as well as the VEGF-mediated pathways on proliferation and death of the ECs. A schematic representation of the incorporated scales in the EC-TC crosstalk model is given in Figure 4.3.

4.2 Numerical Analysis of Pre-treatment Tumor Growth

In this section, we first introduce the parameter values that we can find from the literature. For parameters which there is no information, we estimate them by finding the best fit of the pre-treatment EC-TC model to experimental data. Then we use the estimated parameter valued to numerically explore the impact of EC-IL-6 on tumor growth and compare the results with experimental data. The ultimate goal is to add treatment to the current model and study the responses of TCs to combination therapies.

4.2.1 Experimental data

To begin to evaluate the role of endothelial cell-secreted IL-6 on the tumorigenic potential and survival of primary human HNSCC CSCs, Krishnamurthy et al. Krishnamurthy *et al.* (2014) silenced the IL-6 secretion in endothelial cells and used these cells to generate tumor xenografts with a humanized vasculature. Briefly, immediately after surgical removal of the primary tumor from patients with HNSCC, they sorted and seeded 1'000 HNSCC CSCs ($ALDH^{HIGH}CD44^{HIGH}$ cells) into IL-6 +/+ immunodeficient mice along with 5×10^5 either IL-6-silenced endothelial cells (HDMEC-shRNA-IL-6) or endothelial cells transduced with empty lentiviral vectors (HDMEC-shRNA-C) in poly(L-lactic) acid biodegradable scaffolds. Bilateral scaffolds were implanted subcutaneously in the dorsum of each mouse. Tumor volumes were calculated and recorded over 81 days after implantation. Figure 4.4 shows the relevant data directly taken from Krishnamurthy *et al.* (2014). Red data points in Figure 4.4-C show the volume of xenograft tumors vascularized with IL-6-silenced ECs (HDMEC-shRNA-IL-6) and the blue data points show the volume of the xenograft tumors vascularized with control ECs (HDMEC-shRNA-C) over

days after implantation. When 1'000 $ALDH^{HIGH}CD44^{HIGH}$ cells were transplanted with HDMEC-shRNA-IL-6 cells into the IL-6 +/+ mice, the average tumor volume was smaller as compared to the transplantation of 1'000 $(ALDH^{HIGH}CD44^{HIGH})$ with HDMEC-shRNA-C cells, demonstrating that endothelial cell-secreted IL-6 enhances the tumorigenic potential of CSCs (in vivo). Moreover, they evaluated the percentage of CSCs in those xenograft tumors and observed that ablation of EC-IL-6 within the tumor microenvironment reduced the fraction of CSCs in tumor (Figure 4.4-D).

4.2.2 Estimating baseline parameter values

A list of parameter values found from the literature are tabulated in Table 4.2. The baseline values for the remaining parameters are estimated by fitting the pre-treatment EC-TC model to the control ECs. Similar to the procedure applied in Chapter 2, we use *Monte Carlo parameter sweep method* Cowan (1998) to minimize the Pearson χ^2 statistic by comparing the average tumor volume extracted from the data and the tumor volume predicted by the pre-treatment EC-TC model, over days after implantation. The estimated parameter values are listed in Table 4.3.
Figure 4.5-A depicts the best fit of the model to the data related to the ECs in control case . The blue dots represent the individual tumor volumes over time (for 13 mice), red dots represent the average tumor volume at each time point and the black solid line shows the tumor volumes predicted by the pre-treatment EC-TC model. In addition, we also used the estimated baseline parameter values to predict the percentage of CSC% at day 30 after implantation and compared it with the CSC% given by Figure 4.4-C. Figure 4.5-B illustrates the percentage of $(ALDH^{HIGH}CD44^{HIGH})$ cells in primary human HNSCC. Blue bar shows the CSC% in xenograft tumor vascularized with HDMEC-shRNA-C, and red bar

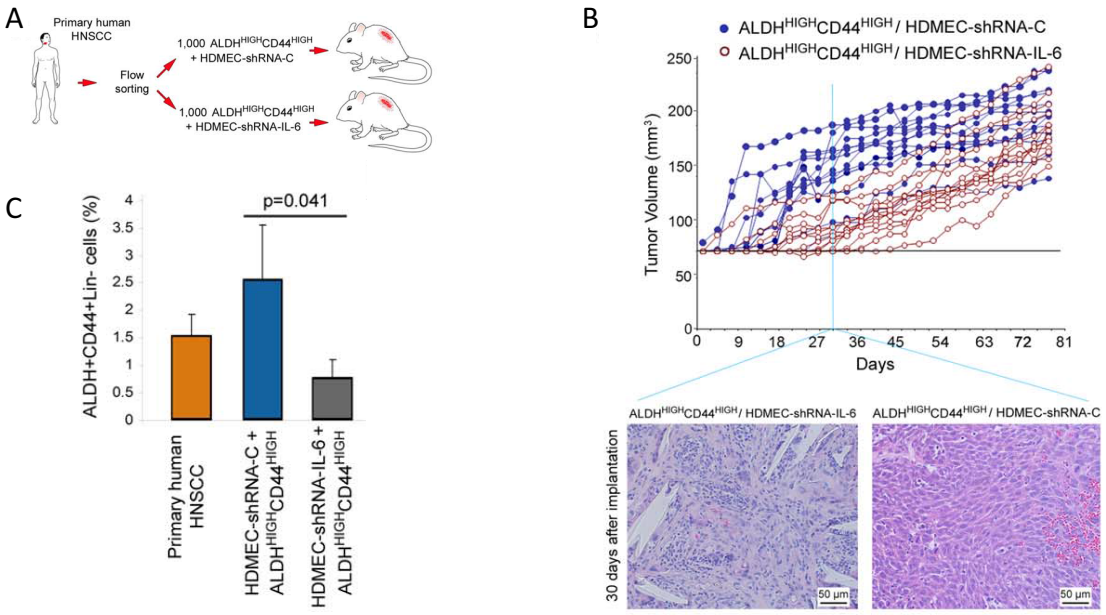

Figure 4.4: Endothelial Cell-Secreted IL-6 Enhances the Tumorigenic Potential of CSCs in HNSCC: (A) Schematic representation of the approach used for testing the role of endothelial cell-secreted IL-6 on the tumorigenic potential of primary human $ALDH^{HIGH}CD44^{HIGH}$ cells. $ALDH^{HIGH}CD44^{HIGH}$ cells were sorted from primary HNSCC and implanted in immunodeficient mice to generate xenograft tumors vascularized with HDMEC-shRNA-IL-6 or control HDMEC-shRNA-C (Figure 2-A in Krishnamurthy *et al.* (2014)). (B) Graph showing individual tumor volume over time. Photomicrographs ($\times$200) of HE-stained tissue sections of scaffolds 30 days after implantation. Few (if any) tumor cells are visible in the implants vascularized with HDMEC-shRNA-IL-6, while the entire microscopy field is populated with tumor cells in the implants vascularized with HDMEC-shRNA-C (Figure 2-C in Krishnamurthy *et al.* (2014)); (C) the percentage of ($ALDH^{HIGH}CD44^{HIGH}$) cells: the orange bar shows the CSC% in primary human HNSCC; blue bar shows the CSC% in xenograft tumor vascularized with HDMEC-shRNA-C; and gray bar shows the CSC% in xenograft tumor vascularized with HDMEC-shRNA-IL-6 at day 30 after implantation (Figure 3-1 in Krishnamurthy *et al.* (2014)).

shows the CSC% predicted by the pre-treatment EC-TC model in the xenograft tumor vascularized with HDMEC-shRNA-C at day 30 after implantation.

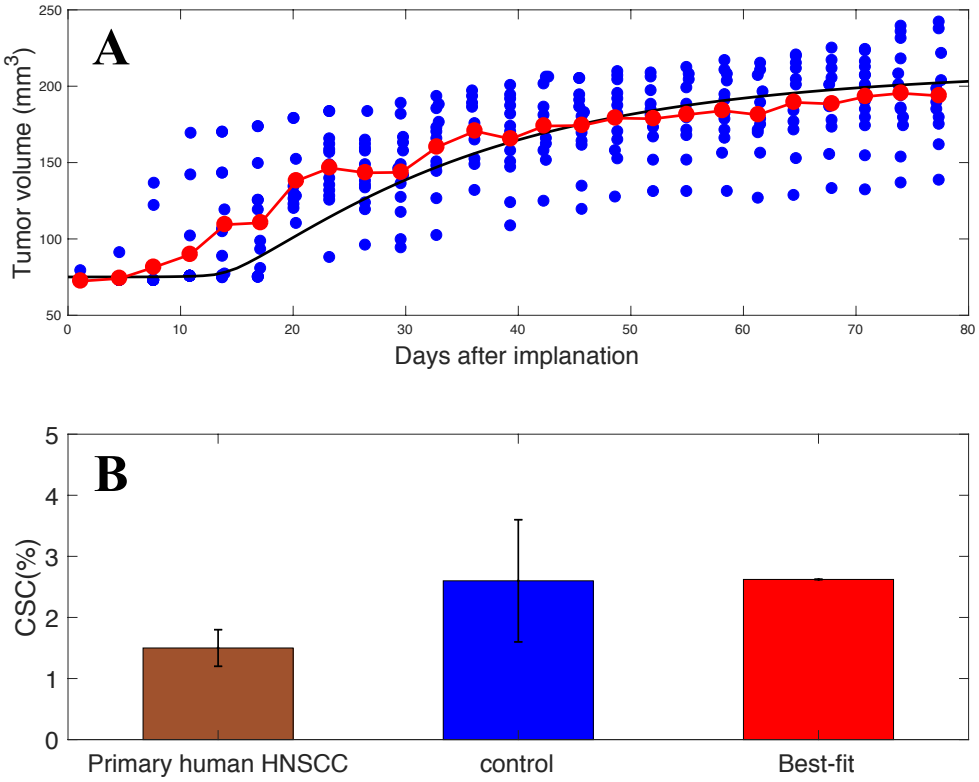

Figure 4.5: The Best-Fit of the Pre-Treatment EC-TC Model to EC-Control Data: (A) 1'000 primary human ALDH^{HIGH}CD44^{HIGH} cells along with HDMEC-shRNA-C cells were seeded in 13 mice; blue dots represent the individual tumor volumes over time, red dots represent the average tumor volume at each time point and the black solid line shows the tumor volumes predicted by the pre-treatment EC-TC model. (B) The percentage of (ALDH^{HIGH}CD44^{HIGH}) cells; the orange bar shows the CSC% in primary human HNSCC; the blue bar shows the CSC% in xenograft tumor vascularized with HDMEC-shRNA-C; and the red bar shows the CSC% predicted by the pre-treatment EC-TC model in the xenograft tumor vascularized with HDMEC-shRNA-C at day 30 after implantation.

Endothelial cell-secreted IL-6 enhances primary HNSCC tumor growth

To evaluate the impact of endothelial cell-secreted IL-6 on tumorigenic potential of CSCs, the IL-6 expression in primary human dermal microvascular endothe-

lial cells was silenced (Figure 4.6). Red data points in Figure 4.6-A show the volume of xenograft tumors vascularized with IL-6-silenced ECs (HDMEC-shRNA-IL-6) and the blue data points show the average volume of the xenograft tumors at each day after implantation.

In order to find the best-fit to HDMEC-shRNA-IL-6, we decreased the secretion rate ofIL-6 by ECs to a very low level (8.9e-07) and then predicted the tumor volume at each time point. The numerical simulations (data is not shown) suggest that some of the parameters that are influenced by IL-6 should be also altered. As we discussed in Chapter 2, disturbance of IL-6 secretion can potentially change A_{in}, P_{N_S} and n values. Therefore, in order to estimate the new altered values of n, A_{in} and P_{N_s}, we fit the pre-treatment model to HDMEC-shRNA-IL-6 when ρ_H is much smaller as compared to HDMEC-shRNA-C data (Figure 4.5).

Model predictions for both HDMEC-shRNA-IL-6 and HDMEC-shRNA-C data indicates that the proposed model is capable of making relatively reliable predictions of tumor growth. In the next sections we will use and extend this pre-treatment model in order to study the tumor cell responses to treatment.

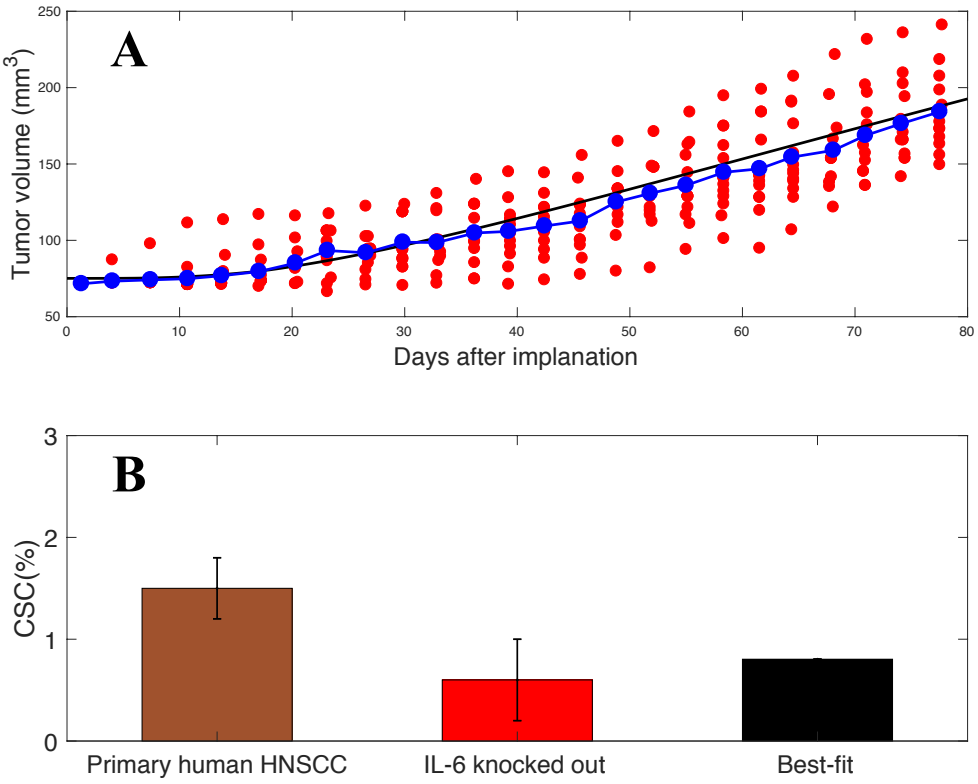

Figure 4.6: The best-Fit of the Pre-Treatment EC-TC Model to EC-IL-6-Silent Data: (A) 1'000 primary human $ALDH^{HIGH}CD44^{HIGH}$ cells along with HDMEC-shRNA-IL-6 cells were seeded in 13 mice; red dots represent the individual tumor volumes over time, blue dots represent the average tumor volume at each time point and the black solid line shows the tumor volumes predicted by the pre-treatment EC-TC model. (B) The percentage of $(ALDH^{HIGH}CD44^{HIGH})$ cells; the orange bar shows the CSC% in primary human HNSCC; red bar shows the CSC% in xenograft tumor vascularized with HDMEC-shRNA-C; and the black bar shows the CSC% predicted by the pre-treatment EC-TC model in the xenograft tumor vascularized with HDMEC-shRNA-Il-6 at day 30 after implantation

Table 4.2: Parameter Values Taken from the Literature and Their Sources.
* Vol_T is the volume of the tumor in μl and is equal to (volume of 1 million ECs)$\times$ H+ (volume of 1 million TCs) $\times$ (S+E+D), where, the volume of 1 EC is $2.2 \times 10^{-6} \mu l$ King *et al.* (2004) and 1 TC is $1 \times 10^{-6} \mu l$ Cunningham *et al.* (1999).

Parameter	**Value**	**Units**	**Source**
α_S	0.6	day^{-1}	Driessens *et al.* (2012); Gao *et al.* (2013)
α_E	$\frac{log(2)}{1.04}$	day^{-1}	Driessens *et al.* (2012); Gao *et al.* (2013)
$P^*_{S_{min}}$	0.014	dimensionless	Weekes *et al.* (2014)
$P_{S_{max}}$	0.90	dimensionless	Weekes *et al.* (2014)
k_f	2.35	$\text{fmol}^{-1}\text{day}^{-1}$	Özbek *et al.* (1998)
k_r	2.24	day^{-1}	Hirabayashi and Lemmey (2012); Özbek *et al.* (1998)
λ_L	0.4152	day^{-1}	Lindmark *et al.* (2001)
ρ_T	7×10^{-7}	$\text{fmol}^{-1}\text{day}^{-1}$per cell	Bran *et al.* (2011); Nilsson *et al.* (2005); PRIES *et al.* (2006)
R_{T_S}	1.66×10^{-6}	fmol^{-1}per cell	Boayue *et al.* (1998); Shkeir *et al.* (2013); Snyers and De Wit (1990); Takizawa *et al.* (1993)
R_{T_E}	$\frac{1}{8} R_{T_S}$	fmol^{-1}per cell	Krishnamurthy *et al.* (2014)
R_{T_D}	$\frac{1}{8} R_{T_S}$	fmol^{-1}per cell	Krishnamurthy *et al.* (2014)
k^f_{H1}	$11.4048/\text{Vol}^*_T$	fmol^{-1} day^{-1}	Mac Gabhann *et al.* (2005); von Tiedemann and Bilitewski (2002)
k^r_{H1}	86.4	day^{-1}	Mac Gabhann and Popel (2007b)
k^p_{H1}	24.1920	day^{-1}	Mac Gabhann and Popel (2007b)
k^f_{H2}	$10.0757/\text{Vol}^*_T$	fmol^{-1} day^{-1}	Cunningham *et al.* (1999); Mac Gabhann *et al.* (2005)
k^r_{H2}	86.4	day^{-1}	Mac Gabhann and Popel (2007b)
k^p_{H2}	24.1920	day^{-1}	Mac Gabhann and Popel (2007b)
$R^t_{H_{A1}}$	6.63e-5	fmol per cell	Wang *et al.* (2002)
$R^t_{H_{A2}}$	1.92e-4	fmol per cell	Wang *et al.* (2002)
λ_A	16.6355	day^{-1}	Yen *et al.* (2011)
δ_B	6.6542	day^{-1}113	Yang *et al.* (2003)

Table 4.3: Estimated Parameter Values

Parameter	Estimated Value	Units	Source
α_H	1.019	per day	Estimated
n_H	0.85	dimensionless	Estimated
δ_H	0.09	per day	Jain and Jackson (2017)
β_H	600	dimensionless	Estimated
N_p	5.5	mmHg	Jain and Jackson (2017)
δ_S	0.0126	day^{-1}	Ch 2
N_d	1	mmHg	Jain and Jackson (2017)
γ_S	2.38	dimensionless	Ch 2
δ_E	0.0612	day^{-1}	Ch 2
γ_E	2.38	dimensionless	Ch 2
δ_D	0.0612	day^{-1}	Ch 2
μ_S	0.018	dimensionless	Ch 2
γ_D	2.38	dimensionless	Ch 2
n_L	2.18	dimensionless	Estimated
A_{in}	4	dimensionless	Ch 2
n	12.66	dimensionless	Ch 2
ρ_H	0.0002	$\text{fmol}^{-1}\text{day}^{-1}\text{cell}^{-1}$	Estimated
k_p	24.95	day^{-1}	Ch 2
P_{N_s}	755500	dimensionless	Ch 2
α_A	1.54×10^{-6}	fmol cell^{-1} day^{-1}	Jain and Jackson (2017)
β_A	0.65	dimensionless	Estimated
ν_A	5e-4	fmol cell^{-1} day^{-1}	Jain and Jackson (2017)
κ_A	2	dimensionless	Jain and Jackson (2017)
N_h	10	mmHg	Jain and Jackson (2017)
χ_H	6.6542	per day	Jain and Jackson (2017)
η_H	1063	per day	Jain and Jackson (2017)
ω_H	0.3341	dimensionless	Jain and Jackson (2017)
n_B	5	dimensionless	Jain and Jackson (2017)
σ_N	1.087	mmHg	Jain and Jackson (2017)

4.3 Treatment of HNSCC Tumor With Tocilizumab and Cisplatin

Based on the stage, location, and histological features, conventional therapies for HNSCC can be surgical resction, radiation therapy, chemotherapy, or a combination of these. Cisplatin is the most common chemotherapeutic drug for the treatment of HNSCC. Although Cisplatin is relatively successful in de-bulking the tumor, it is proposed that CSCs evade therapies with Cisplatin, and, with the passage of time, these cells are activated and regenerate tumors locally or at distant sites Krishnamurthy and Nör (2012); Nör *et al.* (2014) (Figure 4.7-Conventional Therapy).

In the previous sections, we saw that endothelial cell-secreted IL-6 can significantly enhance the survival of CSCs and promote tumor growth. We also observed that the fraction of CSCs was significantly reduced when xenografts were vascularized with IL-6 silenced human endothelial cells. Thus, the significant physiological role of IL-6 provided the rationale for the therapeutic targeting of the IL-6 signaling pathway in HNSCC (Figure 4.7-Perivascular niche-targeted Therapy).
To understand the therapeutic potential of targeting IL-6 signaling in HNSCC, our collaborators in the University of Michigan used UM-SCC-1 and UM-SCC-22B cell lines to conduct a series of treatment experiments with TCZ. The data suggested that inhibition of IL-6 signaling reduced the survival and/or the self-renewal of HNSCC stem cells. Furthermore, they performed a series of individual treatment experiments with only Cisplatin and the combination of Cisplatin with TCZ. Collectively, it was observed that combination therapy with Cisplatin and TCZ has better outcomes than treatment with only Cisplatin or TCZ. All together, these facts motivate us to add treatment with TCZ and Cisplatin to our current model

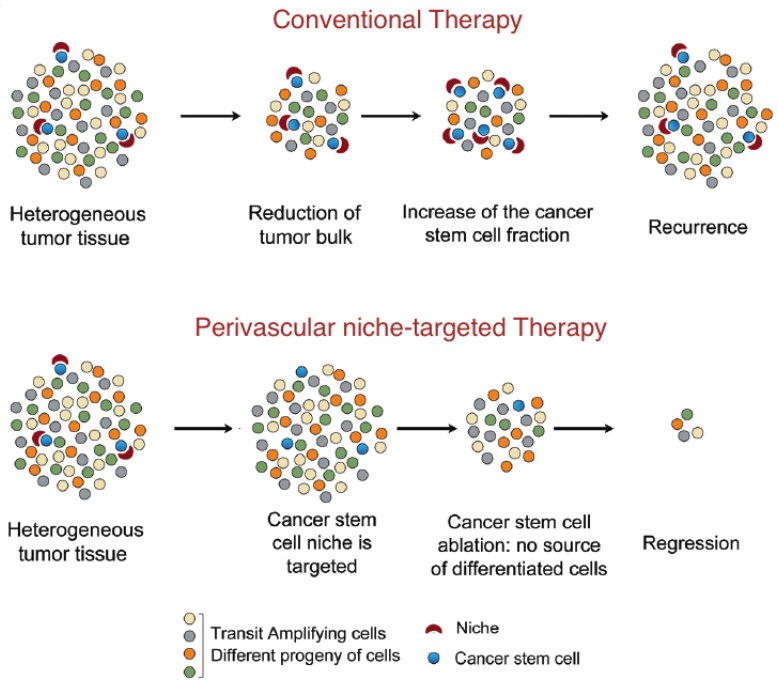

Figure 4.7: Possible Implications of the CSC Hypothesis for Therapy. Conventional chemotherapy targets primarily the bulk of the tumor cells (non-CSCs). As a result, under suitable tumor microenvironment, the CSCs proliferate which leads to tumor recurrence. Perivascular niche-targeted therapy or indirect targeting of CSCs via disruption of their perivascular niche can potentially eliminate them. Ablation of the CSCs may inhibit the regeneration of the tumor and ultimately result in tumor regression. The figure is taken from Krishnamurthy and Nör (2012).

and to explore the ability of our model in predicting the growth rate of tumors generated in mice.

Recall that in the experiment described in Figure 4.4, $ALDH^{HIGH}CD44^{HIGH}$ cells were sorted from "primary" human HNSCC tumor and implanted in mice along with endothelial cells to study the impacts of EC-IL-6 on tumor initiation and tumorigenic properties of CSCs. Primary cells are isolated directly from human or animal tissue and are immediately placed in an artificial environment whereas cell lines have been continually passaged over a long period of time and have acquired homogenous genotypic and phenotypic characteristics. Immortalized or continu-

ous cell lines have acquired the ability to proliferate indefinitely. Moreover, despite the fact that cell lines have lost the true characteristics of the original tissue from which isolated, they are widely used in lab experiments as they are easy to handle. In contrast, primary cells usually are believed to be more biologically relevant tools than cell lines but they have a limited lifespan, slow proliferation and are not well characterized making them hard to maintain. Therefore, since primary cells and cell lines show different behavior, we, firstly, need to find the baseline parameter values for each aforementioned cell lines. Secondly, we add equations related to treatment to the current model and use those obtained baseline parameter values to predict the rate of tumor growth post treatment with TCZ and/or Cisplatin and with the combination therapy of TCZ and Cisplatin. Finally, we use our model to make suggestions/predictions for the most optimized dosing/scheduling combination of Cisplatin and TCZ.

4.3.1 Experimental data

In two separate set of experiments designed specifically for this modeling study, 100,000 unsorted University of Michigan Squamous Cell Carcinoma 1 (UM-SCC-1) and 100,000 University of Michigan Squamous Cell Carcinoma 22B (UM-SCC-22B) cell lines along with 900,000 ECs were implanted bilaterally in mice. When tumors reached approximately 250 mm^3, the mice were assigned into 4 groups and received: (1) 5mg/kg Cisplatin combined with 5mg/kg TCZ; (2) 5mg/kg Cisplatin; (3) 5mg/kg TCZ and (4) control via i.p. injections. Cisplatin was administered weekly for three weeks and the tocilizumab was administered weekly for 9 weeks. Treatment started on day 23 for the UM-SCC-1 cohort and on day 36 for the UM-SCC-22B cohort based on the tumor sizes at those starting day numbers. The tumor sizes were calculated as mm^3 from length and width measurements via (long

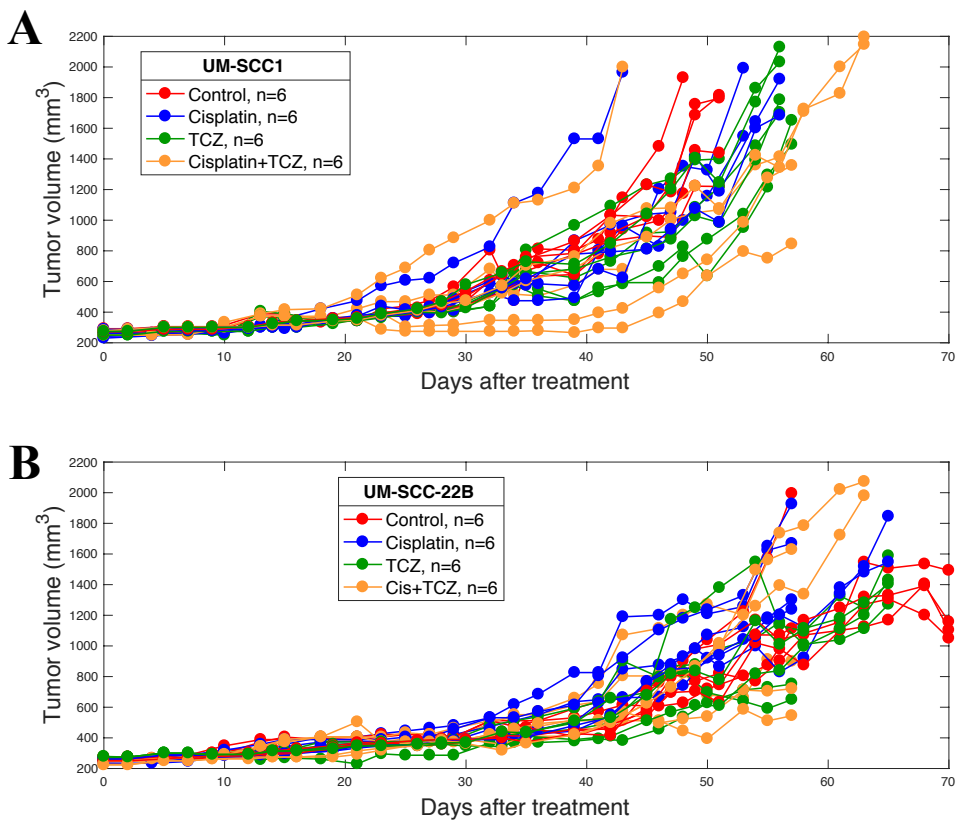

Figure 4.8: Effects of Tocilizumab and/or Cisplatin in the In Vivo Model of HNSCC Described in Subsection 4.3.1. The graphs depict tumor volume over time until the last day of study.

axis$\times$short axis^2)/2. Figure 4.8 shows the data obtained from the experiments. Figure 4.8-A suggests that treating the UM-SCC-1 cohort with single agent TCZ have a better therapeutical effects on tumor growth than treatment with only Cisplatin. Notably, the combination of TCZ with Cisplatin increases the overall effect of therapy leading to a decrease in the tumor volume when compared to the control group. On the contrary, treating UM-SCC-22B cells with only TCZ inhibits tumor growth to the same extent as combination of TCZ and Cisplatin. Treatment with Cisplatin does not show any beneficial therapeutical effects and, interestingly, even

promotes the tumor growth in some of the mice. Collectively, the overall trends suggest that TCZ in combination with Cisplatin group has the most considerable effect on tumor volume compared with control group, and single agent TCZ or Cisplatin.

4.3.2 Estimating baseline parameter values

In order to estimate the baseline parameter values, the pre-treatment EC-TC model is separately fitted to the control treatment data related to UM-SCC-1 and UM-SCC-22 cell line cohorts. Figures 4.9 and 4.10 depict the best fit of the model to the control data for the UM-SCC-1 and UM-SCC-22B cohort, respectively. The blue points depict the tumor volume generate in six mice over time and the red points depict the average tumor volume at each time point. Over the first two or three weeks after treatment starts, our model predicts a slower rate for tumor growth than control data, while for the later weeks the model can fairly predict the tumor growth generated in mice. In the next steps we will first add the equations related to treatment to the current model and then use the estimated parameter values to test the ability of the treatment model to predict the response of cell lines to treatment.

Table 4.4 tabulates all the estimated baseline parameter values.

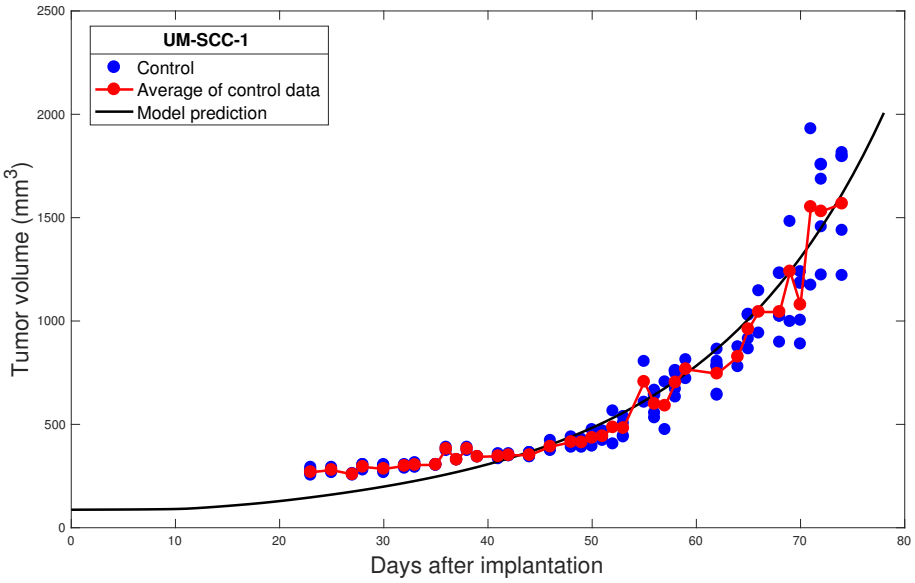

Figure 4.9: The Best Fit of the Pre-Treatment EC-TC Model to the Control Tumor Volume for UM-SCC-1 Group. The blue points depict the tumor volume generate in mice (n=6) over time and the red points depict the average tumor volume at each time point. The black line shows the pre-treatment model predictions.

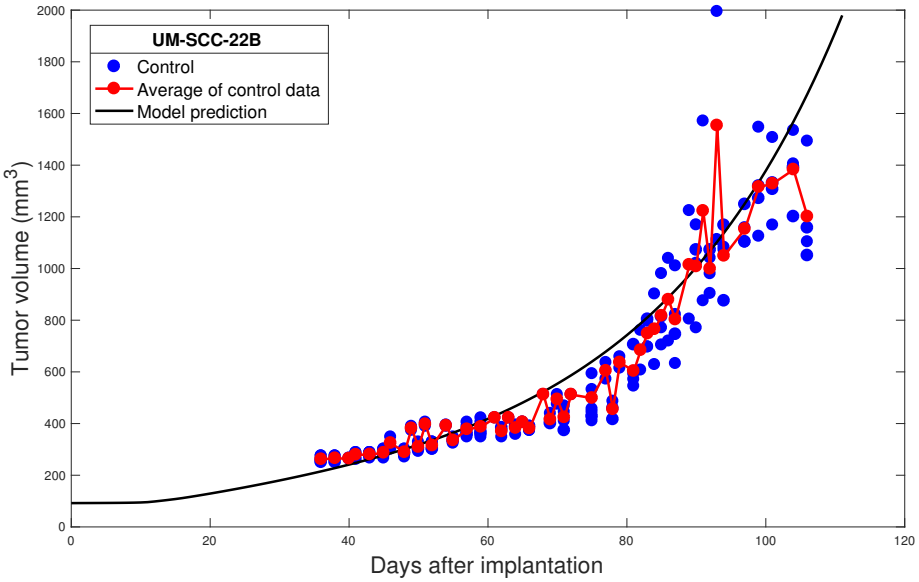

Figure 4.10: The Best Fit of the Pre-Treatment EC-TC Model to the Control Tumor Volume for UM-SCC-22B Group. The blue points depict the tumor volume generate in mice (n=6) over time and the red points depict the average tumor volume at each time point. The black line shows the pre-treatment model predictions.

Table 4.4: Baseline Parameter Values for the Pre-Treatment EC-TC Model Using UM-SCC-1 and UM-SCC-22B Cohort Data

Parameter	**Estimated Value**	**Estimated Value**	**Units**
n_H	0.5	0.5	dimensionless
β_H	1078.7	1457.3	dimensionless
α_H	1.09	1.08	day^{-1}
δ_S	0.0126	0.0126	day^{-1}
δ_E	0.012	0.012	day^{-1}
δ_D	0.5	0.5	day^{-1}
μ_S	0.075	0.035	dimensionless
A_{in}	3	3	dimensionless
n	13.00	17.00	dimensionless
ρ_H	0.0622	0.0622	$\text{fmol}^{-1}\text{day}^{-1}\text{cell}^{-1}$
P_{N_s}	1.5034e+06	1.4242e+06	dimensionless
β_A	0.59	0.59	dimensionless
n_L	0.80	0.86	dimensionless

4.4 Treatment I: Chemotherapy with Cisplatin

4.4.1 Introduction

The published clinical results suggest that some tumor cells can evade chemotherapy with Cisplatin and have the capability to migrate and initiate a new tumor locally or in distance Nör *et al.* (2014). Nör et al. Nör *et al.* (2014) performed a thorough lab experiment to study the effects of Cisplatin therapy on HNSCC tumor lines. Briefly, 100,000 UM-SCC-22B cells were seeded along with 900,000 HDMEC in poly-(L-lactic) acid biodegradable scaffolds in severe combined immunodeficient mice. Bilateral scaffolds were implanted subcutaneously in the dorsum of each mouse (n=12). Mice were treated weekly with 5 mg/kg Cisplatin started when the average volume of the rumors reached 200 mm^3 (Figure CisTherapy-A). In summary, they observed that treatment with Cisplatin enhanced the fraction of CSCs in HNSCC and hypothesized that the combination of Cisplatin with the high expression of IL-6 in tumor niche leads to a dramatic increase in the fraction of CSCs (Figure CisTherapy-B). Furthermore, they reported that Cisplatin has roles in activation of key signaling pathways involved in the regulation of stemness of CSCs (Figure 4.11-C). Finally, to investigate the effect of Cisplatin on stemness in HNSCC, they generated cisplatin-resistant cell lines (UM-SCC-22Cis1, UM-SCC-22Cis6 and UM-SCC-22Cis12) in vitro and saw that these cells are endowed with cancer stemlike features (Figure 4.11-D). Collectively, they observed that IL-6 contributes to Cisplatin-induced stemness, suggesting that a combination therapy involving a platinum-based drug and IL-6R inhibitor might be beneficial for improving more effective treatment and/or cure for HNSCC tumors.

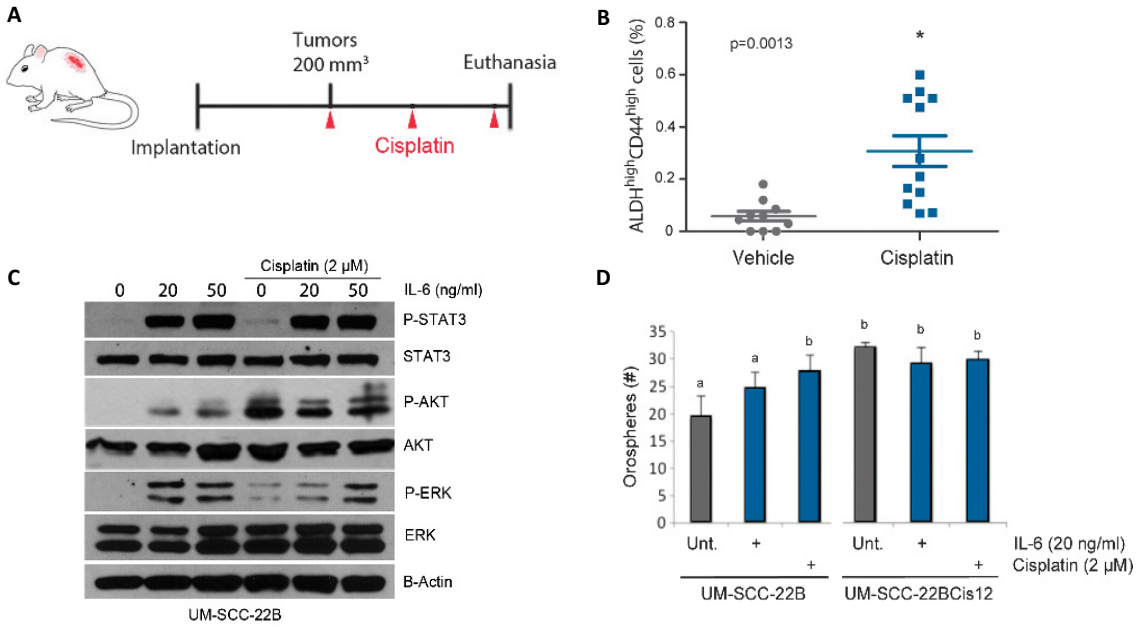

Figure 4.11: Cisplatin Therapy of HNSCC. (A) schematic drawing depicts the experimental design (Figure 1-A in Nör *et al.* (2014)); (B) the percentage of CSCs ($ALDH^{HIGH}CD44^{HIGH}$ cells) in xenograft tumors treated with Cisplatin or vehicle control (n=11) (Figure 1-C in Nör *et al.* (2014)). (C) Western plot for phosphorylated and total key signaling pathways involved in the regulation of stemness including STAT3, ERK, and AKT in UM-SCC-22B (Figure 3-B in Nör *et al.* (2014)); and (D) number of orospheres generated with parental UM-SCC-22B cells or cisplatin-resistant cells (UM-SCC-22BCis12) treated with cisplatin (0 or 2 μM) and/or rhIL-6 (0 or 20 ng/ml) for 10 days in ultralow attachment plates (Figure 4-B in Nör *et al.* (2014)).

In this section, we use the above features to extend the pre-treatment EC-TC model to include Cisplatin therapy of HNSCC tumors. We further use the experimental data described in Subsection 4.3.1 to validate the predictions of the proposed model. Once validated, this model will be used and extended to study the tumor cell responses to combination therapy with TCZ and Cisplatin. Before proceeding to model development, we first estimate the pharmacokinetic parameters of Cisplatin.

4.4.2 *Pharmacokinetics of Cisplatin*

To estimate the pharmacokinetic parameters of Cisplatin we use the analytic solution of PK-model with i.p. injection given by Eq. 3.3.3 in Chapter 2 with the new variables and parameters:

$$X_s(t) = X_p(t_0)\left(A_p e^{-\alpha(t-t_0)} + B_p e^{-\beta(t-t_0)}\right), t \geq t_0 \tag{4.4.1}$$

where,

$$\begin{aligned}
\alpha &= \frac{(k_{12}^C + k_{21}^C + k_{el}^C) + \sqrt{(k_{12}^C + k_{21}^C + k_{el}^C)^2 - 4k_{21}^C k_{el}^C}}{2} \\
\beta &= \frac{(k_{12}^C + k_{21}^C + k_{el}^C) - \sqrt{(k_{12}^C + k_{21}^C + k_{el}^C)^2 - 4k_{21}^C k_{el}^C}}{2} \\
A_p &= \frac{k_{21}^C}{\beta - \alpha} \\
B_p &= \frac{k_{21}^C}{\alpha - \beta}
\end{aligned}$$

where k_{12}^C and k_{21}^C are the distribution rate constants between the systemic central compartment (X_s) and peripheral compartment (X_p). Moreover, k_{el}^C is the elimination rate from central compartment.

In order to estimate the pharmacokinetic parameters, we used the data given in Ling *et al.* (2015). Figure 4.12 shows the best-fit of the pharmacokinetic model to the data and the estimated parameter values are listed in Table 4.5.

4.4.3 *Equations for Cisplatin-therapy*

In this section we modify the pre-treatment EC-TC model to include the equations related to Cisplatin therapy.

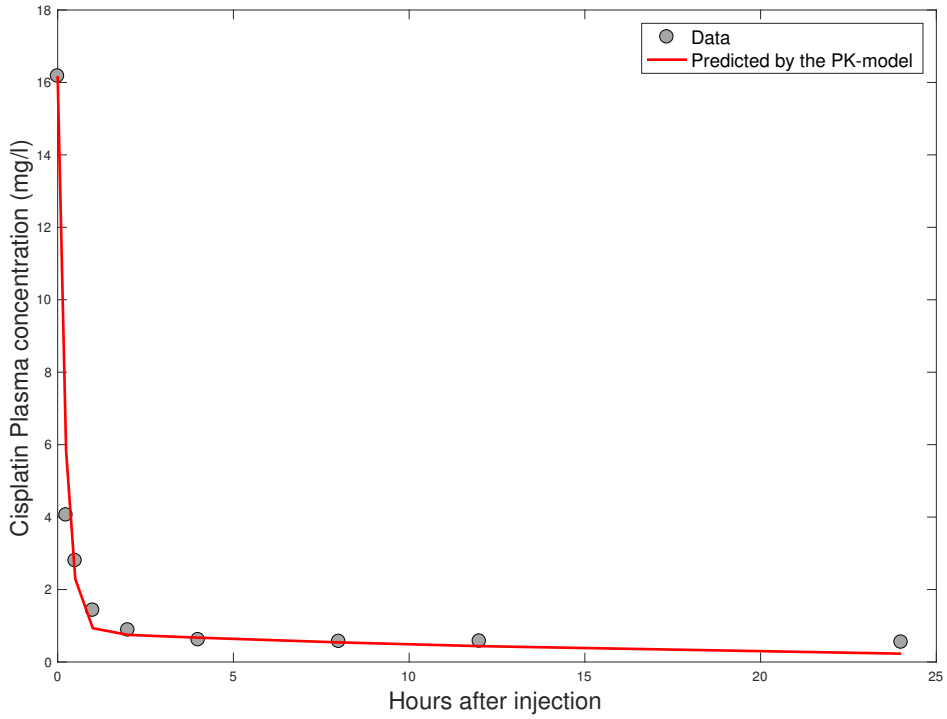

Figure 4.12: Time Profiles of Plasma Cisplatin Concentration Given in Ling *et al.* (2015). The gray points depict Pt concentration in the plasma versus time after a single intravenous injection of cisplatin in rats. Data are presented as mean $\pm$ SD (n = 12) and the solid red line shows the model prediction of Cisplatin elimination from plasma.

Table 4.5: Estimated Pharmacokinetic Parameters of Cisplatin

Parameters	**Values**	**Units**	**Reference**
k_{12}^{C}	84	day^{-1}	Estimated
k_{21}^{C}	7	day^{-1}	Estimated
k_{el}^{C}	20	day^{-1}	Estimated

Cisplatin-induces death of tumor cells

In order to include the Cisplatin-induced death of the tumor cells we use a standard Michaelis-Menten equation as a function of the concentration of Cisplatin

within tumor, X(t), and denoted by:

$$
\begin{aligned}
M_S(X) &= \delta_S(1-\epsilon)\left(\frac{1}{1+\gamma_S\phi_S}+\frac{\Pi_S X}{K_M^S+X}\right)S, \epsilon \neq 1 \\
M_E(X) &= \delta_E(1-\epsilon)\left(\frac{1}{1+\gamma_E\phi_E}+\frac{\Pi_E X}{K_M^E+X}\right)E, \epsilon \neq 1 \\
M_D(X) &= \delta_D(1-\epsilon)\left(\frac{1}{1+\gamma_D\phi_D}+\frac{\Pi_D X}{K_M^D+X}\right)D, \epsilon \neq 1
\end{aligned}
$$

K_M^i, for $i =$ S, E and D, are representing the half maximal inhibitory of Cisplatin concentration and Π_i, denotes the amount by which Cisplatin can increase the maximum natural death rate of CSCs, PCs and DCs, respectively. The parameter ϵ determines the type of interaction between the two ligands (Cisplatin and IL-6). If $\epsilon < 1$ then there are enhanced effects and if $\epsilon > 1$ then there are synergistic effects **?**. For simplicity we assume that $\epsilon = 0$.

Cisplatin enhances the self-renewal capacity of normal and cancer stem cells

As mentioned above, Cisplatin can enhance the stemness of CSCs. In fact, Cisplatin can increase the expression of Bmi-1, a member of the poly comb group family of transcriptional regulators that plays an essential role in stem cell fate decisions and regulates the self-renewal capacity of normal and CSCs Nör *et al.* (2014). Therefore, in order to integrate this feature of Cisplatin, we add a positive feedback function of X (Cisplatin concentration in tumor) to the self-renewal probability function of CSCs (P_S) as following:

$$
\begin{aligned}
P_S(S,\phi_S) &= \frac{(P_{S_{max}} - P_{S_{min}}(\phi_S))P_{N_s}^n}{P_{N_s}^n + S^n} + P_{S_{min}}(\phi_S), \\
P_{S_{min}}(\phi_S) &= \mu_S\left(P_{S_{max}} - P_{S_{min}}^*\right)\left(\phi_S + \frac{X}{K_S+X}\right) + P_{S_{min}}^*
\end{aligned}
$$

Thus, adding the above changes to the pre-treatment EC-TC model gives us the following set of ODEs.

Variables related to pharmacokinetic of Cisplatin are tabulated in Table 4.6.

Table 4.6: Variables Related to Cisplatin-Therapy Model

Variable	Description	Units
X	Free Cisplatin in tumor	fmol
X_s	Free Cisplatin in systemic circulation	fmol
X_p	Free Cisplatin in peripheral compartment	fmol

$$\frac{dS}{dt} = \underbrace{\alpha_S P_S(S,\phi_S)S}_{\text{Stem cell self-renewal}} \underbrace{- \delta_S \left(\frac{1}{1+\gamma_S \phi_S} + \frac{\Pi_S X}{K_M^S + X} \right) S}_{\text{Stem cell death}}$$

$$\frac{dE}{dt} = \underbrace{A_{in}\alpha_S(1-P_S(S,\phi_S))S}_{\substack{\text{Amplified} \\ \text{stem cell differentiation}}} - \underbrace{\alpha_E E}_{\substack{\text{Progenitor cell} \\ \text{differentiation}}} \underbrace{- \delta_E \left(\frac{1}{1+\gamma_E \phi_E} + \frac{\Pi_E X}{K_M^E + X} \right) E}_{\text{progenitor cell death}}$$

$$\frac{dD}{dt} = \underbrace{2\alpha_E E}_{\substack{\text{progenitor cell} \\ \text{differentiation}}} \underbrace{- \delta_D \left(\frac{1}{1+\gamma_D \phi_D} + \frac{\Pi_D X}{K_M^D + X} \right) D}_{\text{differentiated cell death}}$$

$$\begin{aligned} \frac{dL}{dt} = &- \underbrace{k_f L R_S}_{\substack{\text{IL6 binding to} \\ \text{stem cells}}} + \underbrace{k_r C_S}_{\substack{\text{IL6 dissociation} \\ \text{from stem cells}}} - \underbrace{k_f L R_E}_{\substack{\text{IL6 binding to} \\ \text{progenitor cells}}} + \underbrace{k_r C_E}_{\substack{\text{IL6 dissociation} \\ \text{from progenitor cells}}} \\ &- \underbrace{k_f L R_D}_{\substack{\text{IL6 binding to} \\ \text{differentiated cells}}} + \underbrace{k_r C_D}_{\substack{\text{IL6 dissociation} \\ \text{from differentiated cells}}} - \underbrace{\lambda_L L}_{\text{IL6 natural decay}} + \underbrace{\rho_T (S+E+D)}_{\substack{\text{IL-6 Production} \\ \text{by tumor cells}}} \end{aligned}$$

$$\frac{dR_S}{dt} = - \underbrace{k_f L R_S}_{\substack{\text{IL-6 binding to} \\ \text{stem cells}}} + \underbrace{k_r C_S}_{\substack{\text{IL-6 dissociation} \\ \text{from stem cells}}} + \underbrace{k_p C_S}_{\text{Recycling}} + \underbrace{R_{T_S} \mathscr{P}_{\mathscr{S}}(S,\phi_S)}_{\substack{\text{Generation of new } R_S \\ \text{via cell proliferation}}}$$

$$
\begin{aligned}
&\underbrace{-\frac{R_S}{R_S+C_S}R_{T_S}\mathscr{D}_{\mathscr{S}}(S,\phi_S)}_{\substack{\text{Loss of } R_S\\ \text{via cell death}}}\\
\frac{dC_S}{dt} &= \underbrace{+\ k_f L R_S}_{\text{IL6 binding to } R_S} \underbrace{-\ k_r C_S}_{\substack{\text{IL6 dissociation}\\ \text{from } R_S}} \underbrace{-\ k_p C_S}_{\text{Internalization}} \underbrace{-\frac{C_S}{R_S+C_S}R_{T_S}\mathscr{D}_{\mathscr{S}}(S,\phi_S)}_{\substack{\text{Loss of } C_S\\ \text{via cell death}}}\\
\frac{dR_E}{dt} &= \underbrace{-\ k_f L R_E}_{\substack{\text{IL-6 binding to}\\ \text{progenitor cells}}} \underbrace{+\ k_r C_E}_{\substack{\text{IL-6 dissociation}\\ \text{from progenitor cells}}} \underbrace{+\ k_p C_E}_{\text{Recycling}} \underbrace{+\ R_{T_E}\mathscr{P}_{\mathscr{E}}(E,\phi_E)}_{\substack{\text{Generation of new } R_E\\ \text{via cell proliferation}}}\\
&\quad \underbrace{-\frac{R_E}{R_E+C_E}R_{T_E}\mathscr{D}_{\mathscr{E}}(E,\phi_E)}_{\substack{\text{Loss of } R_E\\ \text{via cell death}}}\\
\frac{dC_E}{dt} &= \underbrace{+\ k_f L R_E}_{\text{IL6 binding to } R_E} \underbrace{-\ k_r C_E}_{\substack{\text{IL6 dissociation}\\ \text{from } R_E}} \underbrace{-\ k_p C_E}_{\text{Internalization}} \underbrace{-\frac{C_E}{R_E+C_E}R_{T_E}\mathscr{D}_{\mathscr{E}}(E,\phi_E)}_{\substack{\text{Loss of } C_E\\ \text{via cell death}}}\\
\frac{dR_D}{dt} &= \underbrace{-\ k_f L R_D}_{\substack{\text{IL-6 binding to}\\ \text{differentiated cells}}} \underbrace{+\ k_r C_D}_{\substack{\text{IL-6 dissociation}\\ \text{from differentiated cells}}} \underbrace{+\ k_p C_D}_{\text{Recycling}} \underbrace{+\ R_{T_D}\mathscr{P}_{\mathscr{D}}(E,\phi_D)}_{\substack{\text{Generation of new } R_D\\ \text{via cell proliferation}}}\\
&\quad \underbrace{-\frac{R_D}{R_D+C_D}R_{T_D}\mathscr{D}_{\mathscr{D}}(E,\phi_D)}_{\substack{\text{Loss of } R_D\\ \text{via cell death}}}\\
\frac{dC_D}{dt} &= \underbrace{+\ k_f L R_D}_{\text{IL6 binding to } R_D} \underbrace{-\ k_r C_D}_{\substack{\text{IL6 dissociation}\\ \text{from } R_D}} \underbrace{-\ k_p C_D}_{\text{Internalization}} \underbrace{-\frac{C_D}{R_D+C_D}R_{T_D}\mathscr{D}_{\mathscr{D}}(D,\phi_D)}_{\substack{\text{Loss of } C_D\\ \text{via cell death}}}\\
\frac{dX}{dt} &= \underbrace{+\ k_{12}^C X_s - k_{21}^C X}_{\text{Pharmacokinetics}}
\end{aligned}
$$

Next, we use the baseline parameter values for UM-SCC-1 and UM-SCC-22B cohorts and predict try to test the capability of our proposed model in capturing the tumor growth dynamics after chemotherapy with Cisplatin.

4.4.4 *Cisplatin-therapy does not cause a significant decrease in tumor volume*

We already have introduced the treatment data in Subsection 4.3.1. Figure 4.13 compares the average volume of tumors only in Cisplatin group (n=6) with the average volume of tumors in control group (n=6). The blue dots in Figure 4.13 depicts the average volume of xenograft tumors initiated from UM-SCC-1 (UM-SS-22B) cell lines and treated with 5mg/kg Cisplatin for three weeks starting at day 23 (36) after implantation. The red dots represent the average volume of tumors generated by implanting UM-SCC-1 (UM-SCC-22B) with control vehicle. As it is shown in Figure 4.13, this treatment regimen does not cause a significant decrease (if any) in tumor volume post-treatment in both UM-SCC-1 and Um-SCC-22B cohorts. Notably, UM-SCC-22B cell lines show even higher rate of tumor growth when compared with control group. These results motivate us to use our Cisplatin model to possibly provide some insight into the underlying mechanisms involved in chemotherapeutic effects of Cisplatin.

We use the baseline parameter values obtained from fitting pre-treatment EC-TC model to control data (Figures 4.9 and estimate the parameters related to Cisplatin-therapy (Π_i and K_S). Figures 4.14-A and 4.15-A plot the best fit of the Cisplatin-therapy model to treatment data given in Figure 4.13. The orange line represents the tumor volumes predicted by the Cisplatin-therapy model and the black line represents the tumor volumes for control group predicted by the pre-treatment EC-TC model. The estimated parameter values are given in Table 4.7. Interestingly, the Cisplatin-therapy model suggests that for larger values of K_S, we see the better pro-therapeutic effects of Cisplatin suggesting that when Cisplatin

Finally, we observed that the percentage of CSCs post-treatment is higher for UM-SCC-22B than the post-treatment CSC percentage in UM-SCC-1 group (Fig-

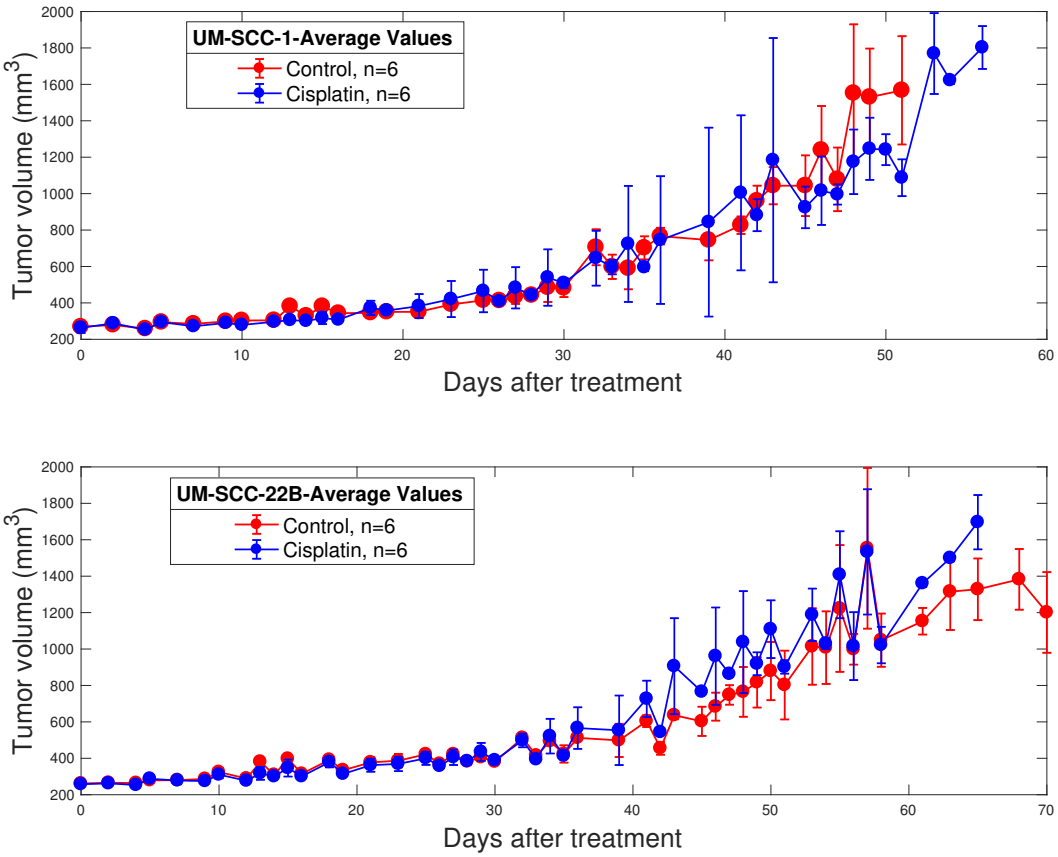

Figure 4.13: Cisplatin-Therapy in Compare to Control

ures 4.14-B and 4.15-B). Collectively, these results suggest that the there is a negative correlation between percentage of CSCs post-treatment and the pro-therapeutic role of Cisplatin.

Table 4.7: Estimated Parameter Values for the Cisplatin-Therapy Model Using data related to Cisplatin Therapy for UM-SCC-1 and UM-SCC-22B Cohorts.

Parameter	**UM-SCC-1**	**UM-SCC-22B**	**Units**	**Source**
Π_S	7.7e-04	3.8e-04	dimensionless	Estimated
Π_E	0.7026	0.080143	dimensionless	Estimated
Π_D	0.0014	0.0027026	dimensionless	Estimated
K_S	5.8277e+19	8.7289e+05	fmol	Estimated
K_M^S	850000	850000	fmol	Nör *et al.* (2014)
K_M^E	850000	850000	fmol	Nör *et al.* (2014)
K_M^D	850000	850000	fmol	Nör *et al.* (2014)

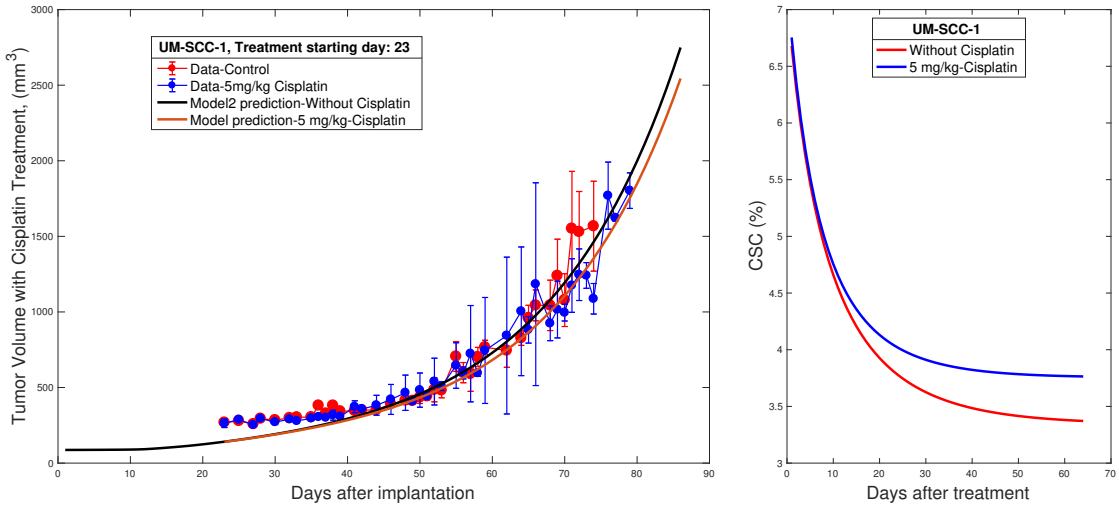

Figure 4.14: At day 23 after tumor implantation, Cisplatin-therapy model is used to predict the tumor volume growth dynamics and the results are compared with the treatment data related to UM-SCC-1 cohort. Model predictions plotted along with experimental data for UM-SCC-1 tumor growth in the control case, without treatment (black line and red dots), and for Cisplatin therapy (orange line and blue dots)

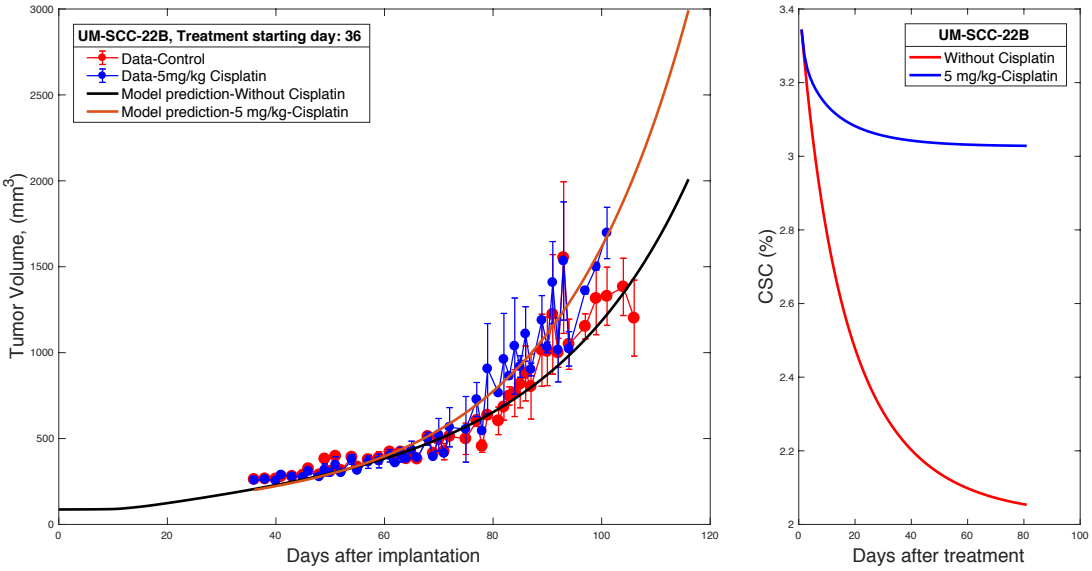

Figure 4.15: At day 36 after tumor implantation, Cisplatin-therapy model is used to predict the tumor volume growth dynamics and the results are compared with the treatment data related to UM-SCC-22B cohort. Model predictions plotted along with experimental data for UM-SCC-22B tumor growth in the control case, without treatment (black line and red dots), and for Cisplatin therapy (orange line and blue dots)

4.5 Treatment II: Treatment of HNSCC Cell Lines With Tocilizumab

4.5.1 Introduction

We have already shown, in the pre-treatment section, that silencing the secretion of IL-6 in endothelial cells (the primary source of IL-6 secretion) leads to a significant reduction in the tumor growth rate and the final percentage of CSCs. Recall that the effects of IL-6 are modeled thorough the fraction of occupied IL-6R on tumor cells. All together, these facts motivate us to add treatment with TCZ (anti-IL-6R antibody), to the pre-treatment EC-TC model and explore its effects on the growth rate of xenograft tumors. Next, we use this model to predict and compare the behavior of tumor growth dynamics with the data related to TCZ-therapy and described in Subsection 4.3.1. Once, we assure that our proposed model can fairly capture the tumor growth dynamics over time then we combine it with the Cisplatin-therapy model developed in the previous section in order to design a model for combination therapy with TCZ and Cisplatin.

4.5.2 Model equations related to TCZ-therapy

In this section we modify the pre-treatment EC-TC model with the equations necessary to describe treatment with TCZ. The treatment model is developed using the same approach used for TCZ-therapy EC-TC model in Chapter 2. However, in this chapter we have additional equations related to endothelial cells and hypoxia. Briefly, TCZ as an anti-IL-6R antibody binds to IL-6R on tumor cells and inhibits formation of IL-6–IL-6R complex molecules. Soon after drug administration, TCZ reaches the tumor environment and binds to IL-6R on tumor cells at a rate k_f^I, and dissociates at a rate k_r^I. Similarly, the complex of TCZ and IL-6R on stem, progenitor and differentiated cells are denoted by C_S^I, C_E^I and C_D^I, respectively. Equation

$\frac{dI}{dt}$ describes the association and dissociation of TCZ in the tumor, $I(t)$, to IL-6 cell-bound receptors on tumor cells. Underlying assumptions for this equations are the same as Chapter 2. Thus, the full model after adding treatment with TCZ can be given by:

$$
\begin{aligned}
\frac{dH}{dt} &= \underbrace{\alpha_H \phi_{H_{A2}}^{n_H} H}_{\substack{\text{Activated VEGFR2-mediated} \\ \text{proliferation}}} - \underbrace{\frac{\delta_H}{1+\beta_H B_H} H}_{\substack{\text{Bcl-2-mediated} \\ \text{apoptosis}}} \\
\frac{dS}{dt} &= \underbrace{\alpha_S P_S(S,\phi_S) S \mathcal{H}(N-N_p)}_{\text{Stem cell self-renewal}} - \underbrace{\frac{\delta_S}{1+\gamma_S \phi_S} S[1+\mathcal{H}(N_d-N)]}_{\substack{\text{IL-6 \& Bcl-2 mediated} \\ \text{apoptosis}}} \\
\frac{dE}{dt} &= \underbrace{A_{in}\alpha_S \left[1-P_S(S,\phi_S)\right] S \mathcal{H}(N-N_p)}_{\substack{\text{Amplified} \\ \text{stem cell differentiation}}} - \underbrace{\alpha_E E \mathcal{H}(N-N_p)}_{\substack{\text{Progenitor cell} \\ \text{differentiation}}} \\
&\quad \underbrace{- \frac{\delta_E}{1+\gamma_E \phi_E} E[1+\mathcal{H}(N_d-N)]}_{\substack{\text{IL-6 \& Bcl-2 mediated} \\ \text{apoptosis}}} \\
\frac{dD}{dt} &= \underbrace{2\alpha_E E \mathcal{H}(N-N_p)}_{\substack{\text{progenitor cell} \\ \text{differentiation}}} - \underbrace{\frac{\delta_D}{1+\gamma_D \phi_D} D[1+\mathcal{H}(N_d-N)]}_{\substack{\text{IL-6 \& Bcl-2 mediated} \\ \text{apoptosis}}} \\
\frac{dL}{dt} &= - \underbrace{k_f L R_S}_{\substack{\text{IL-6 binding to} \\ \text{stem cells}}} + \underbrace{k_r C_S}_{\substack{\text{IL6 dissociation} \\ \text{from stem cells}}} - \underbrace{k_f L R_E}_{\substack{\text{IL-6 binding to} \\ \text{progenitor cells}}} + \underbrace{k_r C_E}_{\substack{\text{IL-6 dissociation} \\ \text{from progenitor cells}}} \\
&\quad - \underbrace{k_f L R_D}_{\substack{\text{IL-6 binding to} \\ \text{differentiated cells}}} + \underbrace{k_r C_D}_{\substack{\text{IL-6 dissociation} \\ \text{from differentiated cells}}} - \underbrace{\lambda_L L}_{\text{IL-6 natural decay}} \\
&\quad + \underbrace{\rho_T (S+E+D)}_{\substack{\text{IL-6 Production} \\ \text{by tumor cells}}} + \underbrace{\rho_H \phi_{H_{A2}}^{n_L} H}_{\substack{\text{Bcl-2-mediated} \\ \text{IL-6 production} \\ \text{by ECs}}}
\end{aligned}
$$

$$
\begin{aligned}
\frac{dI}{dt} &= -\underbrace{k_f^I I R_S}_{\substack{\text{Anti-IL6R binding to}\\ \text{stem cells}}} + \underbrace{k_r^I C_S^I}_{\substack{\text{Ani-IL6R dissociation}\\ \text{from stem cells}}} - \underbrace{k_f^I I R_E}_{\substack{\text{Anti-IL6R binding to}\\ \text{progenitor cells}}} \\
&\quad + \underbrace{k_r^I C_E^I}_{\substack{\text{Anti-IL6R dissociation}\\ \text{from progenitor cells}}} - \underbrace{k_f^I I R_D}_{\substack{\text{Anti-IL6R binding to}\\ \text{differentiated cells}}} + \underbrace{k_r^I C_D^I}_{\substack{\text{IL6 dissociation}\\ \text{from differentiated cells}}} \\
&\quad + \underbrace{k_{12} I_s - k_{21} I}_{\text{Pharmacokinetics}} \\
\frac{dR_S}{dt} &= -\underbrace{k_f L R_S}_{\substack{\text{IL-6 binding to}\\ \text{stem cells}}} + \underbrace{k_r C_S}_{\substack{\text{IL-6 dissociation}\\ \text{from stem cells}}} + \underbrace{k_p C_S}_{\text{Recycling}} - \underbrace{k_f^I I R_S}_{\substack{\text{Anti-IL6R binding to}\\ \text{IL-6R}}} \\
&\quad + \underbrace{k_r^I C_S^I}_{\substack{\text{Anti-IL-6R dissociation}\\ \text{from stem cells}}} + \underbrace{R_{T_S} \mathscr{P}_{\mathscr{S}}(S, \phi_S)}_{\substack{\text{Generation of new } R_S\\ \text{via cell proliferation}}} - \underbrace{\frac{R_S}{R_S + C_S + C_S^I} R_{T_S} \mathscr{D}_{\mathscr{S}}(S, \phi_S)}_{\substack{\text{Loss of } R_S\\ \text{via cell death}}} \\
\frac{dC_S^I}{dt} &= +\underbrace{k_f^I I R_S}_{\substack{\text{Anti-IL6R binding to}\\ \text{IL-6R}}} - \underbrace{k_r^I C_S^I}_{\substack{\text{Ani-IL6R dissociation}\\ \text{from stem cells}}} - \underbrace{\frac{C_S^I}{R_S + C_S + C_S^I} R_{T_S} \mathscr{D}_{\mathscr{S}}(S, \phi_S)}_{\substack{\text{Loss of } C_S^I\\ \text{via cell death}}} \\
\frac{dC_S}{dt} &= +\underbrace{k_f L R_S}_{\text{IL6 binding to } R_S} - \underbrace{k_r C_S}_{\substack{\text{IL6 dissociation}\\ \text{from } R_S}} - \underbrace{k_p C_S}_{\text{Internalization}} - \underbrace{\frac{C_S}{R_S + C_S + C_S^I} R_{T_S} \mathscr{D}_{\mathscr{S}}(S, \phi_S)}_{\substack{\text{Loss of } C_S\\ \text{via cell death}}} \\
\frac{dR_E}{dt} &= -\underbrace{k_f L R_E}_{\substack{\text{IL-6 binding to}\\ \text{progenitor cells}}} + \underbrace{k_r C_E}_{\substack{\text{IL-6 dissociation}\\ \text{from progenitor cells}}} + \underbrace{k_p C_E}_{\text{Recycling}} - \underbrace{k_f^I I R_E}_{\substack{\text{Anti-IL6R binding to}\\ \text{IL-6R}}} \\
&\quad + \underbrace{k_r^I C_E^I}_{\substack{\text{Anti-IL-6R dissociation}\\ \text{from progenitor cells}}} + \underbrace{R_{T_E} \mathscr{P}_{\mathscr{E}}(E, \phi_E)}_{\substack{\text{Generation of new } R_E\\ \text{via cell proliferation}}} - \underbrace{\frac{R_E}{R_E + C_E + C_E^I} R_{T_E} \mathscr{D}_{\mathscr{E}}(E, \phi_E)}_{\substack{\text{Loss of } R_E\\ \text{via cell death}}} \\
\frac{dC_E^I}{dt} &= +\underbrace{k_f^I I R_E}_{\substack{\text{Anti-IL6R binding to}\\ \text{IL-6R}}} - \underbrace{k_r^I C_E^I}_{\substack{\text{Ani-IL6R dissociation}\\ \text{from progenitor cells}}} - \underbrace{\frac{C_E^I}{R_E + C_E + C_E^I} R_{T_E} \mathscr{D}_{\mathscr{E}}(E, \phi_E)}_{\substack{\text{Loss of } C_E^I\\ \text{via cell death}}} \\
\frac{dC_E}{dt} &= +\underbrace{k_f L R_E}_{\text{IL6 binding to } R_E} - \underbrace{k_r C_E}_{\substack{\text{IL6 dissociation}\\ \text{from } R_E}} - \underbrace{k_p C_E}_{\text{Internalization}} - \underbrace{\frac{C_E}{R_E + C_E + C_E^I} R_{T_E} \mathscr{D}_{\mathscr{E}}(E, \phi_E)}_{\substack{\text{Loss of } C_E\\ \text{via cell death}}}
\end{aligned}
$$

$$\frac{dR_D}{dt} = -\underbrace{k_f L R_D}_{\substack{\text{IL-6 binding to}\\ \text{differentiated cells}}} + \underbrace{k_r C_D}_{\substack{\text{IL-6 dissociation}\\ \text{from differentiated cells}}} + \underbrace{k_p C_D}_{\text{Recycling}} - \underbrace{k_f^I I R_D}_{\substack{\text{Anti-IL6R binding to}\\ \text{IL-6R}}}$$
$$+ \underbrace{k_r^I C_D^I}_{\substack{\text{Anti-IL-6R dissociation}\\ \text{from differentiated cells}}} + \underbrace{R_{T_D}\mathscr{P}_{\mathscr{D}}(E,\phi_D)}_{\substack{\text{Generation of new } R_D\\ \text{via cell proliferation}}} - \underbrace{\frac{R_D}{R_D+C_D+C_D^I}R_{T_D}\mathscr{D}_{\mathscr{D}}(E,\phi_D)}_{\substack{\text{Loss of } R_D\\ \text{via cell death}}}$$

$$\frac{dC_D^I}{dt} = + \underbrace{k_f^I I R_D}_{\substack{\text{Anti- nding to}\\ \text{IL-6R}}} - \underbrace{k_r^I C_D^I}_{\substack{\text{Ani-IL6R dissociation}\\ \text{from differentiated cells}}} - \underbrace{\frac{C_D^I}{R_D+C_D+C_D^I}R_{T_D}\mathscr{D}_{\mathscr{D}}(D,\phi_D)}_{\substack{\text{Loss of } C_D^I\\ \text{via cell death}}}$$

$$\frac{dC_D}{dt} = + \underbrace{k_f L R_D}_{\text{IL6 binding to } R_D} - \underbrace{k_r C_D}_{\substack{\text{IL6 dissociation}\\ \text{from } R_D}} - \underbrace{k_p C_D}_{\text{Internalization}}$$
$$- \underbrace{\frac{C_D}{R_D+C_D+C_D^I}R_{T_D}\mathscr{D}_{\mathscr{D}}(D,\phi_D)}_{\substack{\text{Loss of } C_D\\ \text{via cell death}}}$$

$$\frac{dA}{dt} = \underbrace{-k_{H1}^f R_{H_{A1}} A + k_{H1}^r C_{H_{A1}} - k_{H2}^f R_{H_{A2}} A + k_{H2}^r C_{H_{A2}}}_{\text{reaction with VEGFR1/2 on endothelial cells}}$$
$$- \underbrace{\lambda_A A}_{\substack{\text{natural}\\ \text{decay}}} + \underbrace{\alpha_A \frac{B_H}{1+\beta_A B_H} H}_{\substack{\text{Bcl-2-mediated production}\\ \text{by endothelial cells}}} + \underbrace{\frac{\nu_A}{1+e^{-\kappa_A(N_h-N)}}(S+E+D)}_{\substack{\text{hypoxia-mediated VEGF}\\ \text{production by stem/bulk cells}}}$$

$$\frac{dC_{H_{A1}}}{dt} = \underbrace{k_{H1}^f R_{H_{A1}} A - k_{H1}^r C_{H_{A1}} - k_{H1}^p C_{H_{A1}}}_{\substack{\text{VEGFR1 activation by VEGF}\\ \text{on endothelial cells}}} - \underbrace{C_{H_{A1}} \frac{\delta_H}{1+\beta_H B_H}}_{\substack{\text{loss due to}\\ \text{endothelial cell apoptosis}}}$$

$$\frac{dC_{H_{A2}}}{dt} = \underbrace{k_{H2}^f R_{H_{A2}} A - k_{H2}^r C_{H_{A2}} - k_{H2}^p C_{H_{A2}}}_{\substack{\text{VEGFR2 activation by VEGF}\\ \text{on endothelial cells}}} - \underbrace{C_{H_{A2}} \frac{\delta_H}{1+\beta_H B_H}}_{\substack{\text{loss due to}\\ \text{endothelial cell apoptosis}}}$$

$$\frac{dB_H}{dt} = \underbrace{\chi_H}_{\substack{\text{Constitutive}\\ \text{expression}\\ \text{by ECs}}} + \underbrace{\eta_H \frac{\phi_{H_{A2}}^{n_B}}{\omega_H^{n_B}+\phi_{H_{A2}}^{n_B}}}_{\substack{\text{Activated VEGFR2-}\\ \text{mediated production}\\ \text{by ECs}}} - \underbrace{\delta_B B_H}_{\substack{\text{natural}\\ \text{decay}}}$$

$$\frac{dB_T}{dt} = \underbrace{\chi_T}_{\substack{\text{Constitutive}\\ \text{expression}\\ \text{by TCs}}} - \underbrace{\delta_B B_T}_{\substack{\text{natural}\\ \text{decay}}}$$

Similar to the calculation for TCZ-therapy model in Chapter 2, the following equations for treatment model satisfy:

$$\begin{aligned} R_S &= R_{T_S} S - C_S - C_S^I \\ R_E &= R_{T_E} E - C_E - C_E^I \\ R_D &= R_{T_D} D - C_D - C_D^I \end{aligned}$$

Variables and parameter values related to anti-IL-6R treatment are the same as ones tabulated in Tables 3.7 and 3.8 in Chapter 2, respectively.

4.5.3 Predicting the effects of TCZ-therapy on HNSCC tumor growth

We use the model to predict tumor response to administration of TCZ as a single agent therapy in order to understand the mechanism behind the IL-6 role on tumor growth behavior. Furthermore, by directly comparing (i.e. no additional parameter fitting) the model predictions and the TCZ-therapy data we can validate the proposed model. To do so, we use the best fit parameter values obtained from fitting the EC-TC model to the control data for both UM-SCC-1 and UM-SCC-22B cell lines, and predict the tumor growth dynamics post TCZ- therapy.

Figures 4.16 and 4.16 depict model predictions along with experimental data for UM-SCC-1 and UM-SCC-22B cohorts, respectively. The orange dots represent the average volume of UM-SCC-1 (or UM-SCC-22B) tumors post TCZ-therapy and the red plots show the average volume of tumors in control case, without treat-

ment. Comparing the orange and red dots, data suggests that TCZ can cause a considerable decrease in the tumor growth rate in UM-SCC-1 cohort while, treating UM-SCC-22B cell lines does not show a significant decrease in tumor volume when compared to the control case. At day 23 (36) after tumor implantation, TCZ-therapy model is used to predict the tumor volume growth dynamics. Comparing the model outcomes with experimental data for UM SCC-1 (UM-SCC-22B) tumor growth in the control case (purple line and red dots), and in the TCZ therapy case (green line and orange dots) show that our model has fairly reliable predictions in both cases.

Furthermore, the TCZ-therapy model suggests that nine weeks of therapy with 5mg/kg TCZ causes 15 %, and 10% decrease in tumors generated from UM-SCC-1 and UM-SCC-22B cohorts, respectively, as compared to the corresponding control cases. Interestingly, we see where TCZ-therapy causes more reduction in the CSC percentage (i.e. in UM-SCC-1 group), the treatment has a better tumor growth inhibition effects (i.e. more effectively decreases the rate of tumor growth).

In the previous section, we hypothesized that the anti-therapeutic effects of Cisplatin might be because of the observed increased percentage of the CSCs after chemotherapy. Furthermore, the TCZ-therapy model suggested that treating the cell lines with anti-IL-6R antibody could reduce the percentage of CSCs as compared with control case. Together, these findings provide a rationale for trying to treat the tumor cells with a combination of TCZ and Cisplatin. In the next section we use both TCZ-therapy and Cisplatin-therapy model to include the effects of combination therapy with both of the drugs.

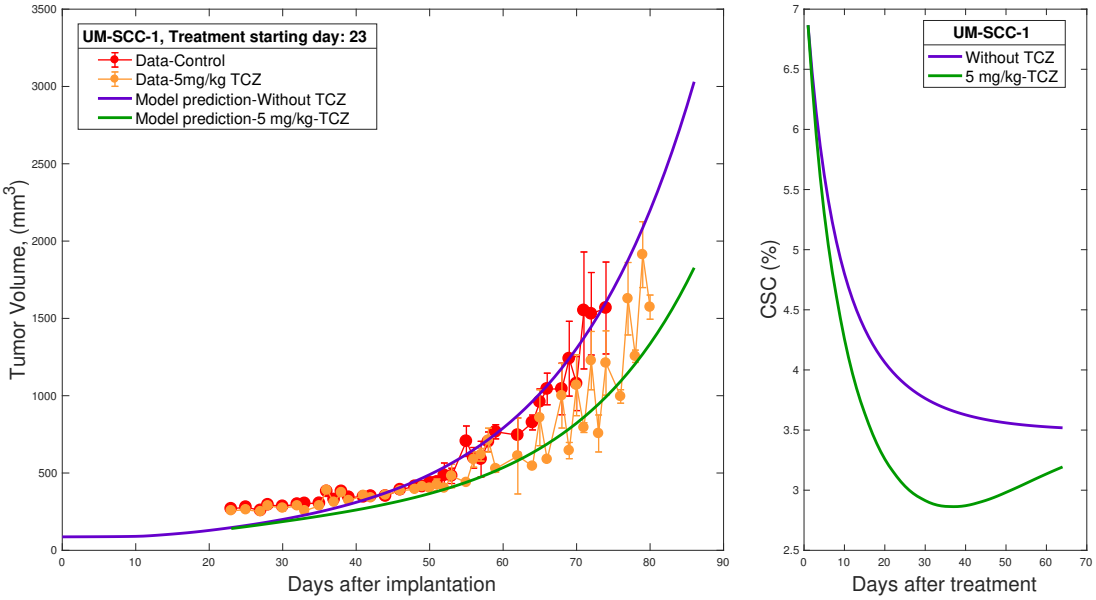

Figure 4.16: At day 23 after tumor implantation, TCZ-therapy model is used to predict the tumor volume growth dynamics and the results are compared with the treatment data related to UM-SCC-1 cohort. Model predictions plotted along with experimental data for UM SCC-1 tumor growth in the control case, without treatment (purple line and red dots), and for combination TCZ therapy (green line and orange dots)

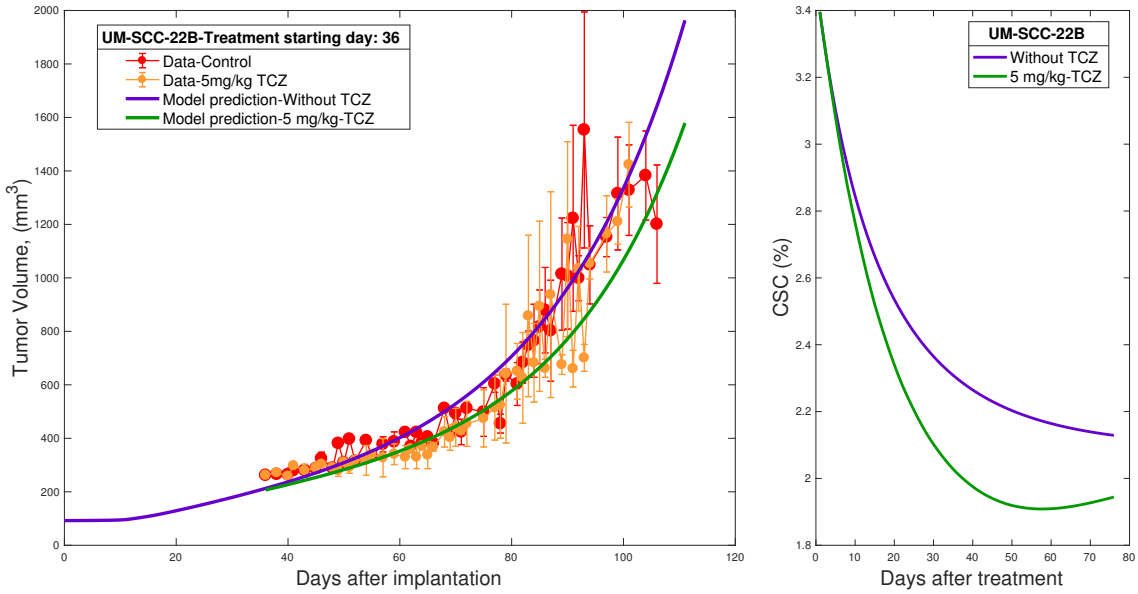

Figure 4.17: At day 36 after tumor implantation, TCZ-therapy model is used to predict the tumor volume growth dynamics and the results are compared with the treatment data related to UM-SCC-22 cohort. Model predictions plotted along with experimental data for UM SCC-22 tumor growth in the control case, without treatment (purple line and red circles), and for TCZ therapy (green line and orange circles)

4.6 Treatment III- Combination Therapy of TCZ and Cisplatin

Nor et al. reported that the combination of Cisplatin treatment with the high expression of IL-6, which is typically observed in HNSCC, leads to a dramatic increase in the fraction of CSCs post treatment Nör *et al.* (2014). They observed that IL-6 enhances the stemness of HNSCC cells and that Cisplatin cannot overcome IL-6-IL-6R induced signaling pathways that are involved in the acquisition of a stemlike phenotype in the cell lines. This result suggest that a combination therapy involving Cisplatin and IL-6R inhibitor (TCZ) might overcome the anti-therapeutic effect of Cisplatin.

In this section, we combine the TCZ- and Cisplatin-therapy models and use it to predict the tumor volumes after combination therapy with TCZ and Cisplatin. Figures 4.18 and 4.19 depict the model predictions and results of the in vivo experiment (described in Subsection 4.3.1) in which UM-SCC-1 and UM-SCC-22B cell lines were treated with a combination of TCZ and Cisplatin. The purple dots represent tumor volume in control case (without treatment) and the orange dots represents tumor volumes for combination therapy. Comparing the tumor volumes before and after combination treatment suggest that UM-SCC-1 cell lines positively responded to treatment and had a slower growth after treatment (Figure 4.19) while the UM-SCC-22B cell lines showed even faster growing rate as compared to tumor volumes in control group (Figure 4.19). We used our TCZ-Cisplatin-therapy model to predict the percentage of CSCs after treatment. Interestingly, our model predicted that in the first 7 weeks after treatment, the CSC percentage in UM-SCC-1 tumors could be decreased to a lower level than the CSC percentage in the control group but started growing faster and getting a higher value than the control group

over the remaining time. In contrast, the combination treatment of UM-SCC-22B cell lines dramatically increased the CSC percentage in tumor suggesting that TCZ could not decrease the Cisplatin-IL-6-mediated growth (as reported in Nör *et al.* (2014)) in UM-SCC-22B cell lines.

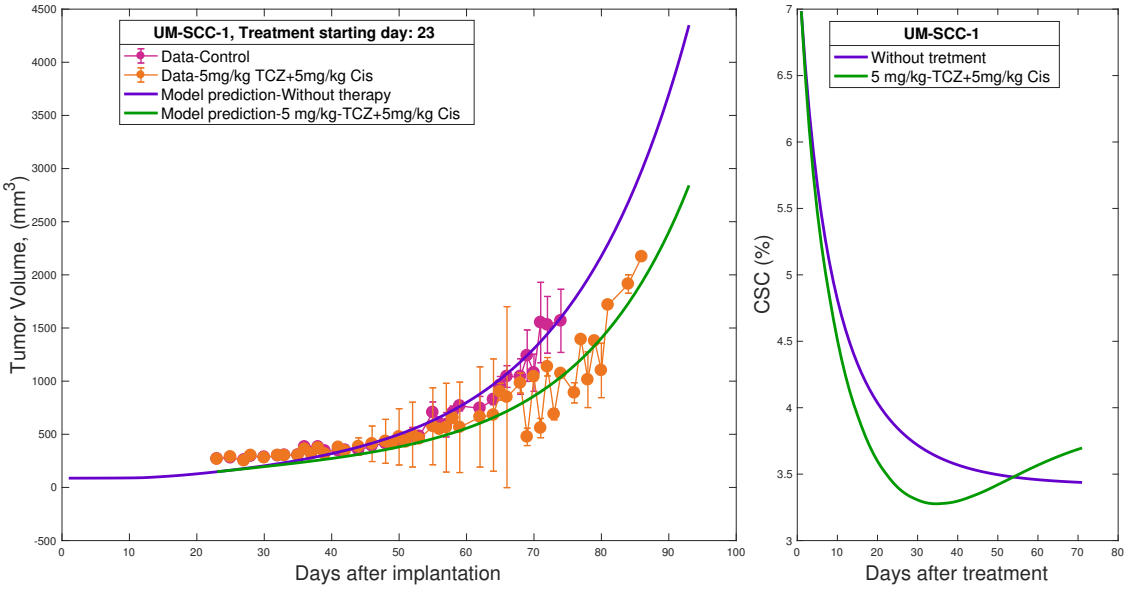

Figure 4.18: Model predictions plotted along with experimental data for UM SCC-1 tumor growth in the control case, without treatment (blue line and purple dots), and for combination TCZ + Cisplatin therapy (green line and orange dots).

Collectively, the partial successes of treating xenograft tumors with combination of TCZ and Cisplatin provide enough rationale for running more simulations in order to find the most effective combinations of these two drugs. In the next section we use the baseline parameter values for UM-SCC-1 cohort and try to suggest/find a dose-scheduling regimen with the most optimal outcome.

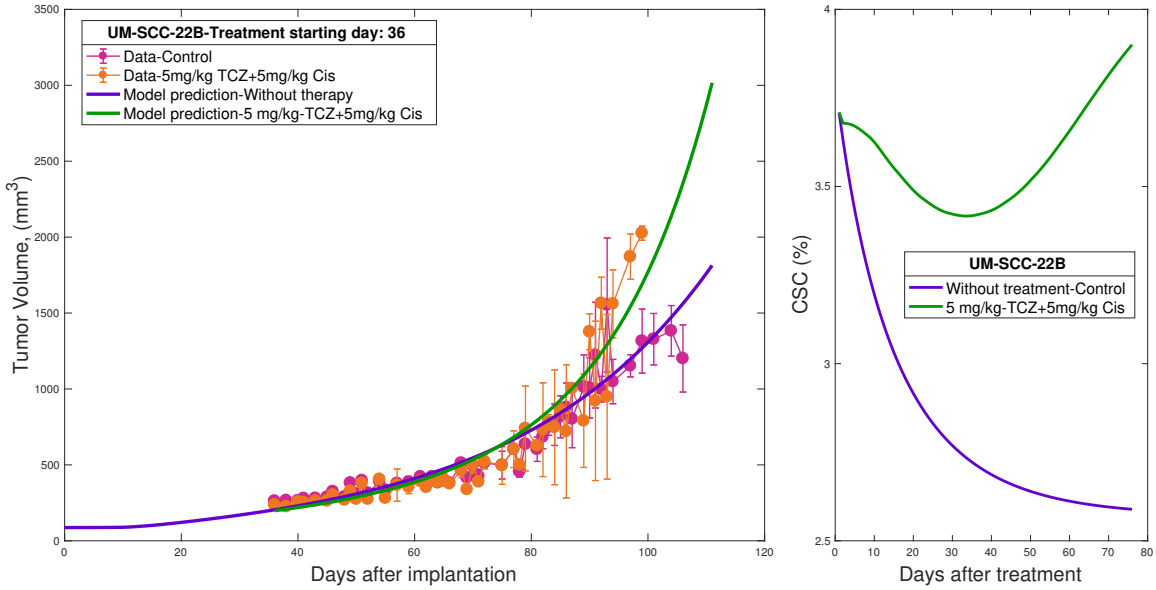

Figure 4.19: Model Predictions Plotted Along the Experimental Data for UM SCC-22B Tumor Growth in the Control Case, Without Treatment (blue line and purple dots), and for Combination TCZ + Cisplatin Therapy (green line and orange dots).

4.7 Treatment Optimization

In order to determine the most favorable combinations and investigate potential synergism between TCZ and Cisplatin, we simulated a number of dose-scheduling regimens (Table 4.8). The ultimate goal is to determine the optimal dosing strategy that minimizes tumor growth, while also minimizing the amount of drug administered. In these simulations, TCZ is administered weekly for nine, six or three weeks starting at day 0 of week 0. The tumor is pre-, co-, or post-treated with 1, 5 or 15 mg/kg Cisplatin weekly for one or three weeks. For each treatment strategy we compute the IC30 value, which corresponds to the amount of TCZ required for 30% reduction (compared to control) in tumor volume at day 63 after treatment. Using the IC30, we define a metric that we refer to as the dose Schedul-

ing Index (S.I.) to indicate the level of synergism between the two drugs. S.I. is defined as a ratio of the predicted IC30 for each dose scheduling strategy with the IC30 for the baseline case, wherein the tumor is co-treated with Cisplatin and TCZ weekly for three weeks followed by treatment with only TCZ for the remainder of the therapeutic window (rows 4, 13, 20, 29, 36 and 42). The S.I. values (the last column of Table 4.8) help us to quantify the therapeutic efficacy of the different dose scheduling strategies. An S.I. value greater than one represents sub-optimal dosing; whereas, a value less than one indicates some level of synergism between the two drugs Cook *et al.* (2015); Jain and Meyer-Hermann (2010).

Therefore, to find an optimal schedule, we need to minimize the amount of TCZ required for a fixed amount of the total Cisplatin (3, 15, or 45 mg/kg) administered by changing the timing/ordering of administering the two drugs with respect to each other. As can be seen in Table 4.8 (rows 10-12, 16, 26-28 and 32), model simulations predict that in general pre-treatment with Cisplatin followed by immediate treatment with TCZ is preferred over post-treatment and co-treatment with Cisplatin. Specially, pre-treatment with 3 mg/kg of Cisplatin, followed by weekly administration of 5mg/kg TCZ for six weeks (rows 28 and 32), totaling 30 mg/kg of TCZ seems to be one of the best options. Strategies that work equally well are the pre-treatment with 1mg/kg (2mg/kg) Cisplatin followed by co-treatment with TCZ for two weeks (one week) and ending with TCZ alone for an additional four (five) weeks (rows 26 and 27). However, if treatment with high doses of 15 mg/kg of Cisplatin for each single injection are allowed, then the TCZ administration schedule can be shortened to a total of 18 mg/kg TCZ over three weeks (rows 34 and 35). Interestingly, post-treatment with Cisplatin in all the cases (for instance, rows 5, 22, and 44) seems to do poorly when compared with pre- or co-treatment and results in some level of antagonism between the two drugs. Finally, the model

Table 4.8: Optimizing Combination Therapy: TCZ is administrated weekly for 9, 6, or 3 weeks (gray cells). Based on the number of weeks that TCZ is administered and the total doses of Cisplatin, treatment strategies are divided into subcategories that are separated by horizontal solid lines in the table. Cisplatin is administered weekly for one or three weeks in doses of 1, 5, and 15 mg/kg. CIS stands for 1mg/kg Cisplatin and W stands for week. Gray cells show the weeks at which TCZ is administered. The pink cells indicate the baseline IC30 for each sub-strategy

	W-3	**W -2**	**W -1**	**W 0**	**W 1**	**W 2**	**W 3**	**W 4**	**W 5**	···	**W 8**	IC30*	S.I.
1		—	5 CIS	5 CIS	5 CIS					···		45	1
2		5 CIS	5 CIS	5 CIS						···		45	1
3	5 CIS	5 CIS	5 CIS							···		45	1
4		—	—	5 CIS	5 CIS	5 CIS				···		45	1
5		—	—		5 CIS	5 CIS	5 CIS			···		54	1.2
6		—	—			5 CIS	5 CIS			···		54	1.2
7			15 CIS							···		45	1
8		15 CIS								···		45	1
9				15 CIS						···		45	1
10		—	CIS	CIS	CIS					···		45	0.91
11		CIS	CIS	CIS						···		45	0.91
12	CIS	CIS	CIS							···		45	0.91
13		—	—	CIS	CIS	CIS				···		49.5	1
14		—	—		CIS	CIS	CIS			···		54	1.09
15		—	—			CIS	CIS			···		54	1.09
16			3 CIS							···		45	0.91
17		—	5 CIS	5 CIS	5 CIS					···		30	1
18		5 CIS	5 CIS	5 CIS						···		30	1
19	5 CIS	5 CIS	5 CIS							···		30	1
20		—	—	5 CIS	5 CIS	5 CIS				···		30	1
21		—	—		5 CIS	5 CIS	5 CIS			···		36	1.2
22		—	—			5 CIS	5 CIS	5 CIS		···		36	1.2
23		—	15 CIS							···		30	1
24		15 CIS								···		30	1
25		—	—	15 CIS						···		30	1
26		—	CIS	CIS	CIS					···		30	0.91
27		CIS	CIS	CIS						···		30	0.91
28	CIS	CIS	CIS							···		30	0.91
29		—	—	CIS	CIS	CIS				···		33	1
30		—	—		CIS	CIS	CIS			···		36	1.1
31		—	—			CIS	CIS	CIS		···		36	1.1
32		—	3 CIS							···		30	0.91
33		—	—	3 CIS						···		33	1

Table 4.8 Continued: Optimal treatment strategies.

	W-3	W -2	W -1	W 0	W 1	W 2	W 3	W 4	W 5	···	W 8	IC30*	S.I.
34		—	15 CIS	15 CIS	15 CIS					···		16.5	0.92
35		15 CIS	15 CIS	15 CIS						···		16.5	0.92
36		—	—	15 CIS	15 CIS	15 CIS				···		18	1
37		—	—		15 CIS	15 CIS	15 CIS			···		19.5	1.08
38		—	—			15 CIS	15 CIS	15 CIS		···		21	1.16
39		—	15 CIS		15 CIS		15 CIS			···		22.5	1.25
40		—	5 CIS	5 CIS	5 CIS					···		18	1
41		5 CIS	5 CIS	5 CIS						···		16.5	0.92
42		—	—	5 CIS	5 CIS	5 CIS				···		18	1
43		—	—		5 CIS	5 CIS	5 CIS			···		19.5	1.08
44		—	—			5 CIS	5 CIS	5 CIS		···		21	1.16
45		—	15 CIS							···		16.5	0.92
46		15 CIS								···		16.5	0.92
47		—	—	15 CIS						···		18	1
48		—	5 CIS		5 CIS		5 CIS			···		22.5	1.25
49					5 CIS		5 CIS		5 CIS	···		25.5	1.41
50		—	5 CIS		5 CIS	5 CIS				···		24	1.33

predicts that alternating between Cisplatin and TCZ results in the worse possible treatment outcomes compared to any other dose scheduling strategy (rows 39 and 48-50). Thus, in all cases, pre-treatment with Cisplatin is predicted to optimize the synergism between Cisplatin and TCZ.

4.8 Summary and Conclusions

Cancer stem cells are highly tumorigenic cells within tumors that exhibit self-renewal and the capacity to differentiate and recapitulate a heterogeneous organ from a single progenitor cell Hermann *et al.* (2010); Krishnamurthy *et al.* (2014); Pearson *et al.* (2016); Prince *et al.* (2007). It also has been hypothesized that these CSCs are responsible for chemotherapy and/or radiotherapy resistance, tumor metastasis and tumor recurrence. All these facts suggest that ablation of CSCs is essential to improve the treatment outcomes for stem-cell driven cancers. However, since CSCs and normal stem cells share similar properties, direct targeting of

CSCs may lead to harming or killing the normal cells. It has been demonstrated that CSCs live in perivascular niches and are highly dependent on crosstalk with those associated endothelial cells for their survival and division. These findings raised the idea of the therapeutic blockade of the crosstalk between endothelial cells and CSCs within the perivascular niche.

Studies of HNSCC have revealed the existences of CSCs and that those tumor-associated endothelial cells express high levels of IL-6. It has also been shown that IL-6 play a major role in enhancing the growth rate of HNSCC Krishnamurthy *et al.* (2014); Neiva *et al.* (2014). Notably, IL-6 binds to its receptor on tumor cells and activates the key pathways involving in regulation of self-renewal, differentiation and survival of CSCs. All together, these discoveries suggest that therapeutic inhibition of the IL-6-mediated pathways by targeting that IL-6 ligand and receptor might be beneficial for patients with head and neck cancer.

In this chapter we developed a mathematical modeling framework for investigating IL-6 mediated, cancer stem cell driven tumor growth and targeted treatment with TCZ alone and/or in combination with Cisplatin. The model is based on a experimental setup in which human tumor cells were seeded along with endothelial cells in poly(L-lactic) acid biodegradable scaffolds, and transplanted into SCID mice. Our model includes the effects of both human tumor and endothelial cell-secreted IL-6 signaling on tumor cell survival and proliferation, and also captures the effects of IL-6 on the probability of self-renewal for cancer stem cells. Specifically, it describes the interaction (crosstalk) between endothelial cells (ECs) and tumor cells (TCs), by tracking the cellular and molecular species used in the experiments described in Figure 4.4. The proposed pre-treatment EC-TC model tracks

the temporal changes in cancer stem cell, progenitor cell and differentiated cell density, free tumor and/or endothelial cell-secreted IL-6 concentration, endothelial cell density, free VEGF concentration and free Bcl-2 mRNA expressed by both tumor and endothelial cells. VEGF can bind to its natural receptors, VEGFR1 and VEGFR2, on endothelial cells to form a signal initiating complex, VEGF–VEGFR2, and a decoy complex, VEGF–VEGFR1 Mac Gabhann and Popel (2007a); Zhang *et al.* (2010). Furthermore, VEGF can also bind to VEGFR1 expressed on the surface of all tumor cell types (cancer stem cells (CSCs), progenitor cells (PCs) and differentiated cells (DCs)) and form the signaling complex for tumor cells, VEGF-VEGFR1 Mac Gabhann and Popel (2007a); Zhang *et al.* (2010). All of the IL-6 binding dynamics that were previously described in Chapter 2 carry over to this model.

To evaluate the impact of endothelial cell-secreted IL-6 on tumorigenic potentials of CSCs, Krishnamurthy et al. Krishnamurthy *et al.* (2014) used a scaffold model and seeded 1'000 HNSCC CSCs in mice along with 500'000 either IL-6-silenced ECs (HDMEC-shRNA-IL-6) or control ECs (HDMEC-shRNA-C) the IL-6 expression in primary human dermal microvascular endothelial cells was silenced. They observed that silencing IL-6 could significantly decrease the tumor growth rate and the percentage of CSCs in primary tumor. In order to calibrate and test the abilities of the proposed pre-treatment model, we first fit it to the control data related to HDMEC-shRNA-C (Figure 4.4) and estimated the unknown parameter values. Then we decreased the secretion rate of IL-6 secretion by ECs and predicted the tumor volumes over time (data is not shown). Comparing the EC-TC model predictions with the HDMEC-shRNA-IL-6 data suggested that in order to get more accurate predictions, some of the parameters which can be influenced by IL-6 should be also altered. As we discussed in Chapter 2, disturbance of the IL-

6 secretion can potentially change the A_{in}, P_{N_S} and n values. Overall, the model predictions were reliably matching the experimental data in both cases where ECs could secrete IL-6 and when the secretion of IL-6 was silenced in ECs. In addition, the model could predict the percentage of CSC observed in the experiment. This allowed us to use and extend the pre-treatment EC-TC model to run a range of simulations for TCZ- and Cisplatin- therapy and for synergistic combinations of TCZ and Cisplatin.

Cisplatin is the most common conventional chemotherapeutic agent used to improve the poor outcomes of standard of care for HNSCC including surgery and radiation. However, it could not significantly change the survival rate of patients due to drug-resistance and metastasis. Attempts to understand the mechanism behind the anti-therapeutic effects of Cisplatin revealed that Cisplatin can not decrease the tumor volume rate as compared to control case without treatment. It also enhances the percentage of CSCs in HNSCC and that percentage is amplified when Cisplatin is combined with IL-6. It was also hypothesized that these CSCs are responsible for drug-resistance and metastasis. In this chapter we extended the pre-treatment model to include the effects of Cisplatin on tumor growth dynamics. The proposed model not only covered the biological characteristics of Cisplatin but it was also developed based on a experimental data in which two cell lines UM-SCC-1 and UM-SCC-22B were seeded in mice along with ECs. When tumors reached approximately 250 mm^3, the mice were assigned into 4 groups and received: (1) 5mg/kg Cisplatin combined with 5mg/kg TCZ; (2) 5mg/kg Cisplatin; (3) 5mg/kg TCZ and (4) control via i.p. injections. Cisplatin was administered weekly for three weeks and the tocilizumab was administered weekly for 9 weeks (Subsection 4.3.1). We calibrated our model by fitting it to the control data for both

UM-SCC-1 and UM-SCC-22B cohort and estimated the baseline parameter values (Figures 4.10 and 4.10). Then we used those estimated baseline parameter values to predict the effects of Cisplatin on tumorigenic potential of HNSCC. The model could reliably predict the tumor growth rate after Cisplatin-therapy. Interestingly, we used the Cisplatin-therapy model to predict the percentage of CSCs in tumor xenografts. Our model suggested that the anti-therapeutic effects of Cisplatin on tumor growth is in a direct positive correlation with the percentage of CSCs after treatment. This result is in line with the experimental results observed by Nör et al. in Nör *et al.* (2014).

It has been demonstrated that growth and survival of CSCs are highly influenced by tumor micro-environmental factors and molecular signaling, including IL-6 Krishnamurthy *et al.* (2014). More interestingly, it has been revealed that HNSCC CSCs reside in perivascular niches and that IL-6 secreted by endothelial cells (ECs) in the tumor niche enhances the survival, self-renewal and tumor initiation potentials of CSCs in primary head and neck tumor Krishnamurthy *et al.* (2014). Therefore, targeting the IL-6-induced signaling pathways may inhibit the survival and self-renewal potential of CSCs. Thus, TCZ as a potential alternative treatment has being used to improve patients outcomes for HNSCC. Therefore, in order to study and make the predictions of tumor cells' responses to TCZ-therapy we extended the pre-treatment model to include the effects of TCZ in our model. Then we used the estimated baseline parameter values and predicted the tumor volumes at each time point in TCZ-therapy data. The prediction results was reliably matched with the TCZ-therapy data for UM-SCC-1 cell lines. However, our model is not capable of capturing the increase observed in tumor volumes after treatment for UM-SCC-22B cell lines.

Furthermore, we combined the TCZ-therapy and Cisplatin-therapy model to study the CSC responses to the combination therapy with TCZ and Cisplatin. Our model predictions matched with the tumor growth dynamics reported in the experimental data (Figures 4.18 and 4.19). In addition, our model predicts that high levels of CSCs after treatment is strongly correlated with the poor therapeutic effects of Cisplatin. It has been observed that combined use of Cisplatin and IL-6 further enhances the stemness of CSCs. Also recall that in this model the the molecular effects of IL-6 binding to its receptor, IL-6R is incorporated via tracking the temporal changes of fractional occupancies of bound receptors on tumor cells. All these facts together, motivated us to look at the dynamics of the fractional occupancies of IL-6R on both UM-SCC-1 and UM-SCC-22B cells lines when treated with a combination of TCZ and Cisplatin (see Figure 4.20).

Surprisingly, we see that the overall fraction of occupied IL-6R is smaller on UM-SCC-22B (4.20-B) cell lines than UM-SCC-1 cell lines (4.20-A). The smaller the fraction of occupied IL-6R by IL-6 means the higher fraction of occupied IL-6R by TCZ. Therefore, we would expect better results for combination therapy for UM-SCC-22B cohort. However, we see that the combination therapy with Cisplatin and TCZ increases the tumor growth rate. One possible explanation might be due to the more available IL-6 in the tumor niche after treating with TCZ. We do not model the other microenvironmental factors and there might be a chance that those free IL-6 indirectly facilitates the tumor growth via binding to its receptor on endothelial cells which results in faster proliferation of them Neiva *et al.* (2009). The other possible read of this result is that TCZ has almost the same impact on tumor volume reduction for both UM-SCC-1 and UM-SCC-22 cell line and since the combination therapy has opposite impacts on tumor growth for the two cell lines we

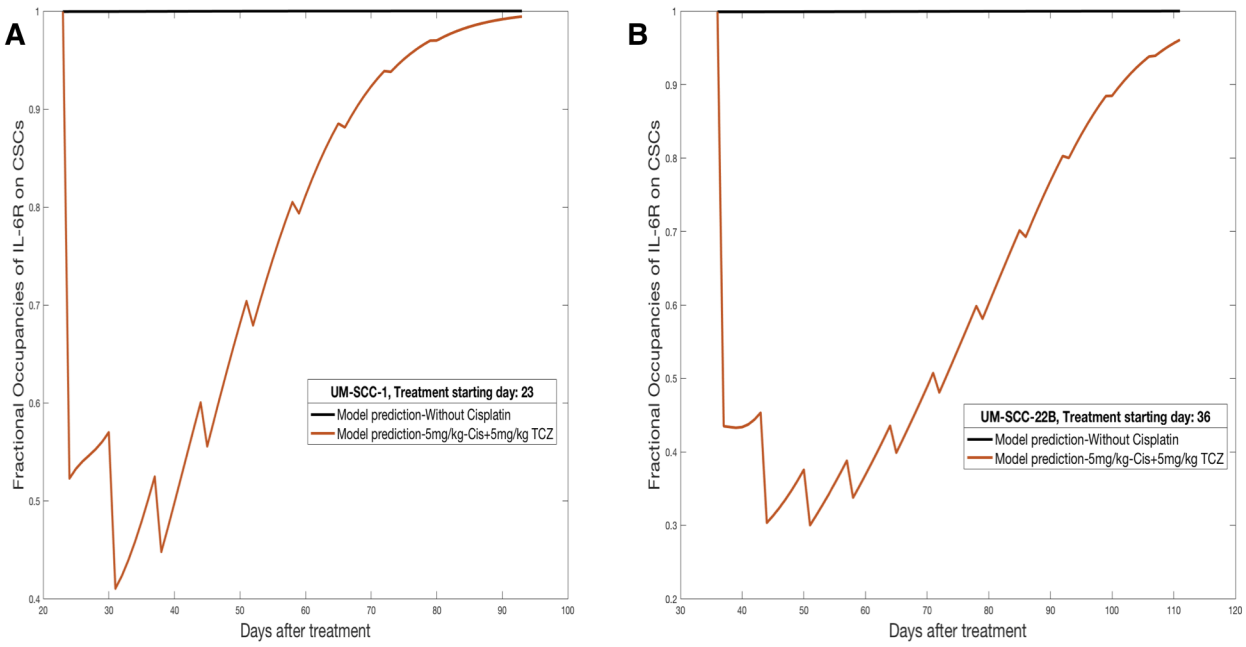

Figure 4.20: Fractional Occupancies of IL-6R on CSCs on UM-SCC-1 (left panel) and UM-SCC-22B (right panel) Cell Lines. The black line is the model prediction for control case without treatment and the orange line is the model prediction after treatment with Cisplatin.

can conclude that Cisplatin might be responsible for the faster growth observed in the data for UM-SCC-22B cell lines. However, the fact that combination therapy of UM-SCC-1 cell line with Cisplatin could successfully decrease the tumor growth in compared with control group along with the contradictory responses of these two cell lines to treatment raise the idea that there might be some levels of antagonism between the two drugs. Therefore, we ran simulations for various dose/scheduling regimens of Cisplatin and TCZ in order to investigate potential synergism between TCZ and Cisplatin. Our simulations suggests that low levels of Cisplatin is enough to be effective and also we concluded that in all cases, pre-treatment with Cisplatin followed by TCZ optimizes the synergism between Cisplatin and TCZ.

Chapter 5

SUMMARY AND CONCLUSIONS

Cancer is a genetic disease caused by the accumulation of mutations in somatic cells Altrock *et al.* (2015). During the multiple steps of evolution from normal to cancerous, altered somatic cells acquire the capabilities of sustaining proliferative signaling, evading growth suppressors, resisting cell apoptosis, enabling replicative immortality, inducing angiogenesis, and activating invasion and metastasis Altrock *et al.* (2015); Hanahan and Weinberg (2011b); Hermann *et al.* (2010). In particular, these mutated cells, so called cancer stem cells (CSCs), do not obey the highly regulated processes of normal cell division and death, which can result in tumor initiation Jackson *et al.* (2014). There are many theories trying to explain the malignancy potential of these mutated tumor cells. Among those, *cancer stem cell hypothesis* has gained credibility within the cancer research community Molina-Peña and Álvarez (2012). According to that, tumors found in adult tissues arise from CSCs that exhibit the ability to self-renew and give rise to differentiated tissue cells Krishnamurthy *et al.* (2014); Nör *et al.* (2014); Zhu *et al.* (2014). Additionally, it states that CSCs make up an often-argued minor subpopulation of cells and the bulk of the tumor tissue is composed of rapidly proliferating cells that lack longevity and have only limited proliferative potential, so called transit-amplifying cells and post-mitotic differentiated cells. These cells do not contribute to tumor initiation. They are derived from the CSCs by differentiation, but are not capable of tumor initiation by themselves Prince and Ailles (2008); Reya *et al.* (2001); Weekes *et al.* (2014). Heterogeneous populations of cancer cells composed of both CSCs and non-CSCs have been identified in a variety of malignancies, in-

cluding tumors of the blood, breast, colon, prostate, brain, and head and neck Al-Hajj *et al.* (2003); Gentry and Jackson (2013); Krishnamurthy *et al.* (2014); Singh *et al.* (2003).

Despite the fact that CSC biology has been extensively studied in the last few years, unfortunately, it is not fully understood yet due to the lack of efficient experimental methods Frank *et al.* (2010); Nguyen *et al.* (2012); Pardal *et al.* (2003); Weekes *et al.* (2014). However, mathematical and computational modeling approaches provide a useful framework to study cancer progression since they can integrate biological parameters and make predictions across different time and/or spatial scales. Moreover, mathematical models provide a powerful tool to facilitate drug development and pre-clinical evaluation of efficacy, which cannot be easily understood by using conventional wet-lab experiments alone Olsen and Siegelmann (2013); Tang *et al.* (2014); Wang *et al.* (2015). Therefore, the contribution of mathematical modeling in cancer biology can be useful in order to restrict the number of lab experiments needed for testing hypotheses and for generating new conjectures.

Several mathematical, physical, computational, stochastic and engineering techniques have been applied to the complex biological system that arises from stem cells and non-stem cell dynamics Dingli *et al.* (2007); Foo *et al.* (2009); Fornari *et al.* (2014); Kapitanov (2012); Kim *et al.* (2008); Komarova and Wodarz (2007); Michor *et al.* (2005); Sottoriva *et al.* (2010); Tomasetti and Levy (2010); Turner *et al.* (2009); Youssefpour *et al.* (2012). In particular, there are several mathematical models of stem cell-driven tumors designed to investigate the mechanism behind the tumor growth dynamics and also the proportion of CSCs that can initiate, propagate and re-initiate tumors. While most of them either neglect asymmetric division, or pro-

genitor cells, or have made assumptions on a fixed symmetric/asymmetric division probability Boman *et al.* (2007); Deleyrolle *et al.* (2011); Gupta *et al.* (2011); Mackillop *et al.* (1983); Molina-Peña and Álvarez (2012); Morton *et al.* (2011); Rodriguez-Brenes *et al.* (2011); Sehl *et al.* (2009), in Chapter 1 we designed a model based on the CSC hypothesis which includes progenitor cells and a negative feedback on the self-renewal probability of CSCs. This assumption is consistent with several experimental reports in which these three main cell subtypes are identified in cancer Bapat *et al.* (2005); Dylla *et al.* (2008). This model is a simplified version of the model developed by Ganguly and Puri (2006), as we described in Section **??**, but instead of adding sub-compartments of progenitor cells, it is assumed that each differentiated stem cell is amplified on upon entry into the progenitor. That is, the efflux from the stem compartment is amplified by a factor A_{in} as soon as the cells enter the progenitor pool. The progenitor cells transition to fully differentiated cells via TA cell division. It is also assumed that differentiated cells do not differentiate any more. Moreover, we used a Hill function to reflect autocrine effects on CSC self-renewal by assuming that if the number of CSCs approaches zero, the probability of CSC self-renewal (based on chemical signaling in the niche) approaches the maximum value. With the inclusion of feedback mechanisms like these that govern stem cell division, cancer cells do not necessarily grow exponentially and tend to reach an equilibrium level Gentry and Jackson (2013). In fact, the results of mathematical analysis of our model, suggested that the qualitative behavior of the model depends on the balance between the net growth rate of CSCs, $\alpha_S P_S$, and the death rate of CSCs, δ_S. For the values of δ_S between the maximum and the minimum net growth rate of CSCs, $\alpha_S P_{S_{min}} < \delta_S < \alpha_S P_{S_{max}}$, tumor growth is bounded and reaches to a steady population whereas $\delta_S < \alpha_S P_{S_{min}}$ causes an exponential growth of CSCs which can results in unbounded exponential growth of tumor.

It was also shown that once the non-trivial exists and is positive, then it is always locally asymptotically stable. That is, once the tumor emerges it reaches to an equilibrium level and relatively small perturbations in parameter values do not change the behavior of the tumor growth dynamics. Furthermore, it was shown that if the death rate of CSCs is below a critical threshold, tumor grows exponentially. Very large division rates of CSCs also lead to a exponential growth of tumor. Consistent with our modeling approach, Liu et al. (2013) developed a set of mathematical models for studying the dynamic interaction between CSCs and non-CSCs both in vitro and in vivo. However, they defined feedback loops from terminally differentiated cells to both division rate of CSCs (PCs) and to self-renewal probabilities of CSCs (PCs) and concluded that the appropriate model needs both of the negative feedbacks in order to obtain the experimentally observed balance between CSCs and non-CSCs. Rodriguez et al. (2013) also described a new model with two negative feedback mechanisms on the symmetric division probability and differentiation probability and their model predictions could show an excellent agreement with the observed experimentally data on the growth curve. Furthermore, Monlina-Peña and Álvarez presented a simple model, with an analytical solution, that also includes the three cell subpopulations (CSCs, progenitors, and terminally differentiated cells) but assumes that each event related to cell division or death of each one of these subpopulations happen at a constant rate. They used their model to fit to experimental data sets from three different tumor growth scenarios and showed that in order to sustain exponential tumor growth with a less than 1% CSCs within the tumor, symmetric and asymmetric CSC division rates must be of the same order of magnitude, and non-stem cancer cells must divide more frequently and have significantly higher cell death rates.

An initially assumed minor subpopulation of CSCs has been challenged with recent data suggesting widely different proportions of CSCs in tumor cells Johnston *et al.* (2010); Liu *et al.* (2013). Therefore, we used our model to predict the asymptotic behavior /proportion of CSCs at equilibrium level and over the tumor's exponential growth phase. Interestingly, our model suggests that depending on the parameter values the percentage of CSCs can vary between 0 and 100. Johnson et al. (2010) also developed an ODE model of stem, progenitor and fully differentiated cell populations and studied constant fractions of CSCs in tumors and reported the same result about the percentage of the CSCs. They showed that depending on the tumor growth and differentiation rates balance, CSCs can comprise any proportion of the tumor, and that higher stem cell proportions likely yield more aggressive tumors.

There is increasing evidence to support the theory that growth and survival of CSCs are highly influenced by tumor micro-environmental factors and molecular signaling, initiated by cytokines and growth factors Li (2002); Morrison and Kimble (2006); Morrison *et al.* (1997); Simons and Cleavers (2011). Interleukin-6 (IL-6) is a pleiotropic cytokine, secreted by a variety of cell types, that is key player in number of cellular processes including proliferation, survival, differentiation, migration and invasion Choudhary *et al.* (2016). IL-6 binds to its natural receptor, IL-6R, on the surface of tumor cells. Once bound to IL-6, the IL-6R-gp130 complex results in the activation of signaling pathways which enhance the CSCs' self-renewal and survival Krishnamurthy *et al.* (2014); Neiva *et al.* (2009). Therefore, in order to quantify the impacts of IL-6 on tumor growth and CSC self-renewal, in Chapter 2 we expanded the model developed in Chapter 1 to incorporate the molecular level details of tumor cell-secreted IL-6 signaling. This model follows

the modeling techniques pioneered by Jackson and Jain Jain *et al.* (2008, 2009). They developed a multi-scale model that operates at three levels: (1) Intracellular level: regulation of signaling pathways that are critical to cell proliferation, apoptosis, and migration; (2) Cellular level: cell-surface dynamics of receptor-ligand binding and receptor activation that lead to intracellular signal transduction cascades; and (3) Tissue level: dynamics of signaling chemicals and anti-cancer agents within the tissue, tumor growth dynamics, and tumor and vascular response to treatment. Their model was used to describe tumor angiogenesis, vascular tumor growth, and response to treatment based on the SCID Mouse Model of Human Tumor Angiogenesis Jain and Jackson (2017); Jain *et al.* (2008, 2009). However, it does not include the heterogenous populations of tumor cells. It is necessary to model CSCs as a distinct subpopulation from other tumor cells since they are identified as "drivers" of the tumorigenic process in cancer. Furthermore, tissue hierarchy must be considered because stem, progenitor, and differentiated cells have very different properties. Our model (and its expansions) is unique in a way that not only it includes assumptions of the CSC hypothesis, but it also includes the molecular level details of IL-6-mediated signaling initiation and its effect on tumor cell survival and CSC self-renewal. To author's knowledge, this is the first model of cancer stem cell driven tumor growth that operates across the scales of receptor-ligand binding and tissue level cancer growth. Tracking the temporal changes in fractional occupancies of IL-6 receptors on tumor cells allows us to quantify the impacts of IL-6 on tumor growth dynamics and also connects the scales.

Another worth mentioning feature of our model is that it is developed based on lab experimental studies of human head and neck primary tumors xenografts generated from a small population of CSCs in mice (described in Krishnamurthy

et al. (2014)). Our model could successfully capture the experimentally observed growth dynamics for these primary tumor xenografts. In addition, it suggested that only a fractional occupancy of 12% on CSCs is sufficient to capture the tumor growth dynamics observed in data. Moreover, our model predicted that each PC undergoes only one round of amplification before differentiating into two terminally differentiated cells leading to a tumor composition that consists of mostly differentiated cells. This is consistent with the relatively slowly growth rate of tumor cells observed in the experimental data.

Although the importance of the role of IL-6 on tumor progression and survival is well documented but the mechanism behind anti-IL-6R therapies is not fully understood yet. Therefore, we modified the model in Chapter 2 to include the therapeutic administration of an anti-IL-6R antibody, Tocilizumab (TCZ), to study the response of tumor cells to this targeted treatment. This model not only quantifies the influence of IL-6 on primary tumor xenografts but also provides some explanations for the various effects of TCZ on tumor growth and CSC percentage. Our TCZ-therapy model tracks the IL-6-TCZ binding dynamics on the tumor cells.

We defined a TCZ dosing schedule based on the experiments described in Mochizuki *et al.* (2015). The simulations predicted that small amounts of TCZ is sufficient to result in tumor reduction and a sustained tumor slowing of tumor growth. Also, for primary tumor xenografts (grown in the absence of human ECs), our model predicts that effect of TCZ on the death rate of the tumor cells is more pronounced than its effect on CSC self-renewal, and this leads to a small increase in the percentage of CSCs after treatment with TCZ. This result is comparable with the results reported in Mochizuki *et al.* (2015). In that study, in an experimental

setting that included human endothelial cells (ECs), the effect of TCZ on Mucoepidermoid carcinoma (MEC) cell lines is investigated and it is shown that TCZ has mixed effects on the fraction of CSCs post therapy. Finally, it was shown that the frequency of dosing does not significantly impact tumor response to TCZ.

In the experimental settings used in Chapter 2, that does not include microenvironmental production of IL-6 by endothelial cells. There is evidence that human endothelial cells associated to HNSCC niche can secrete significantly higher levels of IL-6 than tumor cells Krishnamurthy *et al.* (2014). We already showed that even relatively small amounts of tumor cell-secreted IL-6 can greatly enhance both tumor growth and the fraction of CSCs within xenograft tumors. Interestingly, it has been shown that HNSCC CSCs reside in perivascular niches and depend on that crosstalk with tumor associated endothelial cells for their survival and growth Krishnamurthy *et al.* (2010, 2014). All together, these facts motivated us to extend the model developed in Chapter 2 to include human endothelial cells and further to explore the effects of EC-secreted IL-6 on the survival, self-renewal and tumorigenic potentials of CSCs within the HNSCC tumor niche. As mentioned earlier, this model follows the models introduced in Jain and Jackson (2017); Jain *et al.* (2008, 2009). Among those, Jain and Jackson (2017) developed a model to explore the role of VEGF-mediated cross-talk between endothelial and tumor cells on both cell types' survival and proliferation in both in vitro and in vivo settings. The model in Chapter 3 closely follows their model structure but at the same time it is an extension of the model developed in Chapter 2. To authors' knowledge, this EC-TC cross-talk model is the first model of its kind that goes across the scales from intracellular signaling level to tissue level incorporating the CSC hypothesis and the impacts of microenvironmental molecular factors (IL-6, Bcl-2, VEGF and oxygen)

on CSC-mediated tumor growth dynamics. This is a fully multi-scale approach where the fractional occupancies of IL-6R, VEGF receptors, VEGFR1 and VEGFR2, connect the cellular level (receptor-ligand binding) to both the tissue level (TC and EC growth) and the intracellular level (pro-survival protein, Bcl-2 upregulation).

After discussing the results of mono-therapy, the relevant question is whether combination therapy (always) achieve better results than a single drug therapy. If the population size of CSCs can indeed negatively affect the self-renewal probability of CSCs, removal of them by CSC targeting therapies (such as TCZ) can remove the negative feedback regulation, leading to enhancement of self-renewal of CSCs. In order to address this question for HNSCC tumors, we modified the EC-TC cross-talk model to include the response of tumor cell types, specially CSCs, to combination therapy with TCZ and Cisplatin, the most common chemotherapeutic drug being used in HNSCC treatment Nör *et al.* (2014). Our model is also based on an experimental setup in which human tumor cell (UM-SCC-1 and UM-SCC-22B cell lines) are seeded along with human dermal microvascular endothelial cells (HDMECs) in poly(L-lactic) acid biodegradable scaffolds, and transplanted into SCID mice. The model is calibrated using control data for both UM-SCC-1 and UM-SCC-22B cancer cell lines, and is validated by directly comparing (i.e. no additional parameter fitting) the experimental data and the model predictions for combination treatment of TCZ and Cisplatin. Although there are several mathematical models for describing targeted therapies (see Gallasch *et al.* (2013); Swierniak *et al.* (2009) and Michor and Beal (2015) for reviews), if not any, only in few of them model predictions for treatment might directly be compared to the experimental data. Our model could fairly predict the responses of tumor cells to both mono- and combination therapies. Furthermore, simulations of Cisplatin-therapy suggested

that the anti-therapeutic effects of Cisplatin on tumor growth are directly correlated with the percentage of CSCs after treatment. In addition, the TCZ-therapy reliably predicts the tumor volume growth dynamics observed in tumor volumes after treatment for UM-SCC-1 cell lines. However, our model is not capable of capturing the increase observed in tumor volumes after treatment for some of the UM-SCC-22B cell line data. The combination-therapy model also predicted that high levels of CSCs after treatment is strongly correlated with the poor therapeutic effects of Cisplatin. Finally, our simulations suggested that low levels of Cisplatin is enough to be effective and pre-treatment with Cisplatin followed by TCZ optimizes the synergism between Cisplatin and TCZ.

In summary, our full model has a sufficient resolution to evaluate the molecular details (i.e. cytokine-mediated signal initiation resulting from receptor ligand binding) of phenotype switching among cells, which is the level of detail required to make informed predictions when cells express the same receptors but ultimately integrate signals differently to elicit diverse responses. The model predictions have been validated using experimental data specifically designed for the modeling study. Most models stop at verification ensuring that the model behaves as expected and matches existing experimental data. Here we validated important features of our model by directly comparing the data sets with modeling output (not parameter fitting). Lastly, the model considers the connections between intracellular (up-regulation of survival proteins), cellular (receptor-ligand binding necessary for signal initiation) and tissue level events (Figure 5.1). While some models exist that include one of two the above, few if any, incorporate all three. This type of integration of multilevel descriptions in a single model is novel for computational cancer research.

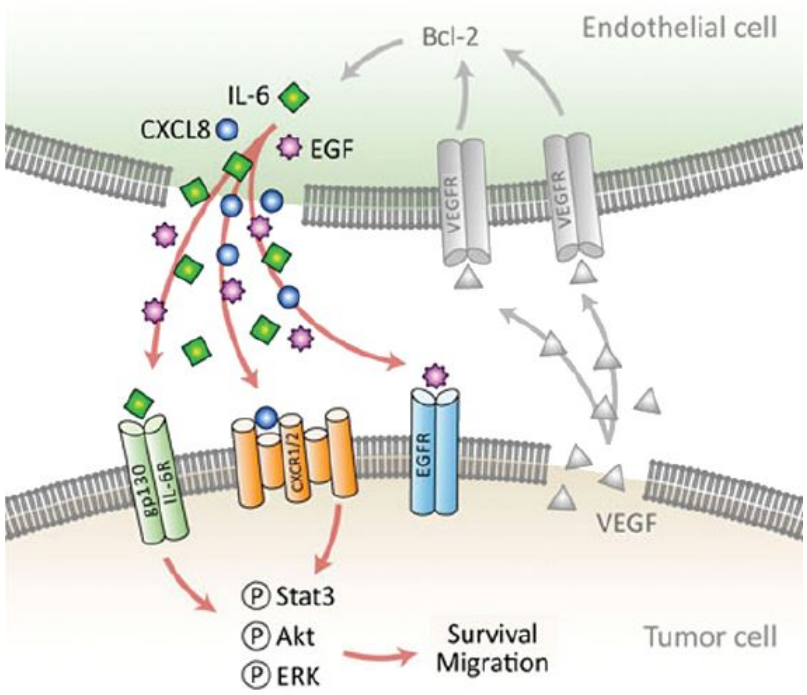

Figure 5.1: Model for Cross-Talk Between Endothelial and Tumor Cells Neiva *et al.* (2009)

The next step is extending these ideas into a spatio-temporal modeling framework. Such a model could be used to investigate the differential motility of cancer stem cells and the subsequent invasion of tumors with multiple cellular phenotypes. The ultimate goal would be to determine the effect of IL-6 signaling on the acquisition of an invasive phenotype by head and neck cancer stem cells. The inherent tumor heterogeneity, manifested by phenotype-dependent proliferation and motility, could lead to the sorting of cells into localized microenvironment (vascular niches) within a solid tumor and enhance invasive and metastatic potential. With a spatiotemporal computational approach, the underlying mechanisms for local tumor invasion can be isolated and studied in detail.

Al-Hajj, M. and M. F. Clarke, "Self-renewal and solid tumor stem cells", Oncogene **23**, 43, 7274–7282 (2004).

Al-Hajj, M., M. S. Wicha, A. Benito-Hernandez, S. J. Morrison and M. F. Clarke, "Prospective identification of tumorigenic breast cancer cells", Proceedings of the National Academy of Sciences **100**, 7, 3983–3988 (2003).

Albers, A. E., C. Chen, B. Köberle, X. Qian, J. P. Klussmann, B. Wollenberg and A. M. Kaufmann, "Stem cells in squamous head and neck cancer", Critical reviews in oncology/hematology **81**, 3, 224–240 (2012).

Altrock, P. M., L. L. Liu and F. Michor, "The mathematics of cancer: integrating quantitative models", Nature Reviews Cancer **15**, 12, 730–745 (2015).

Anderson, L. and M. Mackey, "Resonance in periodic chemotherapy: a case study of acute myelogenous leukemia", J Theo Biol **208**, 113–130 (2001).

Bapat, S. A., A. M. Mali, C. B. Koppikar and N. K. Kurrey, "Stem and progenitor-like cells contribute to the aggressive behavior of human epithelial ovarian cancer", Cancer research **65**, 8, 3025–3029 (2005).

Bernard, S., J. Bélair and M. C. Mackey, "Oscillations in cyclical neutropenia: New evidence based on mathematical modeling", Journal of theoretical biology **223**, 3, 283–298 (2003).

Blower, S. M. and H. Dowlatabadi, "Sensitivity and uncertainty analysis of complex models of disease transmission: an hiv model, as an example", International Statistical Review/Revue Internationale de Statistique pp. 229–243 (1994).

Boayue, K., L. Gu, A. Yeager, R. Kreitman and H. Findley, "Pediatric acute myelogenous leukemia cells express il-6 receptors and are sensitive to a recombinant il6-pseudomonas exotoxin.", Leukemia **12**, 2, 182–191 (1998).

Boman, B. M., M. S. Wicha, J. Z. Fields and O. A. Runquist, "Symmetric division of cancer stem cells–a key mechanism in tumor growth that should be targeted in future therapeutic approaches", Clinical Pharmacology & Therapeutics **81**, 6, 893–898 (2007).

Bran, G., K. Goette, K. Riedel, K. Hoermann and F. Riedel, "Il-6 antisense-mediated growth inhibition in a head and neck squamous cell carcinoma cell line", In Vivo **25**, 4, 579–584 (2011).

Cabrera, M. C., R. E. Hollingsworth, E. M. Hurt *et al.*, "Cancer stem cell plasticity and tumor hierarchy", (2015).

Charusanti, P., X. Hu, L. Chen, D. Neuhauser and J. DiStefano, "A mathematical model of bcr-abl autophosphorylation, signaling through the crkl pathway, and gleevec dynamics in chronic myeloid leukemia", Discrete and Continuous Dynamical Systems Series B **4**, 1, 99–114 (2004).

Choudhary, M., T. France, T. Teknos and K. P, "Interleukin-6 role in head and neck squamous cell carcinoma progression", World J Otorhino-HN Surgery **2**, 90–97 (2016).

Civenni, G., A. Walter, N. Kobert, D. Mihic-Probst, M. Zipser, B. Belloni, B. Seifert, H. Moch, R. Dummer, M. van den Broek *et al.*, "Human cd271-positive melanoma stem cells associated with metastasis establish tumor heterogeneity and long-term growth", Cancer research **71**, 8, 3098–3109 (2011).

Clarke, M. F. and M. Fuller, "Stem cells and cancer: two faces of eve", Cell **124**, 6, 1111–1115 (2006).

Cook, A. B., D. R. Ziazadeh, J. Lu and T. L. Jackson, "An integrated cellular and sub-cellular model of cancer chemotherapy and therapies that target cell survival.", Mathematical biosciences and engineering: MBE **12**, 6, 1219–1235 (2015).

Coulie, P., M. Stevens and J. Van Snick, "High- and low-affinity receptors for murine interleukin 6. distinct distribution on b and t cells", Eur J IImmunol **19**, 2107–2114 (1989).

Cowan, G., *Statistical data analysis* (Oxford University Press, 1998).

Cunningham, S. A., T. M. Tran, M. P. Arrate and T. A. Brock, "Characterization of vascular endothelial cell growth factor interactions with the kinase insert domain-containing receptor tyrosine kinase a real time kinetic study", Journal of Biological Chemistry **274**, 26, 18421–18427 (1999).

Dedrick, R. L. and M. F. Flessner, "Pharmacokinetic problems in peritoneal drug administration: tissue penetration and surface exposure", Journal of the National Cancer Institute **89**, 7, 480–487 (1997).

Deisboeck, T. S., Z. Wang, P. Macklin and V. Cristini, "Multiscale cancer modeling", Annual review of biomedical engineering **13**, 127–155 (2011).

Deleyrolle, L. P., G. Ericksson, B. J. Morrison, J. A. Lopez, K. Burrage, P. Burrage, A. Vescovi, R. L. Rietze and B. A. Reynolds, "Determination of somatic and cancer stem cell self-renewing symmetric division rate using sphere assays", PloS one **6**, 1, e15844 (2011).

Dick, J. E., "Looking ahead in cancer stem cell research", Nature biotechnology **27**, 1, 44–47 (2009).

Dingli, D., A. Traulsen and J. M. Pacheco, "Stochastic dynamics of hematopoietic tumor stem cells", Cell Cycle **6**, 4, 461–466 (2007).

Driessens, G., B. Beck, A. Caauwe, B. D. Simons and C. Blanpain, "Defining the mode of tumour growth by clonal analysis", Nature **488**, 7412, 527–530 (2012).

Dylla, S. J., L. Beviglia, I.-K. Park, C. Chartier, J. Raval, L. Ngan, K. Pickell, J. Aguilar, S. Lazetic, S. Smith-Berdan *et al.*, "Colorectal cancer stem cells are enriched in xenogeneic tumors following chemotherapy", PloS one **3**, 6, e2428 (2008).

Elishmereni, M., Y. Kheifetz, H. Søndergaard, R. V. Overgaard and Z. Agur, "An integrated disease/pharmacokinetic/pharmacodynamic model suggests improved interleukin-21 regimens validated prospectively for mouse solid cancers", PLoS Comput Biol **7**, 9, e1002206 (2011).

Enderling, H., L. Hlatky and P. Hahnfeldt, "Cancer stem cells: a minor cancer subpopulation that redefines global cancer features", Frontiers in oncology **3** (2013).

Finkel, K. A., K. A. Warner, S. Kerk, C. R. Bradford, S. A. McLean, M. E. Prince, H. Zhong, E. M. Hurt, R. E. Hollingsworth, M. S. Wicha *et al.*, "Il-6 inhibition with medi5117 decreases the fraction of head and neck cancer stem cells and prevents tumor recurrence", Neoplasia **18**, 5, 273–281 (2016).

Foley, C. and M. C. Mackey, "Mathematical model for g-csf administration after chemotherapy", Journal of theoretical biology **257**, 1, 27–44 (2009).

Foo, J., M. W. Drummond, B. Clarkson, T. Holyoake and F. Michor, "Eradication of chronic myeloid leukemia stem cells: a novel mathematical model predicts no therapeutic benefit of adding g-csf to imatinib", PLoS computational biology **5**, 9, e1000503 (2009).

Fornari, C., M. Beccuti, S. Lanzardo, L. Conti, G. Balbo, F. Cavallo, R. A. Calogero and F. Cordero, "A mathematical-biological joint effort to investigate the tumor-initiating ability of cancer stem cells", PloS one **9**, 9, e106193 (2014).

Frank, N. Y., T. Schatton and M. H. Frank, "The therapeutic promise of the cancer stem cell concept", The Journal of clinical investigation **120**, 1, 41 (2010).

Gallasch, R., M. Efremova, P. Charoentong, H. Hackl and Z. Trajanoski, "Mathematical models for translational and clinical oncology", Journal of clinical bioinformatics **3**, 1, 23 (2013).

Ganguly, R. and I. Puri, "Mathematical model for the cancer stem cell hypothesis", Cell proliferation **39**, 1, 3–14 (2006).

Gao, X., J. T. McDonald, L. Hlatky and H. Enderling, "Acute and fractionated irradiation differentially modulate glioma stem cell division kinetics", Cancer research **73**, 5, 1481–1490 (2013).

Garbers, C., S. Aparicio-Siegmund and S. Rose-John, "The il-6/gp130/stat3 signaling axis: recent advances towards specific inhibition", Curr Opin Immunol **34**, 75 – 82 (2015).

Gentry, S. N. and T. L. Jackson, "A mathematical model of cancer stem cell driven tumor initiation: implications of niche size and loss of homeostatic regulatory mechanisms", PloS one **8**, 8, e71128 (2013).

Girouard, S. D. and G. F. Murphy, "Melanoma stem cells: not rare, but well done", Laboratory investigation **91**, 5, 647–664 (2011).

Gupta, P. B., C. M. Fillmore, G. Jiang, S. D. Shapira, K. Tao, C. Kuperwasser and E. S. Lander, "Stochastic state transitions give rise to phenotypic equilibrium in populations of cancer cells", Cell **146**, 4, 633–644 (2011).

Hanahan, D. and R. Weinberg, "The hallmarks of cancer (Review)", Cell **100**, 57–70 (2000).

Hanahan, D. and R. Weinberg, "Hallmarks of cancer: the next generation", Cell **144**, 5, 646–674 (2011a).

Hanahan, D. and R. A. Weinberg, "Hallmarks of cancer: the next generation", cell **144**, 5, 646–674 (2011b).

Hermann, P. C., S. Bhaskar, M. Cioffi and C. Heeschen, "Cancer stem cells in solid tumors", in "Seminars in cancer biology", vol. 20, pp. 77–84 (Elsevier, 2010).

Hirabayashi, Y. and A. Lemmey, *The role of tocilizumab in the treatment of rheumatoid arthritis* (INTECH Open Access Publisher, 2012).

Igawa, T., S. Ishii, T. Tachibana, A. Maeda, Y. Higuchi, S. Shimaoka, C. Moriyama, T. Watanabe, R. Takubo, Y. Doi *et al.*, "Antibody recycling by engineered ph-dependent antigen binding improves the duration of antigen neutralization", Nature biotechnology **28**, 11, 1203–1207 (2010).

Insco, M. L., A. Leon, C. H. Tam, D. M. McKearin and M. T. Fuller, "Accumulation of a differentiation regulator specifies transit amplifying division number in an adult stem cell lineage", Proceedings of the National Academy of Sciences **106**, 52, 22311–22316 (2009).

Jackson, T., N. Komarova and K. Swanson, "Mathematical oncology: using mathematics to enable cancer discoveries", The American Mathematical Monthly **121**, 9, 840–856 (2014).

Jain, H. V. and T. Jackson, "Mathematical modeling of cellular cross-talk between endothelial and tumor cells highlights counterintuitive effects of vegf-targeted therapies", Bulletin of Mathematical Biology (2017).

Jain, H. V. and M. Meyer-Hermann, "The molecular basis of synergism between carboplatin and abt-737 therapy targeting ovarian carcinomas", Cancer research pp. canres–3174 (2010).

Jain, H. V., J. E. Nör and T. L. Jackson, "Modeling the vegf–bcl-2–cxcl8 pathway in intratumoral agiogenesis", Bulletin of mathematical biology **70**, 1, 89–117 (2008).

Jain, H. V., J. E. Nör and T. L. Jackson, "Quantification of endothelial cell–targeted anti–bcl-2 therapy and its suppression of tumor growth and vascularization", Molecular cancer therapeutics **8**, 10, 2926–2936 (2009).

Johnston, M. D., P. K. Maini, S. J. Chapman, C. M. Edwards and W. F. Bodmer, "On the proportion of cancer stem cells in a tumour", Journal of theoretical biology **266**, 4, 708–711 (2010).

Kaneko, T., Z. Zhang, M. G. Mantellini, E. Karl, B. Zeitlin, M. Verhaegen, M. S. Soengas, M. Lingen, R. M. Strieter, G. Nunez *et al.*, "Bcl-2 orchestrates a cross-talk between endothelial and tumor cells that promotes tumor growth", Cancer research **67**, 20, 9685–9693 (2007).

Kapitanov, G., "A mathematical model of cancer stem cell lineage population dynamics with mutation accumulation and telomere length hierarchies", Mathematical Modelling of Natural Phenomena **7**, 1, 136–165 (2012).

Kim, P. S., P. P. Lee and D. Levy, "A pde model for imatinib-treated chronic myelogenous leukemia", Bulletin of mathematical biology **70**, 7, 1994 (2008).

Kim, S.-Y., J. W. Kang, X. Song, B. K. Kim, Y. D. Yoo, Y. T. Kwon and Y. J. Lee, "Role of the il-6-jak1-stat3-oct-4 pathway in the conversion of non-stem cancer cells into cancer stem-like cells", Cellular signalling **25**, 4, 961–969 (2013).

King, J., T. Hamil, J. Creighton, S. Wu, P. Bhat, F. McDonald and T. Stevens, "Structural and functional characteristics of lung macro-and microvascular endothelial cell phenotypes", Microvascular research **67**, 2, 139–151 (2004).

Komarova, N. L. and D. Wodarz, "Effect of cellular quiescence on the success of targeted cml therapy", PLoS One **2**, 10, e990 (2007).

Krishnamurthy, S., Z. Dong, D. Vodopyanov, A. Imai, J. I. Helman, M. E. Prince, M. S. Wicha and J. E. Nör, "Endothelial cell-initiated signaling promotes the survival and self-renewal of cancer stem cells", Cancer research **70**, 23, 9969–9978 (2010).

Krishnamurthy, S. and J. Nör, "Head and neck cancer stem cells", Journal of dental research **91**, 4, 334–340 (2012).

Krishnamurthy, S., K. A. Warner, Z. Dong, A. Imai, C. Nör, B. B. Ward, J. I. Helman, R. S. Taichman, E. L. Bellile, L. K. McCauley *et al.*, "Endothelial interleukin-6 defines the tumorigenic potential of primary human cancer stem cells", Stem Cells **32**, 11, 2845–2857 (2014).

Li, H., "The stem-cell niche theory: lessons from flies", Nat Rev Genetics **3**, 931–940 (2002).

Li, L. and W. Neaves, "Normal stem cells and cancer stem cells: the niche matters", Cancer Research **66**, 4553–4557 (2006).

Li, Z. and L. Li, "Understanding hematopoietic stem-cell microenvironments", Trends in Biomedical Sciences **31**, 589–595 (2006).

Lindmark, E., E. Diderholm, L. Wallentin and A. Siegbahn, "Relationship between interleukin 6 and mortality in patients with unstable coronary artery disease: effects of an early invasive or noninvasive strategy", Jama **286**, 17, 2107–2113 (2001).

Ling, X., Y. Shen, R. Sun, M. Zhang, C. Li, J. Mao, J. Xing, C. Sun and J. Tu, "Tumor-targeting delivery of hyaluronic acid–platinum (iv) nanoconjugate to reduce toxicity and improve survival", Polymer Chemistry **6**, 9, 1541–1552 (2015).

Liu, X., S. Johnson, S. Liu, D. Kanojia, W. Yue, U. P. Singh, Q. Wang, Q. Wang, Q. Nie and H. Chen, "Nonlinear growth kinetics of breast cancer stem cells: implications for cancer stem cell targeted therapy", Scientific reports **3** (2013).

Lu, H., K. R. Clauser, W. L. Tam, J. Fröse, X. Ye, E. N. Eaton, F. Reinhardt, V. S. Donnenberg, R. Bhargava, S. A. Carr *et al.*, "A breast cancer stem cell niche supported by juxtacrine signalling from monocytes and macrophages", Nature cell biology **16**, 11, 1105–1117 (2014).

Mac Gabhann, F. and A. S. Popel, "Dimerization of vegf receptors and implications for signal transduction: a computational study", Biophysical chemistry **128**, 2, 125–139 (2007a).

Mac Gabhann, F. and A. S. Popel, "Interactions of vegf isoforms with vegfr-1, vegfr-2, and neuropilin in vivo: a computational model of human skeletal muscle", American Journal of Physiology-Heart and Circulatory Physiology **292**, 1, H459–H474 (2007b).

Mac Gabhann, F., M. T. Yang and A. S. Popel, "Monte carlo simulations of vegf binding to cell surface receptors in vitro", Biochimica et Biophysica Acta (BBA)-Molecular Cell Research **1746**, 2, 95–107 (2005).

Mackillop, W., A. Ciampi, J. Till and R. Buick, "A stem cell model of human tumor growth: implications for tumor cell clonogenic assays.", Journal of the national cancer institute **70**, 1, 9–16 (1983).

Marino, S., I. B. Hogue, C. J. Ray and D. E. Kirschner, "A methodology for performing global uncertainty and sensitivity analysis in systems biology", Journal of theoretical biology **254**, 1, 178–196 (2008).

McKay, M. D., R. J. Beckman and W. J. Conover, "A comparison of three methods for selecting values of input variables in the analysis of output from a computer code", Technometrics **42**, 1, 55–61 (2000).

Michor, F., "Mathematical models of cancer stem cells", Journal of Clinical Oncology **26**, 17, 2854–2861 (2008).

Michor, F. and K. Beal, "Improving cancer treatment via mathematical modeling: surmounting the challenges is worth the effort", Cell **163**, 5, 1059–1063 (2015).

Michor, F., T. P. Hughes, Y. Iwasa, S. Branford *et al.*, "Dynamics of chronic myeloid leukaemia", Nature **435**, 7046, 1267 (2005).

Mihara, M., K. Kasutani, M. Okazaki, A. Nakamura, S. Kawai, M. Sugimoto, Y. Matsumoto and Y. Ohsugi, "Tocilizumab inhibits signal transduction mediated by both mil-6r and sil-6r, but not by the receptors of other members of il-6 cytokine family", International immunopharmacology **5**, 12, 1731–1740 (2005).

Mochizuki, D., A. Adams, K. A. Warner, Z. Zhang, A. T. Pearson, K. Misawa, S. A. McLean, G. T. Wolf and J. E. Nör, "Anti-tumor effect of inhibition of il-6 signaling in mucoepidermoid carcinoma", Oncotarget **6**, 26, 22822 (2015).

Molina-Peña, R. and M. M. Álvarez, "A simple mathematical model based on the cancer stem cell hypothesis suggests kinetic commonalities in solid tumor growth", PloS one **7**, 2, e26233 (2012).

Monk, A. C., N. A. Siddall, T. Volk, B. Fraser, L. M. Quinn, E. A. McLaughlin and G. R. Hime, "How is required for stem cell maintenance in the drosophila testis and for the onset of transit-amplifying divisions", Cell Stem Cell **6**, 4, 348–360 (2010).

Morrison, S. and J. Kimble, "Asymmetric and symmetric stem-cell divisions in development and cancer", Nature **441**, 1068–1074 (2006).

Morrison, S., N. Shah and D. Anderson, "Regulatory mechanisms in stem cell biology", Cell **88**, 287–298 (1997).

Morton, C. I., L. Hlatky, P. Hahnfeldt and H. Enderling, "Non-stem cancer cell kinetics modulate solid tumor progression", Theoretical Biology and Medical Modelling **8**, 1, 48 (2011).

Neiva, K. G., K. A. Warner, M. S. Campos, Z. Zhang, J. Moren, T. E. Danciu and J. E. Nör, "Endothelial cell-derived interleukin-6 regulates tumor growth", BMC cancer **14**, 1, 1 (2014).

Neiva, K. G., Z. Zhang, M. Miyazawa, K. A. Warner, E. Karl and J. E. Nör, "Cross talk initiated by endothelial cells enhances migration and inhibits anoikis of squamous cell carcinoma cells through stat3/akt/erk signaling", Neoplasia **11**, 6, 583–IN14 (2009).

Nguyen, L. V., R. Vanner, P. Dirks and C. J. Eaves, "Cancer stem cells: an evolving concept", Nature reviews. Cancer **12**, 2, 133 (2012).

Nilsson, M. B., R. R. Langley and I. J. Fidler, "Interleukin-6, secreted by human ovarian carcinoma cells, is a potent proangiogenic cytokine", Cancer Research **65**, 23, 10794–10800 (2005).

Noll, J. E., K. Vandyke and A. C. Zannettino, "The role of the ?cancer stem cell niche? in cancer initiation and progression", (2014).

Nör, C., Z. Zhang, K. A. Warner, L. Bernardi, F. Visioli, J. I. Helman, R. Roesler and J. E. Nör, "Cisplatin induces bmi-1 and enhances the stem cell fraction in head and neck cancer", Neoplasia **16**, 2, 137–W8 (2014).

O'Brien, C. A., A. Kreso and C. H. Jamieson, "Cancer stem cells and self-renewal", Clinical Cancer Research **16**, 12, 3113–3120 (2010).

Olsen, M. M. and H. T. Siegelmann, "Multiscale agent-based model of tumor angiogenesis", Procedia Computer Science **18**, 1016–1025 (2013).

Özbek, S., J. Grötzinger, B. Krebs, M. Fischer, A. Wollmer, T. Jostock, J. Müllberg and S. Rose-John, "The membrane proximal cytokine receptor domain of the human interleukin-6 receptor is sufficient for ligand binding but not for gp130 association", Journal of Biological Chemistry **273**, 33, 21374–21379 (1998).

Pardal, R., M. F. Clarke and S. J. Morrison, "Applying the principles of stem-cell biology to cancer", Nature reviews. Cancer **3**, 12, 895 (2003).

Parfenov, M., C. S. Pedamallu, N. Gehlenborg, S. S. Freeman, L. Danilova, C. A. Bristow, S. Lee, A. G. Hadjipanayis, E. V. Ivanova, M. D. Wilkerson *et al.*, "Characterization of hpv and host genome interactions in primary head and neck cancers", Proceedings of the National Academy of Sciences **111**, 43, 15544–15549 (2014).

Pearson, A. T., T. L. Jackson and J. E. Nör, "Modeling head and neck cancer stem cell-mediated tumorigenesis", Cellular and Molecular Life Sciences **73**, 17, 3279–3289 (2016).

Perfahl, H., H. M. Byrne, T. Chen, V. Estrella, T. Alarcón, A. Lapin, R. A. Gatenby, R. J. Gillies, M. C. Lloyd, P. K. Maini *et al.*, "Multiscale modelling of vascular tumour growth in 3d: the roles of domain size and boundary conditions", PloS one **6**, 4, e14790 (2011).

Plaks, V., N. Kong and Z. Werb, "The cancer stem cell niche: how essential is the niche in regulating stemness of tumor cells?", Cell stem cell **16**, 3, 225–238 (2015).

Plank, M., B. Sleeman and P. Jones, "A mathematical model of tumour angiogenesis, regulated by vascular endothelial growth factor and the angiopoietins", Journal of theoretical biology **229**, 4, 435–454 (2004).

PRIES, R., A. THIEL, C. BROCKS and B. WOLLENBERG, "Secretion of tumor-promoting and immune suppressive cytokines by cell lines of head and neck squamous cell carcinoma", in vivo **20**, 1, 45–48 (2006).

Prince, M., R. Sivanandan, A. Kaczorowski, G. Wolf, M. Kaplan, P. Dalerba, I. Weissman, M. Clarke and L. Ailles, "Identification of a subpopulation of cells with cancer stem cell properties in head and neck squamous cell carcinoma", Proceedings of the National Academy of Sciences **104**, 3, 973–978 (2007).

Prince, M. E. and L. E. Ailles, "Cancer stem cells in head and neck squamous cell cancer", Journal of Clinical Oncology **26**, 17, 2871–2875 (2008).

Pulte, D. and H. Brenner, "Changes in survival in head and neck cancers in the late 20th and early 21st century: a period analysis", The oncologist **15**, 9, 994–1001 (2010).

Quintana, E., M. Shackleton, M. S. Sabel, D. R. Fullen, T. M. Johnson and S. J. Morrison, "Efficient tumour formation by single human melanoma cells", Nature **456**, 7222, 593–598 (2008).

Reya, T., S. J. Morrison, M. F. Clarke and I. L. Weissman, "Stem cells, cancer, and cancer stem cells", nature **414**, 6859, 105–111 (2001).

Rodriguez-Brenes, I. A., N. L. Komarova and D. Wodarz, "Evolutionary dynamics of feedback escape and the development of stem-cell–driven cancers", Proceedings of the National Academy of Sciences **108**, 47, 18983–18988 (2011).

Rodriguez-Brenes, I. A., D. Wodarz and N. L. Komarova, "Characterizing inhibited tumor growth in stem-cell-driven non-spatial cancers", Mathematical biosciences **270**, 135–141 (2015).

Sanchez, M. A. and S. M. Blower, "Uncertainty and sensitivity analysis of the basic reproductive rate: tuberculosis as an example", American Journal of Epidemiology **145**, 12, 1127–1137 (1997).

Sanga, S., J. P. Sinek, H. B. Frieboes, M. Ferrari, J. P. Fruehauf and V. Cristini, "Mathematical modeling of cancer progression and response to chemotherapy", Expert review of anticancer therapy **6**, 10, 1361–1376 (2006).

Sehl, M. E., J. S. Sinsheimer, H. Zhou and K. L. Lange, "Differential destruction of stem cells: implications for targeted cancer stem cell therapy", Cancer research **69**, 24, 9481–9489 (2009).

Shirinifard, A., J. S. Gens, B. L. Zaitlen, N. J. Popławski, M. Swat and J. A. Glazier, "3d multi-cell simulation of tumor growth and angiogenesis", PloS one **4**, 10, e7190 (2009).

Shkeir, O., M. Athanassiou-Papaefthymiou, M. Lapadatescu, P. Papagerakis, M. J. Czerwinski, C. R. Bradford, T. E. Carey, M. E. Prince, G. T. Wolf and S. Papagerakis, "In vitro cytokine release profile: Predictive value for metastatic potential in head and neck squamous cell carcinomas", Head & neck **35**, 11, 1542–1550 (2013).

Siegel, R. L., K. D. Miller and A. Jemal, "Cancer statistics, 2017", CA: A Cancer Journal for Clinicians **67**, 1, 7–30, URL `http://dx.doi.org/10.3322/caac.21387` (2017).

Simons, B. and H. Cleavers, "Strategies for homeostatic stem cell self-renewal in adult tissues", Cell **1454**, 851–862 (2011).

Singh, S. K., I. D. Clarke, M. Terasaki, V. E. Bonn, C. Hawkins, J. Squire and P. B. Dirks, "Identification of a cancer stem cell in human brain tumors", Cancer research **63**, 18, 5821–5828 (2003).

Snyers, L. and L. De Wit, "Glucocorticoid up-regulation of high-affinity interleukin 6 receptors on human epithelial cells", Proceedings of the National Academy of Sciences **87**, 7, 2838–2842 (1990).

Sottoriva, A., J. J. Verhoeff, T. Borovski, S. K. McWeeney, L. Naumov, J. P. Medema, P. M. Sloot and L. Vermeulen, "Cancer stem cell tumor model reveals invasive morphology and increased phenotypical heterogeneity", Cancer research **70**, 1, 46–56 (2010).

Sujata, L. and S. Chaudhuri, "Stem cell niche, the microenvironment and immunological crosstalk", Cellular & molecular immunology **5**, 2, 107 (2008).

Swierniak, A., M. Kimmel and J. Smieja, "Mathematical modeling as a tool for planning anticancer therapy", European journal of pharmacology **625**, 1, 108–121 (2009).

Taghizadeh, R., M. Noh, Y. H. Huh, E. Ciusani, L. Sigalotti, M. Maio, B. Arosio, M. R. Nicotra, P. Natali, J. L. Sherley *et al.*, "Cxcr6, a newly defined biomarker of tissue-specific stem cell asymmetric self-renewal, identifies more aggressive human melanoma cancer stem cells", PLoS One **5**, 12, e15183 (2010).

Takizawa, H., T. Ohtoshi, K. Ohta, N. Yamashita, S. Hirohata, K. Hirai, K. Hiramatsu and K. Ito, "Growth inhibition of human lung cancer cell lines by interleukin 6 in vitro: a possible role in tumor growth via an autocrine mechanism", Cancer research **53**, 18, 4175–4181 (1993).

Tang, L., A. L. van de Ven, D. Guo, V. Andasari, V. Cristini, K. C. Li and X. Zhou, "Computational modeling of 3d tumor growth and angiogenesis for chemotherapy evaluation", PloS one **9**, 1, e83962 (2014).

Tarquinio, S. B., Z. Zhang, K. G. Neiva, P. J. Polverini and J. E. Nör, "Endothelial cell bcl-2 and lymph node metastasis in patients with oral squamous cell carcinoma", Journal of Oral Pathology & Medicine **41**, 2, 124–130 (2012).

Tee, D. and J. Distefano Iii, "Simulation of tumor-induced angiogenesis and its response to anti-angiogenic drug treatment: mode of drug delivery and clearance rate dependencies", Journal of cancer research and clinical oncology **130**, 1, 15–24 (2004).

Tomasetti, C. and D. Levy, "Role of symmetric and asymmetric division of stem cells in developing drug resistance", Proceedings of the National Academy of Sciences **107**, 39, 16766–16771 (2010).

Turner, C., A. Stinchcombe, M. Kohandel, S. Singh and S. Sivaloganathan, "Characterization of brain cancer stem cells: a mathematical approach", Cell proliferation **42**, 4, 529–540 (2009).

Turner, P. V., T. Brabb, C. Pekow and M. A. Vasbinder, "Administration of substances to laboratory animals: routes of administration and factors to consider", Journal of the American Association for Laboratory Animal Science **50**, 5, 600–613 (2011).

von Tiedemann, B. and U. Bilitewski, "Characterization of the vascular endothelial growth factor–receptor interaction and determination of the recombinant protein by an optical receptor sensor", Biosensors and Bioelectronics **17**, 11, 983–991 (2002).

Wang, D., R. E. Lehman, D. B. Donner, M. R. Matli, R. S. Warren and M. L. Welton, "Expression and endocytosis of vegf and its receptors in human colonic vascular endothelial cells", American Journal of Physiology-Gastrointestinal and Liver Physiology **282**, 6, G1088–G1096 (2002).

Wang, J., L. Zhang, C. Jing, G. Ye, H. Wu, H. Miao, Y. Wu and X. Zhou, "Multi-scale agent-based modeling on melanoma and its related angiogenesis analysis", Theoretical Biology and Medical Modelling **10**, 1, 41 (2013).

Wang, R., K. Chadalavada, J. Wilshire, U. Kowalik, K. E. Hovinga, A. Geber, B. Fligelman, M. Leversha, C. Brennan and V. Tabar, "Glioblastoma stem-like cells give rise to tumour endothelium", Nature **468**, 7325, 829–833 (2010).

Wang, Z., J. D. Butner, R. Kerketta, V. Cristini and T. S. Deisboeck, "Simulating cancer growth with multiscale agent-based modeling", in "Seminars in cancer biology", vol. 30, pp. 70–78 (Elsevier, 2015).

Weekes, S. L., B. Barker, S. Bober, K. Cisneros, J. Cline, A. Thompson, L. Hlatky, P. Hahnfeldt and H. Enderling, "A multicompartment mathematical model of cancer stem cell-driven tumor growth dynamics", Bulletin of mathematical biology **76**, 7, 1762–1782 (2014).

Wicha, M. S., S. Liu and G. Dontu, "Cancer stem cells: an old idea?a paradigm shift", Cancer research **66**, 4, 1883–1890 (2006).

Yang, E., E. van Nimwegen, M. Zavolan, N. Rajewsky, M. Schroeder, M. Magnasco and J. E. Darnell, "Decay rates of human mrnas: correlation with functional characteristics and sequence attributes", Genome research **13**, 8, 1863–1872 (2003).

Yen, P., S. D. Finley, M. O. Engel-Stefanini and A. S. Popel, "A two-compartment model of vegf distribution in the mouse", PloS one **6**, 11, e27514 (2011).

Youssefpour, H., X. Li, A. Lander and J. Lowengrub, "Multispecies model of cell lineages and feedback control in solid tumors", Journal of theoretical biology **304**, 39–59 (2012).

Zhang, L., D. Badgwell and B. J. et al., "Il-6 signaling via the stat3/socs3 pathway: Functional analysis of the conserved stat3 n-domain", Mol Cell Biochem **288(1-2)**, 179 – 189 (2006).

Zhang, Z., K. G. Neiva, M. W. Lingen, L. M. Ellis and J. E. Nör, "Vegf-dependent tumor angiogenesis requires inverse and reciprocal regulation of vegfr1 and vegfr2", Cell Death & Differentiation **17**, 3, 499–512 (2010).

Zhu, Y., M. Luo, M. Brooks, S. G. Clouthier and M. S. Wicha, "Biological and clinical significance of cancer stem cell plasticity", Clinical and translational medicine **3**, 1, 32 (2014).

APPENDIX A

LATIN HYPERCUBE SAMPLING AND PARTIAL RANK CORRELATION COEFFICIENTS

The sensitivity of each of the parameters of the model to a specified response/output function can be accounted for using Partial Rank Correlation coefficients (PRCC) along with using an appropriate sampling technique, such as Latin Hyperbolic Sampling (LHS) Blower and Dowlatabadi (1994); Marino *et al.* (2008); Sanchez and Blower (1997). The method is briefly described below.

Let $X_1, \ldots, X_d$ be input parameter values that are randomly chosen from a specified sample space (i.e., they are random variables). Furthermore, appropriate probability distribution functions (PDFs) Blower and Dowlatabadi (1994); McKay *et al.* (2000); Sanchez and Blower (1997) for each of the these parameters are chosen (based on the biology cancer being modeled). Any specified PDF describes the range of possible values and the probability of occurrence of any specific value.

Definition A.0.1 McKay *et al.* (2000). *Latin Hypercube Sampling (LHS) is a stratified sampling method for sampling the input parameter values. Using stratified sampling, the sample space S (possible range of each parameter) of X_i are partitioned into N disjoint strata of equal marginal probability $1/N$. LHS ensures us that all portions of sample space are sampled, and each of the input variables has all portions of its distribution represented by input parameter values.*

Definition A.0.2 Blower and Dowlatabadi (1994); Sanchez and Blower (1997). *Sensitivity analysis follows uncertainty analysis to identify critical inputs (parameters and initial conditions) of a model and quantify how input uncertainty impacts model outcome(s).*

Definition A.0.3 Blower and Dowlatabadi (1994). *Partial Rank Correlation Coefficient (PRCC) can be used to evaluate the statistical relationships between each input parameter and each outcome variable, while keeping all of the other input parameters constant at their expected value.*

PRCC can only be used to assess the sensitivity of outcome variables that are monotonically related to the input parameters Blower and Dowlatabadi (1994).

A PRCC between an input parameter X_j, and an output variable Y, can be calculated using formula given by Blower and Dowlatabadi (1994):

$$r_{X_jY} = \frac{Cov(X_j, Y)}{\sqrt{Var(X_j)Var(Y)}} = \frac{\sum_{i=1}^{N}(X_{ij} - \bar{X})(Y_i - \bar{Y})}{\sqrt{\sum_{i=1}^{N}(X_{ij} - \bar{X})^2 \sum_{i=1}^{N}(Y_i - \bar{Y})^2}} := PRCC(Y, X_j) \tag{A.0.1}$$

where, $\mathrm{Cov}(X_j, Y)$ represents the covariance between X_j and Y, while $\mathrm{Var}(X_j)$ and $\mathrm{Var}(Y)$ are the variance of X_j and Y, respectively (the quantities $\bar{X}$ and $\bar{Y}$ are the respective sample means).

It is worth mentioning that PRCC always varies between -1 and $+1$. The sign of PRCC indicates the specific qualitative relationship between input and output variables. Furthermore, the magnitude of the PRCC indicates the importance of the uncertainty in estimating the value of the input variable due to the imprecision in predicting the value of the outcome variable Blower and Dowlatabadi (1994); Sanchez and Blower (1997). The relative importance of the input variables can be directly evaluated by comparing the PRCC values Blower and Dowlatabadi (1994); Sanchez and Blower (1997).

APPENDIX B

TWO-COMPARTMENT PHARMACOKINETIC MODELS

Analytic solution of singe-dose PK-model with i.v. injection given by Eq. 3.3.1

Without loss of generality we assume that $t_0 = 0$. Using matrix notation, the pharmacokinetic equations can be given by:

$$\underbrace{\begin{pmatrix} \frac{dI_s}{dt} \\ \frac{dI_p}{dt} \end{pmatrix}}_{x'(t)} = \underbrace{\begin{pmatrix} -k_{12} - k_{el} & k_{21} \\ k_{12} & -k_{21} \end{pmatrix}}_{=:A} \underbrace{\begin{pmatrix} I_s \\ I_p \end{pmatrix}}_{x(t)} \tag{B.0.1}$$

Applying the Laplace transformation to Eq. B.0.1 we have:

$$\begin{aligned} \mathcal{L}\{\begin{pmatrix} \frac{dI_s}{dt} \\ \frac{dI_p}{dt} \end{pmatrix}\} = \mathcal{L}\{A \begin{pmatrix} I_s \\ I_p \end{pmatrix}\} \quad &\Longleftrightarrow \quad \mathcal{L}\{x'(t)\} = \mathcal{L}\{Ax(t)\} \\ &\Longleftrightarrow \quad sX(s) - x(0) = AX(s) \\ &\Longleftrightarrow \quad (sI - A)X(s) = x(0) \\ &\Longleftrightarrow \quad \underbrace{\begin{pmatrix} s + k_{12} + k_{el} & -k_{21} \\ -k_{12} & s + k_{21} \end{pmatrix}}_{=:L(s)} \underbrace{\begin{pmatrix} X_1(s) \\ X_2(s) \end{pmatrix}}_{=:X(s)} = \underbrace{\begin{pmatrix} I_s(0) \\ I_p(0) \end{pmatrix}}_{=:b} \end{aligned}$$

Solving $L(s)X(s) = b = \begin{pmatrix} I_s(0) \\ 0 \end{pmatrix}$ for $X_1(s)$ and $X_2(s)$ gives:

$$\begin{aligned} X_1(s) &= \frac{(s + k_{21})I_s(0)}{(s + k_{12} + k_{el})(s + k_{21}) - k_{12}k_{21}} \\ X_2(s) &= \frac{k_{12}}{s + k_{21}} X_1(s) \end{aligned}$$

The denominator in the equation of $X_1(s)$ can be re-written as $(s + \alpha)(s + \beta)$ such that

$$\alpha \;\&\; \beta = \frac{(k_{12} + k_{21} + k_{el}) \pm \sqrt{(k_{12} + k_{21} + k_{el})^2 - 4k_{21}k_{el}}}{2}. \tag{B.0.2}$$

In other word,

$$\begin{aligned} \alpha + \beta &= k_{12} + k_{21} + k_{el} \\ \alpha\beta &= k_{el}k_{21} \end{aligned}$$

Therefore,

$$X_1(s) = I_s(0)\frac{(s + k_{21})}{(s + \alpha)(s + \beta)}$$

The original differential equation B.0.1 then can be solved by applying the inverse Laplace transform.

$$\begin{aligned}
\mathcal{L}^{-1}\{X_1(s)\} &= \mathcal{L}^{-1}\left\{I_s(0)\frac{(s+k_{21})}{(s+\alpha)(s+\beta)}\right\} \\
&= I_s(0)\mathcal{L}^{-1}\left\{\frac{s}{(s+\alpha)(s+\beta)}\right\} + I_s(0)\, k_{21}\mathcal{L}^{-1}\left\{\frac{1}{(s+\alpha)(s+\beta)}\right\} \\
&= I_s(0)\left[\frac{-\alpha e^{-\alpha t}}{\beta-\alpha} + \frac{-\beta e^{-\beta t}}{\alpha-\beta} + k_{21}\left(\frac{e^{-\alpha t}}{\beta-\alpha} + \frac{e^{-\beta t}}{\alpha-\beta}\right)\right] \\
&= I_s(0)\left[\frac{k_{21}-\alpha}{\beta-\alpha}e^{-\alpha t} + \frac{k_{21}-\beta}{\alpha-\beta}e^{-\beta t}\right]
\end{aligned}$$

Thus,

$$I_s(t) = I_s(0)\left[\frac{k_{21}-\alpha}{\beta-\alpha}e^{-\alpha t} + \frac{k_{21}-\beta}{\alpha-\beta}e^{-\beta t}\right],$$

Let define

$$A = \frac{k_{21}-\alpha}{\beta-\alpha} \tag{B.0.3}$$

$$B = \frac{k_{21}-\beta}{\alpha-\beta} \tag{B.0.4}$$

Then $I_s(t)$ for a single dose injection can be rewritten as following:

$$I_s(t) = I_s(0)\left(Ae^{-\alpha t} + Be^{-\beta t}\right).$$

This completes the proof.

Multiple-dosing PK-model with i.v. injection

Using the definition of I_s^j given by Eq. 3.3.4, we have

$$\begin{aligned}
I_s^1(t) &= d\left[Ae^{-\alpha(t-\tau_1)} + Be^{-\beta(t-\tau_1)}\right], \quad t \in [\tau_1, \tau_2) \\
I_s^2(t) &= d\left[Ae^{-\alpha(t-\tau_1)} + Be^{-\beta(t-\tau_1)}\right. \\
&+ \left. Ae^{-\alpha(t-\tau_2)} + Be^{-\beta(t-\tau_2)}\right], \quad t \in [\tau_2, \tau_3] \\
&\vdots \\
I_s^m(t) &= d\left[Ae^{-\alpha(t-\tau_1)} + Be^{-\beta(t-\tau_1)}\right. \\
&+ Ae^{-\alpha(t-\tau_2)} + Be^{-\beta(t-\tau_2)}
\end{aligned}$$

$$\begin{aligned} &\vdots \\ &+ \quad Ae^{-\alpha(t-\tau_m)} + Be^{-\beta(t-\tau_m)}\Big], \quad t \geq \tau_m \end{aligned}$$

Therefore, for $t \in [\tau_j, \tau_{j+1}]$, and $1 \leq j \leq m-1$ we have:

$$\begin{aligned} I_s^j(t) &= \sum_{i=1}^{j} d\left[Ae^{-\alpha(t-\tau_i)} + Be^{-\beta(t-\tau_i)}\right] \\ &= d\left[e^{-\alpha(t-\tau_j)}\ A\sum_{i=1}^{j} e^{\frac{-\alpha(t-\tau_i)}{-\alpha(t-\tau_j)}} + e^{-\beta(t-\tau_j)}\ B\sum_{i=1}^{j} e^{\frac{-\beta(t-\tau_i)}{-\beta(t-\tau_j)}}\right] \\ &= d\left[e^{-\alpha(t-\tau_j)}\ A\sum_{i=1}^{j} e^{-\alpha(\tau_j-\tau_i)} + e^{-\beta(t-\tau_j)}\ B\sum_{i=1}^{j} e^{-\beta(\tau_j-\tau_i)}\right] \\ &= d\left[e^{-\alpha(t-\tau_j)}\ A\sum_{k=0}^{j-1} e^{-k\pi\alpha} + e^{-\beta(t-\tau_j)}\ B\sum_{k=0}^{j-1} e^{-k\pi\beta}\right] \\ &= d\left[e^{-\alpha(t-\tau_j)}\ A\frac{1-e^{-j\pi\alpha}}{1-e^{-\pi\alpha}} + e^{-\beta(t-\tau_j)}\ B\frac{1-e^{-j\pi\beta}}{1-e^{-\pi\beta}}\right] \end{aligned}$$

That is,

$$I_s^j(t) = d\left[\ Ae^{-\alpha(t-\tau_j)}\frac{1-e^{-j\pi\alpha}}{1-e^{-\pi\alpha}} + Be^{-\beta(t-\tau_j)}\frac{1-e^{-j\pi\beta}}{1-e^{-\pi\beta}}\right], \quad \tau_j \leq t < \tau_{j+1}\ \&\ 1 \leq j \leq m-1$$

The same approach can be used to show that the above formula also satisfies for $j = m$. This completes the proof.